

OPTIMAL MISSION DESIGN TO LAGRANGIAN POINTS

*A thesis submitted
in partial fulfilment for the award of the degree of*

Doctor of Philosophy

by

RITHWIK N



**Department of Aerospace Engineering
INDIAN INSTITUTE OF SPACE SCIENCE AND TECHNOLOGY
Thiruvananthapuram, India**

March 2024

DECLARATION

I declare that this thesis titled **Optimal Mission Design to Lagrangian Points** submitted in partial fulfilment for the award of the degree of **Doctor of Philosophy** is a record of original work carried out by me under the supervision of **Dr. R.V. Ramanan**, and has not formed the basis for the award of any degree, diploma, associateship, fellowship, or other titles in this or any other Institution or University of higher learning. In keeping with the ethical practice in reporting scientific information, due acknowledgments have been made wherever the findings of others have been cited.

Place: Thiruvananthapuram

Rithwik. N

Date: March 2024

Roll No.:SC16D034

CERTIFICATE

This is to certify that the thesis titled **Optimal Mission Design to Lagrangian Points** submitted by **Rithwik. N (SC16D034)**, to the Indian Institute of Space Science and Technology, Thiruvananthapuram, in partial fulfilment for the award of the degree of **Doctor of Philosophy**, is a bona fide record of the research work carried out by him under my supervision. The contents of this thesis, in full or in parts, have not been submitted to any other Institute or University for the award of any degree or diploma.

Dr. R.V. Ramanan

Research Supervisor,

Outstanding Scientist/Adjunct professor
(Retired)

ISRO/Department of Aerospace
Engineering, IIST

Counter Signature

The Head-of-Department.

Department of Aerospace Engineering,
IIST.

Seal

Place: Thiruvananthapuram

Date : March 2024

This thesis is dedicated to my beloved family

ACKNOWLEDGEMENTS

I would like to express my deepest gratitude and heartfelt acknowledgments to the many individuals who have been instrumental in the completion of my Ph.D. journey.

First and foremost, I want to thank my research supervisor, mentor and guru Dr. R. V. Ramanan for his constructive feedbacks, intellectual stimulation and paternal-like care. The countless hours spent with a programming novice like me at the start of Ph.D. tenure and revising manuscripts must have demanded infinite patience and I truly admire him for that quality. He has been a role model for both academic and non-academic activities and I sincerely hope that our collaboration continues in the future.

I would like to thank my family for their unwavering support throughout this challenging endeavour. My parents and brother for their constant encouragement and belief in my abilities, my spouse Lakshmi for her patience and understanding during countless late nights and weekends dedicated to research. I am especially grateful to my daughter, Naimitra, whose innocence, enthusiasm, and understanding of my pursuit have provided me with immeasurable inspiration and motivation. Your endless love and resilience have been the driving force behind my persistence in achieving this milestone.

I extend my gratitude to my friends, whose unwavering support and encouragement have been a continuous source of strength. I thank my colleagues at Digantara for their understanding and for providing private space amid the hectic work schedule. I would also like to thank my academic advisors and mentors in the doctoral committee for their guidance and expertise. A special mention is required to thank Dr. Anandmayee Tej, IIST for her support in the journal publications.

Lastly, I must acknowledge the countless others who may not be mentioned here but have played a part in my life and academic pursuit. Your impact has not gone unnoticed or unappreciated. Thank you from the bottom of my heart.

Rithwik. N

ABSTRACT

The problem of generating optimal mission design to Lagrangian points is attempted to be solved in this research. Scientific missions to Lagrangian points have the potential to enhance the understanding of the universe and to accelerate the exploration of space. The generation of orbits around the Lagrangian points and constructing optimal transfers to them from the Earth are complicated tasks due to the intricate multi-body dynamics involved. To overcome these complexities, this research employs a two-step approach, first utilizing a basic force model to generate preliminary designs, and then refining them using the full force Ephemeris model. The conventional approach employs the Circular Restricted Three Body Problem (CRTBP) framework and differential correction (DC) techniques for the design of halo orbit and transfer trajectory design. In contrast, this research explores the use of the Elliptic Restricted Three Body Problem (ERTBP) framework and employs the Differential Evolution (DE) optimization technique. Preliminary mission design to Sun-Earth Lagrangian points and Earth-Moon Lagrangian points are constructed under the ERTBP framework. In the Sun-Earth system, multi-revolution (MR) orbits are designed in a single level, single segment approach and the proposed technique identifies multiple options of MR orbits for the same period and generates both Lyapunov and halo orbit MR solutions for the same period. However, the amplitudes of the MR orbits are found to be unacceptably large for scientific missions like the NASA's ISEE-3 mission. For feasible amplitudes, it is found that only quasi-halo orbits are viable and are designed using a DE-based technique in the ERTBP framework and a realistic ephemeris model. The designed quasi-halo orbits do not require any theoretical velocity corrections for about five years (state-of-the-art in literature is about two and half years). Optimal two impulse transfers to the quasi-halo orbit from an Earth parking orbit are generated under the ERTBP framework and the ephemeris model. It is inferred that both the CRTBP and ERTBP reference designs generate the ephemeris design and there is no noticeable advantage of considering ERTBP reference design. This can be attributed to the small eccentricity of the orbit of Earth around the Sun ($e \sim 0.0167$). Then, the Lagrangian point mission design in the Earth-Moon system is attempted. The dynamics of motion near the Earth is significantly different for Earth-Moon Lagrangian point missions compared to the Sun-Earth Lagrangian point missions because in former, the Earth is the larger primary. The proposed design methodology using differential evolution designs the transfer trajectory in a single segment and involving only two velocity impulses. Because of the robustness of the developed technique, there is no need to

tweak the methodology used for generating the orbit or the transfer trajectory in different dynamical systems. The optimal solutions indicate that there exist trajectories with lower cost significantly shorter flight durations than those reported in the literature. In summary, complete Lagrangian point preliminary design in the ERTBP framework is generated. For the mission design in the Sun-Earth system, it is substantively concluded that preliminary design using the ERTBP framework does not provide significant advantages over the CRTBP framework. The differential evolution technique is found to be very versatile in solving Lagrangian point mission design problems and avoids many complexities associated with the differential correction based technique. However, the DE based schemes are found to be computationally more intensive. The proposed methodology based on differential evolution constructs transfer trajectory independent of the characteristics of the target orbit and hence, preserves the fundamental nature as such (not changing the type of orbit from halo to quasi-halo etc.).

List of Publications Based on the Current Research

Publications in Peer Reviewed International Journals

1. Rithwik, N., R. V. Ramanan, February 2021. “Design of multi-revolution orbits in the framework of elliptic restricted three-body problem using differential evolution”, *Journal of Astrophysics and Astronomy*, Vol. 42, No. 5, 2021, <https://doi.org/10.1007/s12036-020-09651-w>.
2. Rithwik, N., R. V. Ramanan, August 2022. “Two-impulse transfer to multi-revolution halo orbits in the Earth–Moon elliptic restricted three body problem framework”, *Journal of Astrophysics and Astronomy*, Vol. 43, No. 50, 2022. <https://doi.org/10.1007/s12036-022-09830-x>
3. Rithwik, N., R. V. Ramanan, August 2023. “Design and analysis of quasi-halo orbits and optimal transfers from the Earth under different Sun–Earth frameworks using differential evolution”, *Journal of Astrophysics and Astronomy*, Vol. 44, No. 81, 2023. <https://doi.org/10.1007/s12036-023-09969-1>.

Publications in International Conferences

1. Rithwik, N., R. V. Ramanan, “Halo orbit design around Lagrangian points using gradient and non-gradient based optimization techniques”, presented at International Conference on Frontiers in Industrial and Applied Mathematics (FIAM2018), NIT Hamirpur, April 26-27, 2018, published in: *AIP Conference Proceedings*, Vol 1975, pp 030019(1)-030019(10) (2018).
2. Rithwik. N, Kiran Jayasurya and R. V. Ramanan, “Analysis of Halo Orbits around Sun-Earth L2 for the ExoWorld mission”, presented at “ExoWorld Team Meet”, IIST, Trivandrum, January 04, 2019.
3. Rithwik, N., R. V. Ramanan, “Design of Halo Orbits in the Framework of Elliptic Restricted Three Body Problem using Differential Evolution”, presented at 11th International Academy of Astronautics (IAA) Symposium on the Future of Space Exploration, June 2019, Torino, Italy.
4. Rithwik, N., R. V. Ramanan, “Improved two-impulse transfer to halo orbits in the Earth-Moon Elliptic Restricted Three Body Problem framework using differential evolution”, presented at 2020 AAS/AIAA Astrodynamics Specialist Conference, paper no. AAS 20-607.

TABLE OF CONTENTS

DESCRIPTION	PAGE NUMBER
DECLARATION	ii
CERTIFICATE	iii
ACKNOWLEDGEMENTS	v
ABSTRACT	vi
PUBLICATIONS BASED ON THIS THESIS	viii
TABLE OF CONTENTS	ix
LIST OF FIGURES	xii
LIST OF TABLES	xv
ABBREVIATIONS	xvii
NOMENCLATURE	xviii
Chapter 1: Introduction and Literature Survey	1
1.1 Introduction	1
1.2 Literature Survey.....	5
1.2.1 Historical Perspective	5
1.2.2 Literature on Design of Orbits around Lagrangian points.....	6
1.2.3 Literature on Transfer Trajectory Design	13
1.3 Motivation of the Research	19
1.4 Objectives of the Research.....	21
1.5 Research Summary.....	22
1.6 Thesis Architecture	25
Chapter 2: Multibody dynamics and frameworks.....	27

2.1	Introduction	27
2.2	N-body problem and the special case of three body problem	27
2.2.1	SEM Ephemeris model	28
2.3	Circular Restricted Three Body Problem (CRTBP) framework	28
2.4	Elliptic Restricted Three Body Problem (ERTBP) framework.....	31
2.5	Coordinate transformations	33
2.6	Locations of Lagrangian points	35
Chapter 3: Preliminary Mission Design in the CRTBP Framework.....		41
3.1	Introduction	41
3.2	Design of Halo Orbits	42
3.2.1	Design Methodology.....	42
3.2.2	Design of Halo Orbits Using Differential Correction.....	42
3.2.3	Design of Halo Orbits Using Differential Evolution	45
3.3	Transfer Trajectory Design to Halo Orbits	56
3.3.1	Design Methodology.....	56
3.3.2	Computational Algorithm	57
3.3.3	Numerical Results	59
3.4	Conclusions	60
Chapter 4: Design of MR orbits in the Sun-Earth system under the ERTBP framework		63
4.1	Introduction	63
4.2	Design of MR Orbits using Differential Evolution.....	64
4.2.1	Terminology and Design Philosophy.....	64
4.2.2	Computational Algorithm	65
4.2.3	Results.....	67
4.3	Comparison Between Differential Correction and Differential Evolution Methodologies for the Design of MR Orbits	79
4.4	Conclusions	83
Chapter 5: Design of quasi-halo orbits and optimal transfers in the Sun-Earth system		85
5.1	Introduction	86
5.1.1	Amplitudes of MR Halo Orbits and Motivation for Design of Quasi-Halo orbits 86	
5.2	Design of Quasi-Halo Orbits.....	88
5.2.1	Design Process for Quasi-Halo orbit in ERTBP and Optimal Numerical Design 88	

5.2.2	Design Process for Quasi-Halo orbit in the SEM Ephemeris model and Optimal Numerical Design	90
5.2.3	Evolution of Radial Distance and Velocity in Quasi-Halo Orbit.	94
5.2.4	Design of Quasi-Halo Orbits for Different Az Amplitudes	95
5.2.5	Validation of the Design of the Orbit in the SEM Ephemeris Model.....	96
5.3	Design of Optimal Transfers to Quasi-Halo Orbits	98
5.3.1	Design Philosophy	98
5.3.2	Optimal Two Impulse Transfer to Quasi-Halo Orbit in the ERTBP framework	99
5.3.3	Optimal Transfers in the SEM Ephemeris Model.....	101
5.3.4	Validation of the Design of the Transfer Trajectory in the SEM Ephemeris Model	102
5.3.5	Sensitivity of the Transfer Trajectory Design.....	103
5.4	Conclusions	105
Chapter 6: Mission design in Earth-Moon system under the ERTBP framework.....		107
6.1	Introduction	108
6.2	Design of MR Halo Orbits	109
6.2.1	Terminology and Design Philosophy.....	109
6.2.2	Computational Algorithm	110
6.2.3	Results.....	112
6.3	Design of Two Impulse Transfers to MR Halo Orbits.....	118
6.3.1	Design Philosophy	118
6.3.2	Computational Algorithm	120
6.3.3	Results.....	121
6.4	Conclusions	136
Chapter 7: Summary and Conclusions.....		139

LIST OF FIGURES

Figure 2.1. Geometry of general three body problem.....	28
Figure 2.2. Rotating coordinate frame in CRTBP	29
Figure 2.3. Coordinate frame in the ERTBP framework.	31
Figure 2.4. Variation of Sun-Earth L_1 with true anomaly of Earth around the Sun	37
Figure 2.5. Variation of Earth-Moon L_1 with true anomaly of Moon around the Earth.....	38
Figure 2.6. Variation of Sun-Earth L_2 with true anomaly of Earth around the Sun	38
Figure 2.7. Variation of Earth-Moon L_2 with true anomaly of Moon around the Earth.....	39
Figure 2.8. Variation of Sun-Earth L_3 with true anomaly of Earth around the Sun	39
Figure 2.9. Variation of Earth-Moon L_3 with true anomaly of Moon around the Earth	40
Figure 3.1 A synthetic diagram of the proposed DE-based solution for the design of halo orbit	48
Figure 3.2. Halo orbit with 120,000 km Az amplitude from DE scheme.....	52
Figure 3.3. Performance of variants of DE in terms of computational effort for halo orbit design around Sun-Earth L_1	54
Figure 3.4 Performance of variants of DE in terms of computational time for halo orbit design around Sun-Earth L_1	54
Figure 3.5 Performance of variants of DE in terms of computational time for halo orbit design around Sun-Earth L_2	55
Figure 3.6 $x - y$ projection of optimal transfer trajectory to halo orbit for $Az = 120,000$ km	60
Figure 4.1 Trajectory and projections of MR halo orbit M5N2 around Sun-Earth L_1	68
Figure 4.2. Period- Az amplitude profile for halo orbits around L_1 in the Sun-Earth system ..	71
Figure 4.3 Evolution of radial distance from Earth in MR orbits.....	72
Figure 4.4 Evolution of velocity in MR orbits.....	73
Figure 4.5 Trajectory and projections of M4N2 halo and M4N2 Lyapunov orbits.....	74
Figure 4.6 Trajectory and projections of MR orbits corresponding to M4N2 design1 and M4N2 design2.....	76
Figure 4.7 Trajectory and projections of MR halo orbit M4N2 belonging to northern and southern families.....	79
Figure 5.1 Variation of SEV angle along different halo orbits.	87
Figure 5.2 Variation of SEV angle along different MR halo orbits	88

Figure 5.3 Trajectory and projections of the CRTBP halo orbit and nine revolutions of ERTBP quasi-halo orbit ($Az \sim 120,000$ km)	90
Figure 5.4 Trajectory and projections of the CRTBP halo orbit and ephemeris quasi-halo orbit ($Az \sim 120,000$ km)	92
Figure 5.5 Trajectory and projections of the ERTBP quasi-halo orbit and ephemeris quasi-halo orbit ($Az \sim 120,000$ km).....	93
Figure 5.6 Evolution of radial distance from the Earth in quasi-halo orbit ($Az \sim 120,000$ km)	94
Figure 5.7 Evolution of velocity in quasi-halo orbit ($Az \sim 120,000$ km)	95
Figure 5.8 Comparison of design simulation and GMAT simulation of the first revolution of quasi-halo orbit.	98
Figure 5.9 $x - y$ projection of the optimal transfer trajectory to the quasi-halo orbit.	100
Figure 5.10 $x - y$ projection of the optimal transfer trajectory to the quasi-halo orbit based on CRTBP framework.....	102
Figure 5.11 GMAT simulation of design of transfer trajectory in the SEM ephemeris model	103
Figure 6.1. Trajectory and projections of MR halo orbit M5N2 around Earth-Moon L_1	113
Figure 6.2 Evolution of radial distance from the Earth in MR halo orbits	117
Figure 6.3. Evolution of velocity in MR halo orbits.....	118
Figure 6.4 $x - y$ projection of the optimal transfer trajectory to MR halo orbit M5N2	122
Figure 6.5 Velocity impulses for optimal transfers to different locations on the MR halo orbit M5N2	126
Figure 6.6 Flight durations for optimal transfers to different locations on the MR halo orbit M5N2	126
Figure 6.7 Velocity impulses for optimal transfer to different locations on MR halo orbit M5N2	128
Figure 6.8 Optimal velocity impulses for different flight durations for the MR halo orbit M5N2	129
Figure 6.9 $x - y$ projections of transfers for different flight durations for the MR halo orbit M5N2	130
Figure 6.10 Variation of geocentric radial distance for different flight durations.....	131
Figure 6.11 Locations of minimum HOI velocity impulse for different revolutions as a function of radial distance from the Earth	133

Figure 6.12. Locations of minimum HOI velocity impulse for different revolutions as a function of radial distance from L_1 133

Figure 6.13. Trajectory and projections of optimal transfers to different revolutions of MR halo orbit M5N2..... 134

LIST OF TABLES

Table 2.1 Location of Lagrangian points in the non-uniformly rotating and pulsating frame in ERTBP and rotating frame in CRTBP	36
Table 3.1 Halo orbit initial conditions generated by different methods.	44
Table 3.2 Comparison of halo orbit amplitudes obtained from DC procedure.	45
Table 3.3 DE performance for different population sizes NP.....	49
Table 3.4 DE performance for varying cross over ratio CR.....	50
Table 3.5 DE performance for varying mutation factor F.	50
Table 3.6 DE performance for varying seeds.	51
Table 3.7 DE performance for varying search bounds.	52
Table 3.8 Performance of Scheme 2 over Scheme 1.	56
Table 3.9. Optimal transfer in the CRTBP framework to halo orbit.....	60
Table 4.1. Performance of DE with varying no of threads	69
Table 4.2. Period and CRTBP initial conditions.....	70
Table 4.3 ERTBP initial conditions for different periods.....	70
Table 4.4. Variation of radial distance and velocity in MR orbits.....	72
Table 4.5 Halo and Lyapunov design solutions for different MR orbits.....	74
Table 4.6 Variation of radial distance and velocity in MR orbits having period 4π	75
Table 4.7 Multiple design solutions for different MR orbits.....	76
Table 4.8 Variation of radial distance and velocity in multiple design solutions for a given MR orbit.....	77
Table 4.9 Az amplitudes of multiple designs of MR halo orbits	78
Table 4.10 Performance of DC and DE methodologies for the design of MR orbits.....	82
Table 4.11 Qualitative comparison of DC and DE processes for the design of MR orbits	83
Table 5.1 Comparison of amplitudes of MR halo orbits and ISEE3 halo orbit.....	86
Table 5.2 Initial conditions of quasi-halo orbits in different frameworks	92
Table 5.3 Comparison of Ephemeris designs of quasi-halo orbits.....	93
Table 5.4 Design of quasi-halo orbits in SEM Ephemeris model for different Az amplitudes.....	96
Table 5.5 Optimal transfer in the ERTBP framework	100
Table 5.6 Optimal transfer in the SEM ephemeris model	101

Table 5.7 Sensitivity analysis of transfer trajectory design in SEM Ephemeris model.....	104
Table 6.1. Performance of DE with varying no of threads	114
Table 6.2 Az amplitudes of MR halo orbits	115
Table 6.3. CRTBP initial conditions and period.....	116
Table 6.4 ERTBP initial conditions and period	116
Table 6.5 Variation of radial distance and velocity in MR halo orbits.....	117
Table 6.6 Performance of the DE based algorithm with different weights in objective function	123
Table 6.7 Performance of the DE based algorithm with different search bounds for velocity components	124
Table 6.8 Performance of the DE based algorithm with different seeds for random number generation.....	124
Table 6.9 Characteristics of transfers identified in Figure 6.8 and Figure 6.9.	129
Table 6.10 Optimal transfer trajectory to different revolutions of MR halo orbit M5N2	132
Table 6.11. Transfer trajectory designs for different CAA's.	135
Table 6.12 Initial conditions and period of target MR orbits	136
Table 6.13 Transfer trajectory designs for different MR orbits.....	136

ABBREVIATIONS

CPU	Central Processing Unit
CRTBP	Circular Restricted Three Body Problem
DC	Differential Correction
DE	Differential Evolution
EPO	Earth Parking Orbit
ERTBP	Elliptic Restricted Three Body Problem
GMAT	General Mission Analysis Tool (a NASA provided open source software system for space mission design, optimization, and navigation.)
ISEE	International Sun-Earth Explorer
ISRO	Indian Space Research Organization
JPL	Jet Propulsion Laboratory
LEO	Low Earth Orbit
MR	Multi Revolution
NASA	National Aeronautics and Space Administration
OS	Operating System
RK	Runge-Kutta
RKF	Runge-Kutta-Fehlberg
SEM ephemeris model	Sun-Earth-Moon ephemeris model
SEV	Sun-Earth-Vehicle
SEZ	Solar Exclusion Zone
STM	State Transition Matrix
TDB	Temps Dynamique Barycentrique (Barycentric Dynamical Time)
TOI	Target Orbit Insertion

NOMENCLATURE

<i>CAA</i>	Closest Approach Altitude
<i>M</i>	Number of third body revolutions around the Lagrangian point (for an MR orbit)
<i>N</i>	Number of primary revolutions around the barycentre (for an MR orbit)
<i>A_z</i>	Out of plane amplitude
ΔV	Velocity impulse required
μ	Mass ratio
υ	True anomaly
\emptyset	State Transition Matrix
<i>NP</i>	Size of population in differential evolution
<i>OBJ</i>	Objective Function
<i>F</i>	Mutation scale factor in differential evolution
<i>CR</i>	Cross over frequency in differential evolution
ε	A very small tolerance value
$[\Delta\dot{x}, \Delta\dot{y}, \Delta\dot{z}]$	Components of halo orbit insertion velocity impulse.
T_E	Period of MR orbit in ERTBP framework
T_C	Period of halo orbit in CRTBP framework
<i>h</i>	Step size for numerical integration

Chapter 1: Introduction and Literature Survey

*"Somewhere, something incredible is waiting to be known."
- Carl Sagan*

1.1 Introduction

The interest of humanity in space dates back to ancient times, with early civilizations looking up at the night sky and developing their own stories and beliefs about the stars and planets. Ancient civilizations, such as the Indians, Greeks, Egyptians, and Babylonians, studied the movements of celestial bodies and developed methods of observing and predicting astronomical events. As civilizations progressed, so did our understanding of space. With the advent of telescopes and other advanced technologies, astronomers were able to observe and study the cosmos in greater detail.

In the 20th century, the launch of the first artificial satellite Sputnik by the Soviet Union in 1957 marked the beginning of the *new* space age and ignited a global interest in space exploration. Since then, humanity's interest in space has continued to grow. The first human spaceflight by Yuri Gagarin in 1961 marked a major milestone in space exploration and inspired a generation of space enthusiasts. The launch of the Apollo program in the 1960s, which culminated in the first moon landing in 1969, rekindled the imagination of people around the world and sparked a renewed interest in space exploration. Since then, space exploration has continued to expand, with missions to Mars and the discovery of new planets and galaxies.

One area of space exploration that has gained increasing attention in recent years is the use of Lagrangian point dynamics. The concept of Lagrangian points was first proposed by French mathematician Joseph-Louis Lagrange in 1772, and refers to the five points in space where the gravitational forces of two large celestial bodies (such as the Earth and the Sun) balance the centrifugal force felt by a smaller object, such as a spacecraft. These points are ideal locations for spacecraft to observe the Sun, Earth, and other celestial bodies with minimal interference from Earth's atmosphere and magnetic field. They offer a unique vantage point for observing distant stars, galaxies, and other celestial objects, and can provide valuable insights into the origins and evolution of the universe. In addition, Lagrangian point missions can be

used for a range of scientific and technological applications, including communications and space weather monitoring.

In 1978, NASA launched the International Sun-Earth Explorer 3 (ISEE-3) mission, which was the first spacecraft to explore the L_1 Lagrangian point between the Earth and the Sun. The spacecraft studied the solar wind, the magnetic field of the Earth, and the composition of the interstellar medium. In addition to its scientific observations, the mission was also notable for its innovative use of the Earth's gravity to change its orbit and allow it to explore other areas of space. In 1996, the European Space Agency (ESA) launched the Solar and Heliospheric Observatory (SOHO) mission, which also placed a spacecraft in an orbit around the L_1 point. The mission has made ground-breaking observations of the Sun, including the discovery of coronal mass ejections and the first detection of seismic waves on the Sun. It has also provided valuable data on the impact of solar activity on Earth's climate and weather. In 2001, NASA launched the Wilkinson Microwave Anisotropy Probe (WMAP) mission, which was placed in orbit around the L_2 Lagrangian point on the opposite side of the Earth from the Sun. The mission provided detailed observations of the cosmic microwave background radiation, which is the afterglow of the Big Bang. The data collected by WMAP has been used to refine our understanding of the composition, age, and evolution of the universe. Recently, the James Webb Space Telescope (Gardner et al., 2006) was inserted in a halo orbit around Sun-Earth Lagrangian point L_2 for deep space exploration. The Webb telescope is the largest and most powerful space telescope ever built, with a primary mirror over six times larger than that of the Hubble Space Telescope. It is expected to make ground-breaking observations in areas such as galaxy formation, star birth, and the atmospheres of exoplanets. The Aditya L_1 mission is a space mission by the Indian Space Research Organization (ISRO) to study the Sun. The spacecraft will carry several scientific instruments, including a coronagraph to study the Sun's corona, a solar ultraviolet imaging telescope, and a magnetometer to study the Sun's magnetic field. The Aditya L_1 spacecraft was launched in September 2023 and will make important contributions to our understanding of the Sun and its effects on Earth.

A typical mission design to an orbit around the Lagrangian points from the Earth involves two steps. In the first step, an orbit with prescribed geometrical characteristics is designed and in the second step, an optimal transfer trajectory to the orbit from an Earth parking orbit is generated. Both these steps are executed first in a basic force model to generate reference preliminary designs and then refined in the full force ephemeris model.

The design of orbits around the Lagrangian points in the Sun-Earth and Earth-Moon systems under realistic frameworks is a challenging task due to the complex multi-body dynamics of the problem. The complexity is the same for generating transfers also. It is well known that the N -body (multi-body) equations of motion have no analytical solution and that the numerical solution process requires a good initial guess. A well-known design approach for Lagrangian point missions is to generate design in the framework of Circular Restricted Three Body Problem (CRTBP) first and then refine this design under an ephemeris model. The CRTBP framework assumes that the primaries (large, celestial bodies) revolve around their barycentre in circular orbits. The CRTBP framework-based designs serve as an initial approximation to initiate the real mission design involving full force ephemeris models. Furthermore, these CRTBP designs are used for preliminary mission analysis purposes.

The current research focuses on exploring a higher fidelity dynamical model (compared to the CRTBP framework) for the preliminary designs of orbits around the Lagrangian points and transfer trajectory to them from the Earth. The dynamical model explored is known as the Elliptic Restricted Three Body Problem (ERTBP) Framework, wherein the eccentricities of the orbits of the primaries are also modelled. The motivation to utilize the ERTBP framework is that the orbits designed in the ERTBP framework closely mimic the characteristics of the actual quasi-periodic orbits in the ephemeris model. The advantages and disadvantages of the initial approximations using the CRTBP, ERTBP frameworks on generating the ephemeris designs are compared and analysed.

First, the design of multi-revolution (MR) halo orbits around the Lagrangian point L_1 in the Sun-Earth system is generated using a differential evolution based methodology. The MR halo orbits are perfectly periodic, multi-revolution orbits in the ERTBP framework and differ from the quasi-periodic orbits in the sense of temporal repetition of geometry (the quasi-periodic orbits do not repeat the geometry, but the positions in subsequent revolutions are very close to that in the first revolution). In the design process of MR orbits, unlike in the differential correction-based method, the proposed methodology produces both Lyapunov and halo orbit MR solutions for the same period. *However, the amplitudes of the generated MR halo orbits in the Sun-Earth system are large compared to the halo orbits used for scientific missions such as the ISEE-3 mission (Minimum average Az amplitude of all MR halo orbits in the Sun-Earth system is around 490,300 km whereas the Az amplitude of halo orbit used in ISEE3 mission was 120,000 km).* Such large amplitudes of MR halo orbits result from the use of the

commensurability constraint used in the design methodology and violate the communication system constraint on the maximum Sun-Earth-Vehicle angle possible in the orbit. Therefore, it is found that MR halo orbits in the Sun-Earth system cannot be used for meeting the objectives of a scientific mission similar to ISEE-3 and the focus is shifted to the generation of quasi-periodic orbits.

The quasi-halo orbit is generated under the ERTBP framework using a differential evolution based methodology. The quasi-halo orbit and the CRTBP halo orbit are used as reference designs and the quasi-halo orbit design is obtained in the higher fidelity ephemeris model. The design methodology based on DE generates a ten-revolution quasi-halo orbit (previously reported is five) without any maneuvers and has demonstrated that generation of orbits for a wide range of Az amplitudes is possible. ***Both the CRTBP and ERTBP reference designs generate the ephemeris design and there is no noticeable advantage of considering ERTBP reference design.*** Transfers under three frameworks (CRTBP, ERTBP and ephemeris) are constructed and it is found that the least cost is incurred when the transfer is generated under the ephemeris model.

Motivated by the success of the proposed methodology in the Sun-Earth system, the design of MR halo orbits in the Earth-Moon system is attempted. The proposed methodology does not require a close initial guess and generates MR halo orbits under the ERTBP framework in a single segment, single level scheme (avoiding the need for multiple segments and numerical continuation methods). Next, two-impulse transfer trajectories from Earth parking orbit to the MR halo orbits are generated, based on a differential evolution based methodology. The proposed method does not make use of the manifold theory and avoids the bridge segment resulting in a single segment design process. The optimal solutions obtained indicate that there exist trajectories with lower cost and for significantly lower time of flight than those reported in the literature for similar problems.

This chapter is organized as follows: In Section 1.2, a literature review that includes an exhaustive survey of the currently available orbit and trajectory design techniques is presented. Section 1.3 outlines the limitations of the conventional techniques for the design of orbits and transfer trajectories which form the motivation for the current research. The objectives of the research are presented in Section 1.4. Section 1.5 provides a summary of the research. Section 1.6 provides the thesis architecture.

1.2 Literature Survey

1.2.1 Historical Perspective

The history of research on the three-body problem can be traced back to the 17th century, when Isaac Newton developed the laws of motion and universal gravitation. Newton himself studied the three-body problem, but his methods were limited to analytical approximations and he was not able to obtain exact solutions. In the 18th century, several mathematicians attempted to solve the problem using various methods. In 1772, Joseph-Louis Lagrange developed a mathematical framework for the problem based on the principle of least action and found three collinear equilibrium points (Moulton, 1914). Lagrange's work laid the foundation for later developments in the field of celestial mechanics. Leonhard Euler built upon the work of Lagrange and developed a number of techniques for finding approximate solutions to the problem. Euler's methods were based on perturbation theory, which involves breaking the problem down into a series of simpler problems that can be solved analytically. In the 19th century, the problem continued to attract the attention of mathematicians and astronomers. Carl Friedrich Gauss made significant contributions to the field, developing a method for determining the orbits of celestial bodies based on the principle of least squares. Henri Poincare developed analytical techniques for solving differential equations and applied the concepts to compute periodic orbits (Moulton et al., 1920; Green, 1993).

A significant leap in the understanding of the three-body problem and its potential applications was made when George William Hill studied the motion of the Moon in the Sun-Earth-Moon system (Hill, 1878). Hill's work on the restricted three-body problem was motivated by his desire to improve the accuracy of lunar ephemerides, which were used by astronomers to predict the position of the Moon in the sky. Hill developed a powerful analytical technique for studying the problem, known as the method of canonical variables. Using this method, Hill was able to derive a series of perturbation equations that described the effect of the Sun's gravitational pull on the motion of the Moon. Using these equations, he could calculate the Moon's position with much greater accuracy than previous methods. Hill's work also had broader implications for the field of celestial mechanics. His techniques for studying the restricted three-body problem were later applied to other systems in the solar system, such as the motion of asteroids and comets.

The work on Elliptic Restricted Three Body Problem began as early as the 1900s. Moulton worked on the planar restricted three body problem, where the motion of all the bodies was assumed to be restricted to one plane (Moulton, 1920). Moulton derived approximate analytical solutions for the motion of the third body assuming both circular and elliptical motion of the primaries. Among many significant fundamental findings, Moulton presented a condition for an orbit to be periodic in ERTBP, as stated below:

“For an orbit to be periodic it is sufficient that it has two perpendicular crossings with the syzygy-axis, and that the crossings happen at moments when the two primaries are at an apse, (i.e., at maximum or minimum elongation, or apoapsis and periapsis).”

Here, the syzygy axis denotes the straight line connecting the two primary, celestial bodies and the property of ‘perpendicular’ or ‘orthogonal’ crossing is emphasized. This fundamental characteristic of periodic orbits can be found ubiquitously in the design methodologies formulated by later researchers in the field.

Broucke (1969) studied the stability of periodic orbits systematically in the ERTBP. Broucke considered the simplified form of planar motion of the primaries and generated periodic orbits for a wide range of eccentricities and mass ratios.

1.2.2 Literature on Design of Orbits around Lagrangian points

Until the mid-twentieth century, the approaches to solving restricted three body problem were mostly analytical. A quantum leap in the numerical computations happened with the invention of computers. Researchers began to investigate a wider range of exact numerical solutions including the three-dimensional orbits. In 1967, a comprehensive summary of the research efforts till date on restricted three body problem was consolidated by Szebehely in his classical work (Szebehely, 1967). Starting from a simplified circular two-dimensional problem, Szebehely elegantly combined aspects of analytical results and numerical results to characterize the motion near Lagrangian points and also touched upon the more complex three dimensional and elliptic restricted problems.

Around this time, analytic studies on a specific type of orbit named as ‘halo orbit’ was undertaken by Robert Farquhar. The term ‘halo orbit’ was coined by Farquhar because when viewed from the Earth, the orbit would seem to appear as a halo about the Moon. The halo orbit is a three dimensional, perfectly periodic orbit around the Lagrangian point under the restricted

three-body problem framework (Farquhar, 1967). This novel concept resulted from Farquhar's efforts to establish an effective communication link with the far side of the moon, as a part of the Apollo mission 18 (the mission was canceled later). The original proposal involved the use of only two satellites, one at each of L_1 and L_2 Lagrangian points of the Earth-Moon system to ensure uninterrupted communications with the Earth (Farquhar, 1967). These efforts eventually resulted in NASA's ISEE-3 mission, which was the first scientific mission to a Lagrangian point (L_1 of the Sun-Earth system). The scientific objectives of the ISEE-3 mission were to study the interactions between the Earth's magnetic field and the solar wind, as well as to investigate the physical processes that occur in the magnetosphere and the space plasma environment. After completing its original mission as the ISEE-3, the spacecraft was repurposed to become the International Cometary Explorer (ICE).

Following the success of the ISEE-3 mission, a series of analytical works on the methodology and formulation of the halo orbit was published (Farquhar and Kamel, 1973; Richardson and Cary, 1975; Richardson, 1980a; Richardson, 1980b). Specifically, Richardson developed a third order analytical solution for the halo orbit using successive approximations and Lindstedt-Poincaré method (Richardson, 1980b). Using the analytical approximation, a numerical solution of the halo orbit was also presented using a methodology based on differential correction (DC). The deviations between the analytically constructed and numerically constructed halo orbits were evaluated and Richardson concluded that the deviations were of the order of the truncation error of the third order approximation (Richardson, 1980b), proving the effectiveness of the analytical approximation. As an extension of this work, Richardson and Cary also developed a fourth order analytic approximation for Lissajous orbits (Richardson and Cary, 1975).

Howell and Pernicka used Richardson's third order solution as an initial approximation and generated halo orbits using the multiple shooting method, based on differential correction (Howell, 1984; Howell and Pernicka, 1987). The algorithm involves a numerical optimization technique in which the orbit is divided into a series of sub-intervals, each of which is treated as a separate boundary value problem. The boundary conditions at the end of each segment are used to determine the state of the spacecraft at the beginning of the next segment. The procedure involves two broad levels. In the first level, the algorithm computes the difference between the desired final positions and the current positions at the end of the different segments. This difference is called the residual error and the algorithm then adjusts the initial

conditions of each segment of the trajectory in order to minimize the residual error. This process is repeated until the residual error is minimized to be within a desired tolerance and the first level is completed. Now, a trajectory continuous in time and positions, but discontinuous in velocities is obtained. In the next step, the same procedure is repeated, while correcting the velocity discontinuities. A very good initial guess is required for the process, otherwise the algorithm diverges quickly. Provided with a good initial guess, typically, the numerical procedure is robust, quick and converges within less than 10 iterations.

The design of halo orbits using the differential correction, however, does not achieve the desired out-of-plane amplitude in a single level scheme. The halo orbit formulation based on the DC scheme needs one of the (three) unknown coordinates obtained using higher order analytical solution to be fixed. Because of this fixation of a variable, the resulting halo orbit design will not have the same out-of-plane amplitude that is used in Richardson solution. That means, the initial design based on the multiple shooting and differential correction methodology needs to be refined using some numerical continuation procedure such as pseudo arc continuation (Paffenroth et al., 2001), making it a multi-level effort. Further, the methodology for the design of orbits in ERTBP framework requires numerical continuation on eccentricity also. That means, the initial design is based on the CRTBP framework and the design needs to be refined by incrementing the value of eccentricity in several small steps until the eccentricity of the desired physical system.

Apart from the perfectly periodic halo orbits, researchers also found quasi-periodic orbits around the Lagrangian points in different dynamical systems (Howell and Pernicka, 1987; Pernicka, 1990; Dunham et. al, 1992). These (theoretical) orbits do not come back to the initial point (like the halo orbits do), but return to the vicinity of the initial point. The actual orbits designed in the ephemeris model are also quasi-periodic in nature, even though a perfectly periodic halo orbit is used as the reference trajectory. Also, the station-keeping requirements for the quasi-periodic orbits are not as stringent as those for the halo orbits, when used as the reference trajectories. These facts motivated the researchers to explore more into the dynamics of the quasi-periodic orbits. Howell and Pernicka (1987) designed Lissajous orbits in CRTBP using the differential correction and multiple shooting algorithm, similar to the design methodology of halo orbits. Sarris (1989) used numerical continuation methods to generate periodic orbits in systems with large mass ratios. Pernicka (1990) extended the methodology to compute Lissajous orbits and investigated their station keeping aspects in

ERTBP. His work involved a Z-axis control for avoiding the solar exclusion zone, wherein the maneuver was applied along the out-of-plane axis. Following this work, Gordon (1991) treated the curve fit approximation to the halo and Lissajous orbits in the Sun-Earth ERTBP and concluded that cubic splines best approximate the trajectories resulting from numerical integration. David and Bong formulated the halo orbit control problem in Earth-Moon CRTBP linearly first and modeled the nonlinearities as trajectory dependent persistent disturbance inputs (David and Bong, 1994; David and Bong, 1996).

The 1990s also saw a number of scientific missions launched to the vicinity of Lagrangian points in the Sun-Earth and Earth-Moon systems. Farquhar (1991) consolidated the past missions and emphasized the use of Lunar gravity for such missions. As a later effort, Dunham and Farquhar (2003) extended the effort to include further missions till 2002. Both these works explained the scientific objectives of the missions, their target orbits and transfer trajectory designs in detail.

Around this time, the use of manifold theory to construct transfer trajectories to different orbits around the Lagrangian points was conceptualized. Some attempts were made to extend the same concepts to the design of orbits as well. Martin Lo (1997) generated small amplitude halo and Lissajous orbits in the Sun-Earth system using dynamical systems theory. Barden and Howell (1998) conceptualized that the halo and Lissajous orbits form a part of the motion in a torus around the center manifold. Jorba and Gomez constructed quasi-halo orbits using a semi-analytical method employing Lindstedt-Poincare method (Jorba and Masdemont, 1997; Gomez et al., 1998). The manifold theory was extensively used in the trajectory design of the Genesis mission, a technologically challenging mission to return solar wind samples from the vicinity of Sun-Earth L_1 (Bell et al., 1999). This mission also explored innovative use of the dynamics of the three body systems such as heteroclinic connection between the L_1 and L_2 points in the Sun-Earth system and the possible interaction between dynamics of motion near the Lagrangian points of Sun-Earth and Earth-Moon systems (Koon et al., 1999). On similar lines, Koon et al. (2000a) conceptualized the relation between the unstable manifolds of periodic orbits in the Sun-Earth system and stable manifolds of the periodic orbits in the Earth-Moon system. Martin and Ross (2001) found that the energy levels of the Sun-Earth and Earth-Moon Lagrangian points are nearly the same (the difference is about 50 m/s) and based on this, formed the concept of low energy paths leading ultimately to interplanetary superhighways. All of their work on dynamical systems theory was summarized in a textbook

(Koon et al., 2000b). A similar but broader consolidation effort resulted in a series of works by Gomez et al. (Gomez et al., 2001a-c) and Canalias et al. (Canalias et al., 2004, Canalias and Masdemont, 2006).

Howell (2001) consolidated the attempts to construct halo and quasi-halo orbits in the CRTBP, starting with the history of Poincare and extending through the applications of dynamical systems theory. Folta and Beckman (2002) reviewed the numerical and dynamical design techniques used by NASA for Lagrangian point missions. McCaine (2004) used optimization techniques from a MATLAB based optimization software named DIDO and generated halo orbits. Farquhar et al. (2004) reinstated the usability of orbits around Lagrangian points for space exploration and proposed an ambitious 35-day servicing mission to an orbit around Sun-Earth L_2 .

Rausch (2005) generated halo orbits, Lissajous orbits in the CRTBP and transitioned them to a higher fidelity SEM ephemeris model, where the gravitational effects of Sun, Earth and Moon on the spacecraft are modeled. Although the focus of his work was on transfer trajectories, Rausch demonstrated the transition of baseline halo orbits in CRTBP to quasi-halo orbits in the ephemeris model. Kolenen et al. (2007) generated quasi-halo orbits based on a Newton iteration scheme built over the Poincare method. Mondelo et al. (2007) parameterized the invariant tori around the Earth-Moon Lagrangian points and generated halo and Lissajous orbits based on a two-parameter scheme, wherein an orbit can be uniquely specified.

Extending the concepts of periodicity of orbits formulated by Moulton (1920) and Broucke (1969), Campagnola et al. (2008) proposed the condition for periodicity of orbits in the 3D ERTBP. They used the fundamental symmetry of the orbits about the $x - z$ plane (denoted as Eq. (1.1) and Eq. (1.2) below) and formed the periodicity condition Eq. (1.3).

$$S1 : (k\pi + f, x, y, z, \dot{x}, \dot{y}, \dot{z}) \rightarrow (k\pi - f, x, -y, -z, -\dot{x}, \dot{y}, \dot{z}) \quad (1.1)$$

$$S2 : (k\pi + f, x, y, z, \dot{x}, \dot{y}, \dot{z}) \rightarrow (k\pi - f, x, -y, z, -\dot{x}, \dot{y}, -\dot{z}) \quad (1.2)$$

Periodicity conditions:

“For an orbit to be periodic in the ERTBP, it is sufficient that it has two perpendicular crossing with either the normal plane (from S1) or the syzygy axis (from S2), or both of them, when the primaries are at an apse”.

$$T_E = MT_c = 2N\pi \quad (1.3)$$

where T_E is the period of the orbit in ERTBP, T_c is the period of the orbit in CRTBP, N is the number of primary revolutions around the barycentre and M is number of third body revolutions around the Lagrangian point.

Olikara and Howell computed quasi-periodic invariant tori by formulating the problem in the form of an invariant partial differential equation and used pseudo arc-length continuation technique to generate families of tori (Olikara and Howell, 2010; Olikara, 2010). Alessi et al. combined the concepts of multiple shooting technique and an optimization technique to ease the transition of baseline CRTBP solutions into an ephemeris model (Alessi, 2010; Alessi et al., 2012). Zhang et al. (2011) took a different approach to the mathematical formulation of the halo orbit and used the concept of flow map, which relates the state of a spacecraft at a time to its initial state. On a slightly different dynamical problem, Mahajan and Pernicka (2012) designed halo orbits near very small primaries like asteroids, comets etc.

In 2014, Hao Peng commenced research about some perfectly periodic resonant orbits in the ERTBP framework (Peng and Xu, 2014a; Peng and Xu, 2017). Peng utilized the periodicity conditions proposed by Campagnola et al. (2008) and constructed perfectly periodic, multi revolution halo orbits in the ERTBP framework. These orbits were obtained using numerical continuation on eccentricity, with the conditions of circular halo orbit as the initial guess. They called these orbits as multi-revolution elliptic halo orbits. Peng used the multiple shooting method and posed the problem as an optimization problem. Multiple segments were used to avoid problems associated with numerically integrating the equations of motion for the long term.

Folta et al. (2015) proposed the concept of a dynamic and interactive catalog of orbit and transfer solutions in the Earth-Moon system. The fundamental idea is to arrive at faster mission design solutions and to facilitate intuitive tradeoffs. The proposed concept architecture

could incorporate new families of orbits as and when they are identified and provides provisions for transforming the baseline CRTBP solutions into ephemeris models. This concept was later extended to the Sun-Earth system and Bosanac et al. (2017) generated the mission design for a proposed NASA mission to Sun-Earth L_2 (the mission was initially named as WFIRST, but later changed to Roman telescope).

In 2016, Nath and Ramanan developed a methodology which produces precise halo orbit design in a single level scheme based on an evolutionary technique known as Differential Evolution (Nath and Ramanan, 2016). In this methodology, there is no need for a close initial guess because the process works from search bounds for the unknowns. The required out-of-plane amplitude is achieved by defining it as a part of the objective function and therefore, it's a single level scheme.

Vineet et al. (2018) modeled the solar radiation pressure and the oblateness of the smaller primary in CRTBP and designed halo orbits for different dynamical systems. They found that the contribution of solar radiation pressure leads to changes in the amplitude, period and stability indices of the halo orbit. Similar conclusions were drawn by Elbaz et al. (2021) also, although the study was restricted to the Sun-Earth system. Baresi et al. (2018) compared a number of numerical computation techniques for the design of quasi-periodic tori and concluded that the approach by Gomez and Mondelo (2001) is the most accurate method. Ferrari and Lavagna (2018) generated resonant orbits in the Earth-Moon and Sun-Earth systems and classified them based on the number of revolutions. On a similar but larger research effort, Antoniodou and Libert (2018) generated multiple resonant orbits and studied their stability in detail. However, neither these research efforts looked into the viability of using the designed orbits for a scientific mission (like ISEE-3) nor extended the baseline orbits into ephemeris models.

Wu et al. (2019) generated a halo orbit ($Az \sim 280,000$ km) in the Sun-Earth CRTBP framework and extended the orbit to the ephemeris model. They used a generic algorithm based process to formulate the halo orbit design and report that a five period orbit is generated. With a one-time maneuver of about 8.77 m/s, the orbit could be extended up to 10 periods (~five years).

Lujan and Scheeres (2022) generated a number of quasi-halo orbits in the Earth-Moon system and systematically studied their stability aspects. Paez and Guzzo (2022) derived an analytical method for constructing halo orbits in the ERTBP using a nonlinear Floquet-Birkhoff normal form.

1.2.3 Literature on Transfer Trajectory Design

Transfer trajectory in Lagrangian point missions refers to the part of the space craft's trajectory from an Earth parking orbit to the target orbit around the Lagrangian point. Typically, the spacecraft is launched from a ground station on the Earth to an Earth parking orbit (EPO), which the launch vehicle is capable of launching to. From the Earth parking orbit, the spacecraft is inserted into the 'transfer trajectory' to the target orbit using its propulsion system. The design of transfer trajectory has been attempted in two broad approaches in the literature (Folta and Beckman, 2002). In the first approach, the initial conditions of the transfer trajectory near the Earth are determined through forward propagation in time using some numerical search methods. In the second and most popular approach, the analysis starts from the insertion point on the target orbit and the initial conditions near the Earth are determined through backward propagation in time from the insertion point, such that the requirement on Closest Approach Altitude (CAA) to the Earth is satisfied. In the second approach, the methodology can either be based on numerical search or utilization of dynamical systems theory to find a suitable manifold originating from the target orbit.

In 1973, D'Amario presented the first analysis on transfer trajectory between a parking orbit and a Lagrangian point (D'Amario, 1973). D'Amario used analytical and numerical approaches with primer vector theory, to establish an approximate method for quickly calculating transfer trajectories from the Earth and Moon to the Earth-Moon Lagrangian point L_2 (D'Amario and Edelbaum, 1974). D'Amario used his multiconic technique to determine families of locally optimum two- and three-impulse transfers. After this period, the ISEE-3 mission was designed (Farquhar et al., 1977). The ISEE-3 transfer trajectory intersected the halo orbit at the point where the ecliptic plane crossed on the near side of the Earth. The transfer was considered "slow" since the Time of Flight (TOF) was around 102 days. The reason this particular transfer trajectory was chosen over a "fast" transfer trajectory (flight time around 35 days) to the halo orbit is because numerical simulations showed that it is less expensive in terms of velocity impulse.

Farquhar (1980) performed a post-flight mission study of ISEE-3 flight data in 1980. Rodriguez and Hechler (1989) generated transfer trajectory design by choosing a location on the halo orbit, adding a velocity impulse, and then numerically propagating backwards to reach the Earth parking orbit. In this investigation, gradient-based optimization techniques such as recursive quadratic programming and the conjugate gradient method were employed for the numerical search. Rodriguez and Hechler (1989) also discussed the well-known difficulties of optimization using gradient-based methods. Later, Hiday (1992) investigated the impulsive transfers between parking orbits and Lagrangian Point Trajectories to L_1 in the Sun Earth system by applying primer vector theory to the problem.

Around this time, Gomez et al. (1991) started investigating the Moon's influence on the transfer trajectory to an orbit around Sun-Earth Lagrangian point, culminating in a key development of use of nonlinear dynamical systems theory for transfer trajectory design (Gomez et. al, 1993). This methodology proved to provide a thorough understanding of the transfer scenarios. The stable manifolds from the target halo orbit that approach the Earth on backward numerical integration are identified to be possible transfer trajectories. Finding the appropriate manifold that satisfies the mission criteria and putting the spacecraft into this manifold became the solution to the problem of transfer to halo orbits. Although very promising for the design of transfer trajectories to higher amplitude target halo orbits, an operational difficulty was identified in choosing the right manifold for the transfer to smaller amplitude target halo orbits, like the one chosen for ISEE-3 mission ($Az = 120,000$ km). The minimum of the closest approach distances to the Earth of all the stable manifolds originating from such smaller amplitude halo orbits is around 3000 km; the transfer to such large altitudes using then existing launch vehicles proved to be nearly impossible. Therefore, it became apparent that using dynamical systems theory alone is insufficient if a mission has to be planned from a low Earth altitude to a low amplitude halo orbit. In the approach of dynamic system theory, the direction of backward propagation is determined by computing the eigenvalues and eigenvectors of a monodromy matrix. Howell et al. (1994) applied the concept of differential correction on the design generated using the dynamical systems theory. Numerical propagation of the state transition matrix, involving 42 differential equations is carried out. By investigating a very large number of points on the target halo orbit at small intervals and using a DC-based scheme for each of the points, the position on the target orbit that results in the lowest velocity impulse is found. It is clear that the search process is discrete in nature and that the demand for preciseness needs the number of exploratory points to be very high. A number of researchers

later attempted the problem on similar lines (Barden et al., 1997; Wilson, 1999; Wilson and Howell, 1999; Folta et al., 2001; Rausch; 2005).

Mains (1993) conducted a comprehensive numerical investigation and was interested in developing approximations that may be used in future automated transfer trajectory determination techniques. Mains investigated transfers from several parking orbits with varying durations of flight, including one comparable to that of the ISEE-3 mission. Mains' research was further broadened by Barden using a mix of numerical approaches and dynamical systems theory (Barden, 1994; Howell et al., 1994; Sharer, 1996). Wilson, Barden, and Howell developed design approaches for determining the Genesis trajectory in the mid-1990s (Wilson, 1998; Wilson and Howell, 1998). Anderson, Guzmán, and Howell proposed an efficient approach to study transfers from Earth to Lissajous trajectories in the ephemeris model (Anderson, 2001; Howell et al., 2001). Farquhar (2001) summarized the key mission objectives and the transfer trajectory design aspects of the ISEE-3 mission in a detailed manner.

Rausch (2005) conducted a comprehensive numerical investigation of transfer trajectories to orbits around Lagrangian points in both Sun-Earth and Earth-Moon systems. Rausch employed differential correction upon the dynamical systems theory-based design to construct transfer trajectories and also generated two-impulse direct transfers. Rausch also transitioned these baseline trajectories into an ephemeris model. The methodology based on differential correction necessitates the division of transfer trajectory into multiple segments and requires very good initial guesses at all patch points. Further, Rausch (2005) also mentions that the shape of the target halo orbit needs to be altered when realizing transfers to higher amplitude halo orbits in the Earth-Moon system. On a slightly different modeling aspect, Correa et al. (2007) compared the transfer cost to a halo orbit in the Earth-Moon system using two different dynamical models; the first one being the classical restricted three body problem framework and the second, a quasi-bicircular problem involving the Sun also. They concluded that the total velocity impulse required in the quasi-bicircular problem framework is less compared to that in the restricted three body problem framework. Correa et al. essentially modeled the influence of Sun in the transfer cost. A similar approach was followed later by Rosales et al. (2021), where the halo orbits were identified to be quasi-periodic and the manifolds originating from these orbits were found to interact with the Earth. Although using a different dynamical system (an ephemeris model), the findings of this investigation also found similar results.

Hou et al. (2007) constructed transfer trajectory designs to the L_3 Lagrangian point in the Sun-Earth system using the invariant manifolds about the other two collinear Lagrangian points. Gordon (2008) examined the use of Lunar gravity to aid the insertion of spacecraft into the manifold of Earth-Moon Lagrangian point orbits. Gordon initially considered the transfer to the planar Lyapunov orbit and extended the analysis to halo orbits and found that the choice of Lunar altitude at which the insertion maneuver takes place has a profound influence on the ΔV requirement.

In 2008, Parker and Born conducted a comprehensive numerical determination of transfer trajectories to halo orbits around L_1 and L_2 Lagrangian points in the Earth-Moon system (Parker and Born, 2008). In the Earth-Moon system, unlike in the Sun-Earth system, the manifolds do not pass close to the Earth, as the Earth is the larger primary. So, the transfer trajectory is typically divided into two segments: (i) bridge segment and (ii) manifold segment (Parker and Born, 2008). In this approach, two large maneuvers are performed to realize the transfer to a halo orbit. The first maneuver moves the spacecraft from an Earth parking orbit (EPO) into the bridge segment which intersects the manifolds from the Moon. The second maneuver is performed at the manifold injection point, which is the intersection of bridge segment and the manifold segment and this maneuver injects the spacecraft into the manifold that takes the space vehicle to the desired halo orbit asymptotically. A third, small maneuver is required to precisely insert the spacecraft into the required halo orbit. Parker and Born classified the transfers into short and long transfers requiring less than 5 days and around 3 weeks respectively. It was found that the short transfers need significantly larger ΔV compared to long transfers.

Alessi et al. modeled the transfer trajectory to Lissajous orbits around Lagrangian points in the Earth-Moon system by including two maneuvers and refined the initial approximation in CRTBP to an ephemeris model by modeling as an optimization problem (Alessi et al., 2009; Alessi et al., 2010). Li and Zheng (2010 a, b) used Lunar flyby and the perturbed stable manifold to study indirect transfer to the Earth-Moon L_1 Lagrangian point and found that compared to direct transfer, indirect transfer saves around 420 m/s of ΔV . The corresponding flight time was found to be 20 days longer. A similar conclusion was also drawn by Folta et al. (2013). In addition to two impulse transfers and transfers utilizing Lunar flybys, Folta et al. (2013) also constructed round trip Earth - Earth Moon L_1/L_2 - Earth trajectories.

Renk et al. (2010) explored the use of Lunar flybys and trajectories around different Lagrangian points in the Earth-Moon system to reduce the ΔV compared to direct transfer options. In both cases, the ΔV requirement was lesser than direct transfer at the expense of increase in flight duration. They also concluded that the variation of ΔV requirement over time for transfer to smaller amplitude Lissajous orbit ($Az \sim 2000$ km), is smaller compared to large amplitude orbits. Zanzottera et al. (2011) combined two CRTBP physical systems and generated transfer trajectories to halo orbits around Lagrangian point L_2 in the Earth-Moon system. First, the Sun-Earth CRTBP framework is utilized to design the transfer trajectory from the Earth as is done in WSB transfers; next the ballistic capture into the halo orbit is modeled using the Earth-Moon CRTBP framework. Using this combined model, they optimized the insertion point into the manifold of the target halo orbit and found that a single impulse maneuver demands lowest in terms of ΔV .

Davis et al. (2013) constructed transfers to halo orbits around Lagrangian point L_3 in the Earth-Moon system, using a concept called pseudo-manifold. The stable pseudo-manifolds are generated similar to the stable manifolds, but with three orders of magnitude larger perturbation values and the perturbation is applied only to the velocity components of the spacecraft's state vector. The transfer trajectories from an LEO parking orbit to the stable manifold of the target halo orbit using this approach has a minimum flight duration of about 46 days, whereas direct transfer can be constructed with flight duration around 5 days for similar ΔV . This is because all the transfer trajectories involved Lunar flybys. Folta et al. (2013) also performed similar analysis and drew similar conclusions and constructed round trips from Earth parking orbits (Earth - Earth Moon L_1/L_2 - Earth). Bihan et al. (2014) conducted a survey of the transfer trajectory strategies to halo orbits around the Earth-Moon L_2 and proposed optimal configuration based on the scientific requirements. For example, a series of manned missions culminating in a deep space habitat requires transfer duration less than 20 days and therefore, direct transfers are found to be most suitable costing around 3.45 km/s. For the transport of cargo to such stations, which can afford longer flight durations around 100 days, the weak stability boundary transfers are identified to be optimal.

Nath and Ramanan (2016) generated two-impulse transfer trajectories to the halo orbit around the L_1 point in the Sun-Earth system using a single step scheme based on differential evolution. The location of insertion onto the halo orbit and the components of velocity impulse

required from the EPO are treated as unknowns and determined using the DE based scheme. This formulation of the problem identifies the precise halo orbit insertion point whereas the DC based scheme needs to explore a large number of locations and eventually selects the location from a pre-defined discrete set. Further, the need for a close initial guess is eliminated because the DE based scheme can work with search bounds for unknown parameters and there is flexibility to explore different mission scenarios. Nath and Ramanan report three domains with flight durations with minimal cost solutions. Additionally, it has been noted that even with longer flight times, some regions on the halo orbit could only be reached with very high insertion impulses from low CAAs.

Zeng et al. (2017) incorporated mission constraints in the LEO parking orbit into the design of transfer trajectories to Sun-Earth L_1 and found that the parameters inclination and RAAN of the parking orbit together with the Az amplitude and insertion point on the halo orbit causes the total variation in requirement of ΔV from a few m/s to hundreds of m/s. Conte et al. generated transfer trajectories around halo orbits around the L_2 point in the Earth-Moon system utilizing an optimization method known as fireworks optimization and generated both direct transfers and manifold transfers (Conte et al., 2018; He et al., 2020). Wu et al. (2019) constructed transfers to a halo orbit around Sun-Earth L_1 and designed the mid-course maneuver to account for error due to launch deviation and perturbation. Also, the launch window analysis was performed taking into consideration the inclination of the EPO. Mezentsev and Aksenov (2021) systematically studied the transfers to the Sun-Earth L_1 halo orbits by varying the Az amplitude of target orbits and altitude of the EPO. They identified a number of transfer trajectories reaching the desired CAA in the first close approach near the Earth and several subsequent approaches. They conclude that transfers to large amplitude halo orbits ($Az \sim 350,000$ to $1,000,000$ km) have the shortest transfer duration of about 25 days. The relation between Az amplitude of target orbit and transfer time is found to be nonlinear and complex. Similar inference can be drawn from the findings of Nath and Ramanan (2016) also. Ren et al. (2022) constructed direct transfers to the halo orbits around Earth-Moon L_4 by utilizing primer vector theory. They also generated indirect transfers utilizing lunar gravity assist, modeled using optimal control theory.

Constructing transfers to an orbit around the Lagrangian points using the ERTBP framework is a relatively unexplored research area. Campagnola and Martin Lo (2007) constructed transfer trajectory design to Lissajous orbits around Sun-Mercury Lagrangian

point, similar to that used for the BepiColombo mission. They concluded that even though the BepiColombo mission was designed without utilizing the dynamical systems theory, the eventual trajectory was part of the stable manifold of the target quasi-periodic orbit.

Peng and Xu conducted research efforts targeting the resonant orbits in the Earth-Moon system and Sun-Mercury system (Peng and Xu, 2015 a, b). Similar to the CRTBP counterpart, transfers to multi-revolution elliptic halo orbits were constructed using the dynamical systems theory utilizing the three-dimensional stable manifolds and the bridge concept. But in contrast to the structure of the manifold in the CRTBP framework, the manifold generated from the periodic orbit in the ERTBP framework has two stable directions, designated as main and redundant stable directions. First, they generated transfers to the perigee of the stable manifold as the manifold insertion point and then optimized the insertion point (Peng and Xu, 2015a).

Specifically, there is no study available in the literature to the best of knowledge of the author that deals with entire aspects of preliminary mission design (design of orbit, transfer trajectory and transition to realistic ephemeris models) completely conducted using the Elliptic Restricted Three Body Problem Framework.

1.3 Motivation of the Research

Lagrangian point missions have the potential to enhance the understanding of the universe and to accelerate the exploration of space. Innovative and technologically demanding missions such as the James Webb Telescope are being conceptualized to satisfy the needs and quest for innovation of modern humanity. However, the design of orbits around the Lagrangian points and transfers to them from Earth under realistic frameworks are challenging tasks due to the intricate multi-body dynamics of the problem. The inherent nonlinear nature of the N -body (multi-body) gravity problem prevents the formulation of analytical solutions and hence lends numerical means as the only viable solution strategy. It is well known that the numerical solution process requires a good initial guess.

The CRTBP framework has been conventionally used to generate the approximate guess to initiate the actual mission design involving high fidelity ephemeris models. However, the planets in our solar system exhibit a wide range of average eccentricities in their orbits

around the Sun varying from ~ 0.0067 (Venus) to ~ 0.2056 (Mercury). Therefore, it is natural to investigate the feasibility of using the ERTBP framework to generate the initial guess and quantify the advantages (if any) over the initial guess from the CRTBP framework. The fact that the orbits generated in the ERTBP framework (reported in the existing literature) are innately multi-revolution in nature, resembling the actual orbits generated in the ephemeris models, further strengthens the above mentioned intuition.

Although the use of ERTBP framework to generate orbits around Lagrangian points is not uncommon in literature, the following points are worth noting.

1. There are few studies which attempt the complete preliminary mission design using ERTBP and extend the results to high fidelity ephemeris models. In other words, the focus of existing research is mostly on generating the orbit and not the transfer trajectory from Earth. Even in the area of generation of the quasi periodic halo orbits, there is no or very little research effort in the Sun-Earth system.
2. The existing techniques for the design of orbits (in both CRTBP and ERTBP frameworks) are largely based on differential correction techniques and require a very good initial guess. The sensitivity of the DC based solution to the initial guess, the inability to achieve the orbit's desired out of plane amplitude in a single level scheme and the need for modification of the target orbit while constructing transfer trajectories (using patch points) are well reported issues in the literature.
3. The use of widely popular manifold theory for the construction of transfer trajectories necessitates tweaking of the methodology to suit different dynamical systems. This happens because the process being dependent on the natural flow near the primaries, the methodology for designing transfer trajectories from Earth for a Sun-Earth Lagrangian point mission (where the Earth is the smaller primary) and that for an Earth-Moon Lagrangian point mission (where the Earth is the larger primary) are different in nature. The latter requires an additional segment known as the bridge segment which connects the Earth parking orbit and the stable manifolds from the target orbit.
4. The transfer trajectory design methodologies existing in the literature rely heavily on the characteristics of the target orbit. There are two reasons for this. The first reason is the use of dynamical systems theory where the transfer trajectory is part of the manifolds emanating from the target orbit. The second reason is the use of a differential correction based process which demands patching of the various points and *may* result in tweaking the characteristics of the target orbit. For example, even though the target

orbit is a halo orbit at the beginning of the process, the orbit may have to be modified into a quasi-halo orbit by the patching process.

To overcome the insufficiencies and shortcomings of the existing techniques and methodologies, the current research focuses on generating complete mission design using the CRTBP/ERTBP frameworks and extending/generating the results in high fidelity ephemeris models. The next section elaborates how the current work addresses each of the points (1-4) mentioned in this section.

1.4 Objectives of the Research

The aims of the current research are to generate numerical design techniques that serve the following objectives:

1. **Explore the suitability of the complete preliminary Lagrangian point mission design under the ERTBP framework:** For the scientific missions to the Lagrangian points in the Sun-Earth and Earth-Moon systems, generate the preliminary designs for both the orbit and transfer trajectory from Earth under the ERTBP framework and generate/extend these to the ephemeris models. The pros and cons of the preliminary reference designs in generating ephemeris design and potential advantages (or disadvantages) compared to the preliminary design using the CRTBP framework are to be quantified.
2. **Investigate the utility of differential evolution technique as an alternative to differential correction:** Differential evolution is an evolutionary optimization technique widely used for solving numerical problems in aerospace engineering. This technique offers a wide variety of features (such as no need for a close initial guess, flexibility of incorporating multiple objective functions etc.) which renders it suitable for the design of Lagrangian point missions. The advantages and disadvantages of using differential evolution in the design methodologies for generation of orbit and transfer trajectory are to be analyzed.
3. **Formulate a design methodology independent of the characteristics of the dynamical system:** The design methodology should be versatile enough to generate

Lagrangian point missions in any dynamical system such as Sun-Earth, Earth-Moon, Sun-Mars or Earth-Asteroid restricted three body systems.

4. **Formulation of a transfer trajectory design methodology independent of target orbit characteristics:** The transfer trajectory design should be versatile enough to construct transfers to any kind of target orbit, be it periodic halo orbit/quasi-halo orbit/Lissajous orbit etc.

1.5 Research Summary

With the goal of achieving the aforementioned objectives, the current research is initiated by implementing the existing techniques for Lagrangian point preliminary mission design to understand the advantages, drawbacks and scope for improvement. The CRTBP framework and differential correction methodology are first used to generate halo orbits and construct transfer trajectories in the Sun-Earth and Earth-Moon systems. As is well known, it is found that the differential correction-based design requires a very good initial guess (for the design of halo orbits, this was provided by the third order analytical approximation (Richardson, 1980b)). Such is the sensitivity of the DC technique that even when the initial conditions for the unknowns are perturbed in the fourth decimal place (in normalized form), the DC based process fails to converge.

In the next step, the design of halo orbit and transfer trajectory in CRTBP are generated using a differential evolution-based methodology (as outlined in Nath and Ramanan, 2016). The numerical technique to find numerical designs of orbit and transfer trajectory is tested, validated and the DE parameters are tuned for the reduction of computational time.

As the first step towards generating the orbits in the ERTBP framework, the multi-revolution (MR) halo orbits around the Lagrangian point L_1 in the Sun-Earth system are generated using the DE technique. The MR halo orbits are perfectly periodic halo orbits in the ERTBP framework. The initial state of the orbit at the first $x - z$ plane crossing is treated as unknown and is determined using a DE based methodology. The proposed design methodology using DE technique requires neither a close initial guess nor continuation methods to generate orbit for a desired eccentricity of the smaller primary around the larger primary (both are quintessential for the existing methods). Further, the whole trajectory (MR halo orbit) is treated as a single segment in the proposed design methodology, whereas the existing methodologies divide the orbit into a number of segments to avoid problems associated with long term

propagation of equations of motion. Unlike in the differential correction-based method, the proposed methodology generates both Lyapunov and halo orbit MR solutions for the same period. Further, it could capture multiple solutions for each of the halo or Lyapunov MR orbits. For multiple options of MR halo orbits with the same period, it is found that the variation of radial distance from Earth and the variation of velocity in orbit increases as the number of third body revolutions increases. *However, the amplitudes of the generated MR halo orbits in the Sun-Earth system are large compared to the halo orbits used for scientific missions such as the ISEE-3 mission.* Such large amplitudes of MR halo orbits violate the communication system constraint on the maximum Sun-Earth-Vehicle angle possible in the orbit. The commensurability constraint used in the design methodology, which is an expression relating the period of MR halo orbit with the period of the primaries, leads to large amplitude orbits.

As the next logical step, the design of quasi-halo orbits of desirable amplitudes, independent of the commensurability constraint, is generated under the ERTBP framework. The focus is shifted to the quasi-halo orbits as it is realized that no (theoretical) perfectly periodic halo orbit exists in the Sun-Earth system which meet the requirements of a scientific mission similar to ISEE-3. The quasi-halo orbit and the CRTBP halo orbit are used as reference designs and the quasi-halo orbit design is obtained in the higher fidelity ephemeris model. The design methodology based on DE generates a ten-revolution quasi-halo orbit (previously reported is five) without any maneuvers and has demonstrated that generation of orbits for a wide range of Az amplitudes is possible. Both the CRTBP and ERTBP reference designs generate the ephemeris design and there is no noticeable advantage of considering ERTBP reference design. Transfers under three frameworks (CRTBP, ERTBP and ephemeris) are constructed and it is found that the least cost is incurred when the transfer is generated under the ephemeris model.

Motivated by the success of the proposed methodology for the design of MR orbits in the Sun-Earth system, the design of MR orbits in the Earth-Moon system is attempted. A number of MR halo orbits around the Earth-Moon Lagrangian point L_1 is generated and the methodology is found to be easily adaptable to other Lagrangian points as well. The average of Az amplitudes of individual revolutions of MR halo orbits are found to be nearly equal to that of corresponding halo orbits in CRTBP.

As the next step, the transfer trajectory design to the MR halo orbits in the Earth-Moon system is carried out. The proposed methodology using the DE technique designs the transfer trajectory in a single segment, unlike the existing techniques which divide the transfer trajectory into multiple segments. The direct transfer technique does not utilize the manifold

theory and hence, completely avoids the manifold segment. The location of insertion on to the MR halo orbit and the components of the insertion velocity from the single segment transfer trajectory into the MR halo orbit are treated as unknowns and obtained using differential evolution. The proposed technique is a unified approach to generate optimal transfer trajectory design to halo orbits under CRTBP framework and to MR halo orbits under ERTBP framework. The geometry of the transfer trajectory is found to be entirely different from the one obtained using the manifold approach. The trajectories are in the neighborhood of Earth for the most part of the flight duration whereas the transfer trajectory of the manifold approach is in the neighborhood of the Lagrangian point L_1 of Earth-Moon system. There is no significant variation in the HOI velocity impulse for different closest approach altitudes from the Earth and the optimal solutions indicate that there exist trajectories with lower cost and for significantly lower time of flight than those reported in the literature for similar problems.

In summary, through various research studies, the objectives of the research are met in the following terms:

1. Complete Lagrangian point preliminary design using the ERTBP framework is generated. For the mission design in the Sun-Earth system, it is substantively concluded that preliminary design using the ERTBP framework does not provide significant advantages over the CRTBP framework. This can be attributed to the small eccentricity of the orbit of Earth around the Sun ($e \sim 0.0167$).
2. The differential evolution technique is found to be very versatile in solving Lagrangian point mission design problems and avoids many complexities associated with the differential correction based technique. However, the DE based schemes are found to be computationally more intensive.
3. The proposed methodology based on differential evolution constructs transfer trajectory independent of the characteristics of the target and hence, preserves the fundamental nature as such (not changing the type of orbit from halo to quasi-halo etc.). The geometry of the transfer trajectory remains nearly the same even when generated in the ephemeris model.

1.6 Thesis Architecture

The current thesis has six chapters, which are outlined below.

- **Chapter 1 (Introduction and Literature Survey):** This chapter introduces the topic of the research. A survey of the available literature for the design of halo orbit and transfer trajectory to the halo orbit is consolidated. The limitations of the existing schemes, which motivated the current research, are discussed. The objectives of the research and a brief research summary are presented along with thesis architecture.
- **Chapter 2 (Multibody Dynamics and Frameworks):** This chapter presents an overview of the various dynamical models employed in this research. First the equations of motion governing the motion of a spacecraft in the actual N -body (multibody) dynamics is explained and modified to the higher fidelity force model used in this research (SEM ephemeris model). Then the CRTBP and ERTBP frameworks are explained together with the locations of Lagrangian points in each framework. The equations of motion and the coordinate transformations explained in this chapter are used in subsequent chapters.
- **Chapter 3 (Preliminary Mission Design in the CRTBP Framework):** This chapter gives an account of the preliminary Lagrangian point mission design in the CRTBP framework. Two steps of the mission design (halo orbit design and transfer trajectory design) are accomplished under the CRTBP framework. The problems associated with the design of halo orbit using the conventional DC-based technique are demonstrated and to overcome those issues, DE-based technique is employed. The transfer trajectory design to halo orbits is also generated using DE-based technique and does not involve the manifold theory.
- **Chapter 4 (Design of MR orbits in the Sun-Earth System under the ERTBP Framework):** This chapter gives an account of the design of Multi-Revolution (MR) orbits around the Lagrangian points in the Sun-Earth system under the ERTBP framework. The MR orbits in the Sun-Earth system are generated using a DE-based technique and reported for the first time in literature. The design and analysis of different MR orbits in the Sun-Earth system are presented.
- **Chapter 5 (Design of Quasi-Halo Orbits and Optimal Transfers in the Sun-Earth System):** This chapter gives an account of the design of quasi-halo orbits around the Lagrangian points and transfers to them in the Sun-Earth system using the ERTBP

framework and SEM ephemeris model. The generation of small amplitude quasi-halo orbits ($Az \sim 120,000$ km) is demonstrated and the quasi-halo orbits in SEM ephemeris model which doesn't need theoretical correction maneuvers for more than five years are generated. Optimal two impulse transfers to the quasi-halo orbit are generated, utilizing a DE-based technique.

- **Chapter 6 (Mission Design in Earth-Moon System under the ERTBP Framework):** This chapter gives an account of design of MR halo orbits and design of transfer trajectory to the MR orbits under the ERTBP framework in the Earth-Moon system. For the transfer trajectory design, it is demonstrated that the use of manifold theory and the associated bridge segment is not necessary. Optimal two impulse transfers to the MR halo orbit are generated, utilizing a DE-based technique.
- **Chapter 7 (Summary and Conclusions):** This chapter consolidates the summary of the research and lists the major contributions. The scope for future work is also presented.

Chapter 2: Multibody Dynamics and Frameworks

2.1 Introduction

Formulating trajectory computation strategies and interpreting the related results depend on fundamental assumptions which are dependent on the frameworks. So, the various dynamic models under different frameworks, used in this research, are described in detail in this chapter. They are a) SEM ephemeris model b) model under CRTBP framework (CRTBP model) and c) model under ERTBP framework (ERTBP model). The initial designs of the orbit around the Lagrangian point and the optimal transfer trajectory to the orbit are generated using the CRTBP and ERTBP models. These designs are refined using higher fidelity SEM ephemeris model and used to evaluate the closeness of the designs in the other two frameworks.

2.2 *N*-body Problem and the Special Case of Three Body Problem

In astrodynamics, an *N*-body (multi-body) problem refers to the gravitational interaction problem involving multiple celestial bodies. The gravitational interaction among multiple bodies can be modeled using the equations of motion. These equations describe the forces acting on each body and the resulting acceleration. The equations of motion for the *N*-body problem are derived from Newton's laws of motion and the law of universal gravitation.

The force acting on the *i*-th body is the sum of the gravitational forces due to all other bodies in the system. The direction of the force is along the line joining the centers of mass of the two bodies and the magnitude is determined by the masses and distance between the bodies.

The equation of motion for the *i*-th body in an inertial frame is:

$$\ddot{\vec{r}}_{qi} = -GM_q \left(\frac{\vec{r}_{qi}}{r_{qi}^3} \right) + G \sum_{\substack{j=1 \\ j \neq i, q}}^n m_j \left(\frac{\vec{r}_{ij}}{r_{ij}^3} - \frac{\vec{r}_{qj}}{r_{qj}^3} \right) \quad (2.1)$$

In Eq. (2.1) the suffixes q represents the central body, i represents the spacecraft and j represents the gravitational bodies other than the central body. Figure 2.1 represents the geometry of the special case of three body problem.

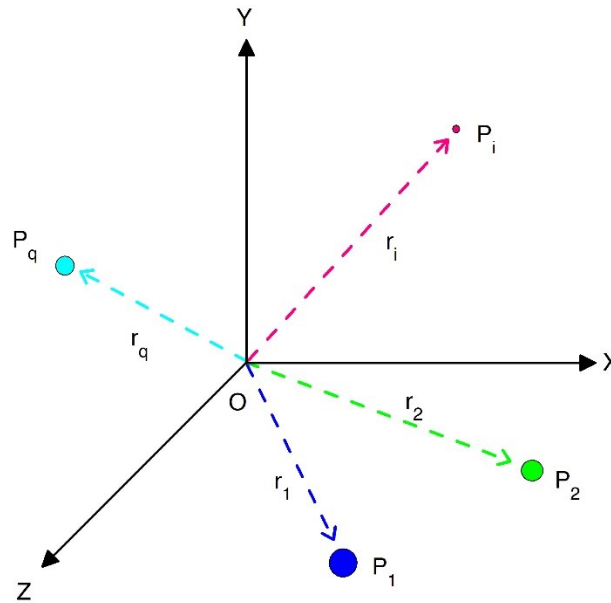


Figure 2.1. Geometry of general three body problem

2.2.1 SEM Ephemeris Model

The higher fidelity force model used in this research considers three major celestial bodies (the Sun, the Earth and the Moon) influencing the motion of a spacecraft near the Sun-Earth and Earth-Moon Lagrangian points and is designated as the SEM ephemeris model. The DE431 planetary ephemerides from NASA Jet Propulsion Laboratory (JPL) are used to generate the positions and velocities of the celestial bodies in the SEM ephemeris model.

2.3 Circular Restricted Three Body Problem (CRTBP) Framework

The circular restricted three body problem describes the motion of a small (third) body under the gravitational attraction of two large celestial bodies. The literature has various terminologies for designating the bodies under consideration. The convention followed in this research adopts the definitions given by Szebehely (1967). The two large bodies are termed primaries and are assumed to revolve around their common barycenter in circular orbits. The

third body is assumed to be so small that it cannot influence the motion of the primaries and moves in the plane of the motion of the primaries. A coordinate frame with origin at the barycentre of the primaries and which rotates with the rotation of primaries is the most useful to express the equations of motion in a concise and elegant form. The rotating coordinate frame is represented in Figure 2.2.

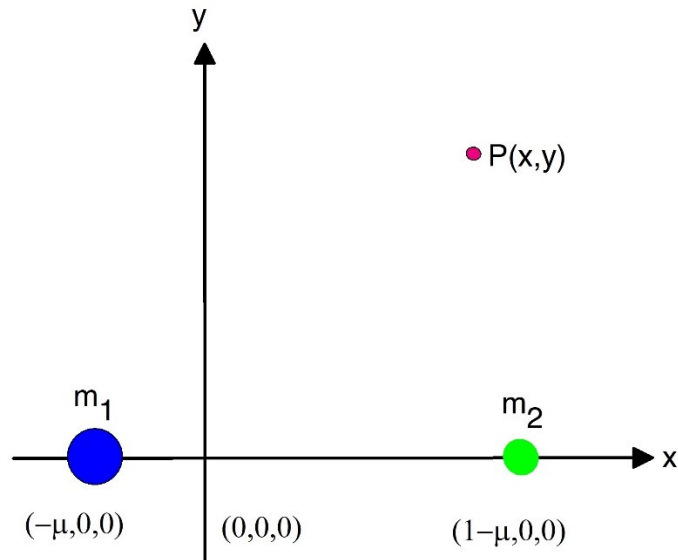


Figure 2.2. Rotating coordinate frame in CRTBP

The equations of motion of the third body in CRTBP framework are:

$$\begin{aligned}
 \ddot{x} &= x + 2\dot{y} - \frac{1-\mu}{r_1^3}(x+\mu) - \frac{\mu}{r_2^3}(x-(1-\mu)) \\
 \ddot{y} &= y - 2\dot{x} - \frac{1-\mu}{r_1^3}y - \frac{\mu}{r_2^3}y \\
 \ddot{z} &= -\frac{1-\mu}{r_1^3}z - \frac{\mu}{r_2^3}z
 \end{aligned} \tag{2.2}$$

where

$$\mu = \frac{m_2}{m_1 + m_2} \tag{2.3}$$

In Eq. (2.2), x , y and z represent the coordinates of the third body and r_1 and r_2 are the distances of the third body from the primaries in the rotating coordinate system.

Five (theoretical) equilibrium points known as Lagrangian points, exist in the CRTBP framework. At these points, the gravitational attractions of the primaries and the centrifugal force about the barycentre of primaries on the third body exactly balance, hence an equilibrium of forces exist. As an implication of the force equilibrium, a body (like a spacecraft) placed at these points with theoretical zero velocity stays there forever. Note that the Lagrangian points exist only in the restricted three body formulation and as seen from the rotating frame. In reality, there are regions of space around the theoretical Lagrangian points where the spacecraft will experience very little acceleration. Hence, station keeping is required to keep the spacecraft in the desired scientific orbit. There are five Lagrangian points for a restricted three body system. Three of them (L_1 , L_2 and L_3) lie on the straight line joining the primaries and two of them (L_4 and L_5) form an equilateral triangle with the primaries. However, only 2 of these five points (L_4 and L_5) are stable, whereas L_1 , L_2 , and L_3 are unstable. The spacecraft is placed into an orbit around a Lagrangian point rather than at the point because the eccentricity of Earth's orbit around the Sun and other perturbations prevent these points from truly being stationary with respect to Earth. Additionally, it is not advisable to position the spacecraft precisely on the Sun-Earth line since it would require a lot of fuel for station keeping and would not be acceptable for communication.

The calculation of location of Lagrangian points involves equating the acceleration terms to zero in the equations of motion (Eq. (2.2)). The location of Lagrangian points in the CRTBP framework exactly coincide with those under the ERTBP framework in the pulsating coordinate system and are described in Section 2.6.

2.4 Elliptic Restricted Three Body Problem (ERTBP) Framework

In the ERTBP framework, the primaries are assumed to revolve around their barycentre in Keplerian elliptical orbits. The distance between the primaries R is a function of true anomaly v (Figure 2.3) and is given by:

$$R(v) = \frac{a(1 - e^2)}{1 + e \cos(v)} \quad (2.4)$$

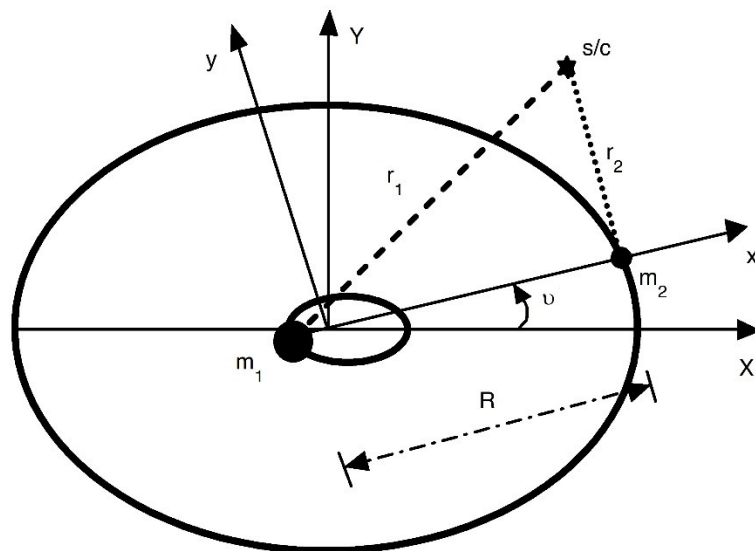


Figure 2.3. Coordinate frame in the ERTBP framework.

In Eq. (2.4), a and e are the semi-major axis and eccentricity of smaller primary around the other.

The equations of motion in ERTBP can be expressed using two different coordinate systems.

- A synodic coordinate frame, which moves with the same angular velocity of the primary system.
- A non-uniformly rotating and pulsating frame.

The first frame, the synodic frame has its origin at the barycenter of the primaries and the x axis along the line joining the primaries, similar to those in CRTBP. The z axis is coincident with inertial Z axis and the y axis forms the right handed system, as shown in Figure 2.3.

The normalized equations of motion in this frame are (Pernicka, 1990):

$$\begin{aligned}\ddot{x} - 2\dot{v}\dot{y} - \ddot{v}y - \dot{v}^2x &= -\frac{(1-\mu)(x+\mu R)}{r_1^3} - \frac{\mu[x-(1-\mu)R]}{r_2^3} \\ \ddot{y} + 2\dot{v}\dot{x} + \ddot{v}x - \dot{v}^2y &= -\frac{(1-\mu)y}{r_1^3} - \frac{\mu y}{r_2^3} \\ \ddot{z} &= -\frac{(1-\mu)z}{r_1^3} - \frac{\mu z}{r_2^3}\end{aligned}\tag{2.5}$$

where

$$R = 1 - e\cos E\tag{2.6}$$

$$\dot{v} = \frac{h}{R^2} = \frac{\sqrt{1-e^2}}{(1-e\cos E)^2}\tag{2.7}$$

$$\ddot{v} = -2e\sin E \frac{\sqrt{1-e^2}}{(1-e\cos E)^4}\tag{2.8}$$

$$\vec{r}_1 = (x + \mu R)\hat{x} + y\hat{y} + z\hat{z}\tag{2.9}$$

$$\vec{r}_2 = [x - (1 - \mu)R]\hat{x} + y\hat{y} + z\hat{z}\tag{2.10}$$

In these equations, ' μ ' represents the mass ratio (c.f. Eq. (2.3), h is the angular momentum and ' E ' is the eccentric anomaly. r_1 and r_2 are the distances of the third body from the larger and smaller primaries respectively.

The second frame, the non-uniformly rotating and pulsating rotating frame also has its origin at the barycenter of the primaries. Here, the system is instantaneously normalized by the distance between primaries. In this frame, the independent variable is transformed from time ' t ' to true anomaly ' v ' using the chain rule (Campagnola, Lo and Newton, 2008):

$$\frac{d}{dt} = \frac{dv}{dt} \frac{d}{dv} \quad (2.11)$$

$$\frac{d}{dt} = \frac{(1 + e \cos v)^2}{(1 - e^2)^{3/2}} \quad (2.12)$$

The normalized equations of motion of the third body in the ERTBP in the pulsating frame are (Szebehely, 1967):

$$\begin{aligned} \ddot{x} - 2\dot{y} &= \omega_x \\ \ddot{y} + 2\dot{x} &= \omega_y \end{aligned} \quad (2.13)$$

$$\ddot{z} = \omega_z$$

where

$$\omega(x, y, z, v) = (1 + e \cos v)^{-1} \tilde{\Omega}(x, y, z) \quad (2.14)$$

$$\tilde{\Omega}(x, y, z) = \frac{1}{2}(x^2 + y^2) + \frac{(1 - \mu)}{r_1} + \frac{\mu}{r_2} + \frac{\mu(1 - \mu)}{2} - \frac{1}{2}e \cos v z^2 \quad (2.15)$$

The epoch when primaries are at their periapsis is set as the reference epoch. It can be seen from the equations of motion that the ERTBP is a periodic system with period 2π .

2.5 Coordinate Transformations

The state vector of the spacecraft in the barycentric rotating frame is transformed to the geocentric inertial J2000 frame for the numerical integration of N -body equations of motion. The transformation is described below (Pavlak, 2010).

The locations of the combined Earth-Moon center and the Sun in the barycentric rotating frame are $(1 - \mu, 0, 0)$ and $(-\mu, 0, 0)$ respectively, where μ is the mass ratio:

$$\mu = \frac{mass_{Earth} + mass_{Moon}}{mass_{Sun} + mass_{Earth} + mass_{Moon}} \quad (2.16)$$

First, the position vector of the spacecraft in the barycentric rotating frame is transformed to a geocentric rotating frame by the following simple translation:

$$\vec{r}_{BC} = \begin{bmatrix} x_{BC} - (1 - \mu) \\ y_{BC} \\ z_{BC} \end{bmatrix} = \begin{bmatrix} x_{EC} \\ y_{EC} \\ z_{EC} \end{bmatrix} \quad (2.17)$$

where the subscripts BC and EC represents barycentric and Earth centric respectively.

An instantaneous rotating frame is defined in terms of the unit vectors relative to the inertial J2000 frame and utilises the ephemeris data from the JPL ephemerides (DE431 is used in this research). The unit vectors of the axes of the instantaneously rotating frame are given by:

$$\begin{aligned} \tilde{x} &= \frac{\vec{R}}{|\vec{R}|} \\ \tilde{z} &= \frac{\vec{R} \times \vec{V}}{|\vec{R} \times \vec{V}|} \\ \tilde{y} &= \tilde{z} \times \tilde{x} \end{aligned} \quad (2.18)$$

Here, \vec{R} and \vec{V} represent the position and velocity vectors of the Earth relative to the Sun at a given epoch in the inertial J2000 frame, as obtained from the ephemeris files. These unit vectors form the components of the transformation matrix for the transformation of the position vector of the spacecraft from the geocentric rotating frame to the geocentric inertial J2000 frame. The transformation is given by the following relation:

$$\begin{bmatrix} X_{EC} \\ Y_{EC} \\ Z_{EC} \end{bmatrix} = \begin{bmatrix} \tilde{x}_1 & \tilde{y}_1 & \tilde{z}_1 \\ \tilde{x}_2 & \tilde{y}_2 & \tilde{z}_2 \\ \tilde{x}_3 & \tilde{y}_3 & \tilde{z}_3 \end{bmatrix} \begin{bmatrix} x_{EC} \\ y_{EC} \\ z_{EC} \end{bmatrix} \quad (2.19)$$

where X_{EC} , Y_{EC} and Z_{EC} are the components of the position vector of the spacecraft in the geocentric inertial J2000 frame.

For the transformation of the velocity components, the following kinematic relation is used:

$$\frac{d\vec{r}_{EC}^I}{dt} = \frac{d\vec{r}_{EC}^R}{dt} + \omega^{I-R} \times \vec{r}_{EC} \quad (2.20)$$

$$\frac{d\vec{r}_{EC}^I}{dt} = (\dot{x}_{EC} - \dot{\theta}y_{EC})\tilde{x} + (\dot{y}_{EC} + \dot{\theta}x_{EC})\tilde{y} + (\dot{z}_{EC})\tilde{z} \quad (2.21)$$

Here the superscripts I and R denote the inertial and rotating frames, ω^{I-R} is the angular velocity vector given by $\omega^{I-R} = \dot{\theta}\tilde{z}$. Here, $\dot{\theta} = \frac{|\vec{R}X\vec{V}|}{|\vec{R}|^2}$ is instantaneous angular velocity. \dot{x}_{EC} , \dot{y}_{EC} and \dot{z}_{EC} are the velocity components of the spacecraft in the geocentric rotating frame. The transformation of the velocity components from the geocentric rotating frame to the geocentric inertial J2000 frame is given by:

$$\begin{bmatrix} \dot{X}_{EC} \\ \dot{Y}_{EC} \\ \dot{Z}_{EC} \end{bmatrix} = \begin{bmatrix} \dot{\theta}\tilde{y}_1 & -\dot{\theta}\tilde{x}_1 & 0 & \tilde{x}_1 & \tilde{y}_1 & \tilde{z}_1 \\ \dot{\theta}\tilde{y}_2 & -\dot{\theta}\tilde{x}_2 & 0 & \tilde{x}_2 & \tilde{y}_2 & \tilde{z}_2 \\ \dot{\theta}\tilde{y}_3 & -\dot{\theta}\tilde{x}_3 & 0 & \tilde{x}_3 & \tilde{y}_3 & \tilde{z}_3 \end{bmatrix} \begin{bmatrix} x_{EC} \\ y_{EC} \\ z_{EC} \\ \dot{x}_{EC} \\ \dot{y}_{EC} \\ \dot{z}_{EC} \end{bmatrix} \quad (2.22)$$

Combining the separate expressions for the transformations of position vector and velocity vector, the following expression using a 6×6 transformation matrix is used for the transformation of the state vector of the spacecraft from geocentric rotating frame to geocentric inertial J2000 frame:

$$\begin{bmatrix} X_{EC} \\ Y_{EC} \\ Z_{EC} \\ \dot{X}_{EC} \\ \dot{Y}_{EC} \\ \dot{Z}_{EC} \end{bmatrix} = \begin{bmatrix} \tilde{x}_1 & \tilde{y}_1 & \tilde{z}_1 & 0 & 0 & 0 \\ \tilde{x}_2 & \tilde{y}_2 & \tilde{z}_2 & 0 & 0 & 0 \\ \tilde{x}_3 & \tilde{y}_3 & \tilde{z}_3 & 0 & 0 & 0 \\ \dot{\theta}\tilde{y}_1 & -\dot{\theta}\tilde{x}_1 & 0 & \tilde{x}_1 & \tilde{y}_1 & \tilde{z}_1 \\ \dot{\theta}\tilde{y}_2 & -\dot{\theta}\tilde{x}_2 & 0 & \tilde{x}_2 & \tilde{y}_2 & \tilde{z}_2 \\ \dot{\theta}\tilde{y}_3 & -\dot{\theta}\tilde{x}_3 & 0 & \tilde{x}_3 & \tilde{y}_3 & \tilde{z}_3 \end{bmatrix} \begin{bmatrix} x_{EC} \\ y_{EC} \\ z_{EC} \\ \dot{x}_{EC} \\ \dot{y}_{EC} \\ \dot{z}_{EC} \end{bmatrix} \quad (2.23)$$

2.6 Locations of Lagrangian Points

The calculation of location of Lagrangian points involves equating the acceleration terms to zero in the equations of motion (Eq. 2.2 for the CRTBP framework, Eq. 2.5 and Eq. 2.13 for the ERTBP framework). In the CRBTP framework and non-uniformly rotating and pulsating coordinate frames in the ERTBP framework, the computation of abscissas of locations of collinear Lagrangian points involves the solution of the following quintic equations:

$$\xi^5 \mp (3 - \mu)\xi^4 + (3 - 2\mu)\xi^3 - \mu\xi^2 \pm 2\mu\xi - \mu = 0 \quad (2.24)$$

$$x_L = 1 - \mu \mp \xi \quad (2.25)$$

The equation for calculating the location of L_3 is:

$$\xi^5 + (2 + \mu)\xi^4 + (1 + 2\mu)\xi^3 - (1 - \mu)\xi^2 - 2(1 - \mu)\xi - (1 - \mu) = 0 \quad (2.26)$$

In the non-uniformly rotating and pulsating frame in the ERTBP framework, the system is normalised by the instantaneous varying distance (R) between the primaries. Hence, the solution of the quintic equation yields $\frac{\xi}{R}$, which can be used to compute the abscissa of the Lagrangian points (Eq. (2.25)). This makes the locations of Lagrangian points to coincide exactly with those in the CRTBP framework and are tabulated in Table 2.1

Table 2.1 Location of Lagrangian points in the non-uniformly rotating and pulsating frame in ERTBP and rotating frame in CRTBP

Lagrangian point	Sun-Earth system	Earth-Moon system
L_1	0.989985982342937, 0, 0	0.836889533921712, 0, 0
L_2	1.010075200022544, 0, 0	1.155702168107331, 0, 0
L_3	-1.0000005067407, 0, 0	-1.00207970230233, 0, 0
L_4	0.499996959576596, 0.8660254037844, 0	0.487844212727104, 0.8660254037844, 0
L_5	0.499996959576596, - 0.8660254037844, 0	0.487844212727104, - 0.8660254037844, 0

In the synodic frame, solution of Eq. (2.24) yields ξ , which can be directly used to compute the abscissa of the Lagrangian points. In this frame, the stationary equilibrium points in the same sense as in CRTBP do not exist, they oscillate about their average values. The variation of Lagrangian points with respect to the true anomaly of smaller primary around the larger primary are depicted in Figure 2.4 to Figure 2.9. The variation of locations of Sun-Earth Lagrangian points L_1 (c.f. Figure 2.4) and L_2 (c.f. Figure 2.6) from the corresponding locations in the CRTBP framework are about 25,400 km 27,000 km respectively. This amounts to about 0.018% of the Sun-Earth distance and this variation is less than that for the Earth-Moon system (about 0.86%), possibly due to a lower eccentricity of the system.

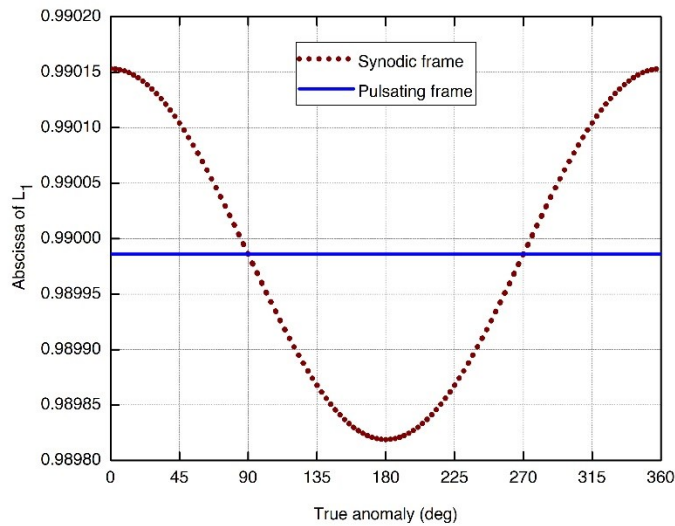


Figure 2.4. Variation of Sun-Earth L_1 with true anomaly of Earth around the Sun

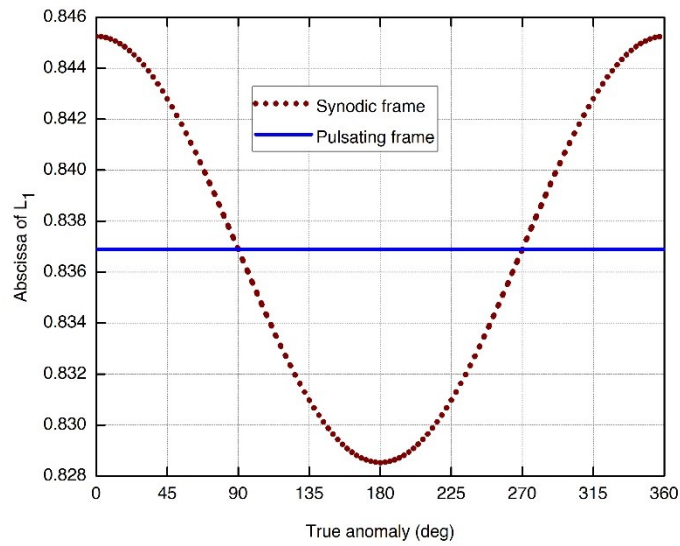


Figure 2.5. Variation of Earth-Moon L_1 with true anomaly of Moon around the Earth

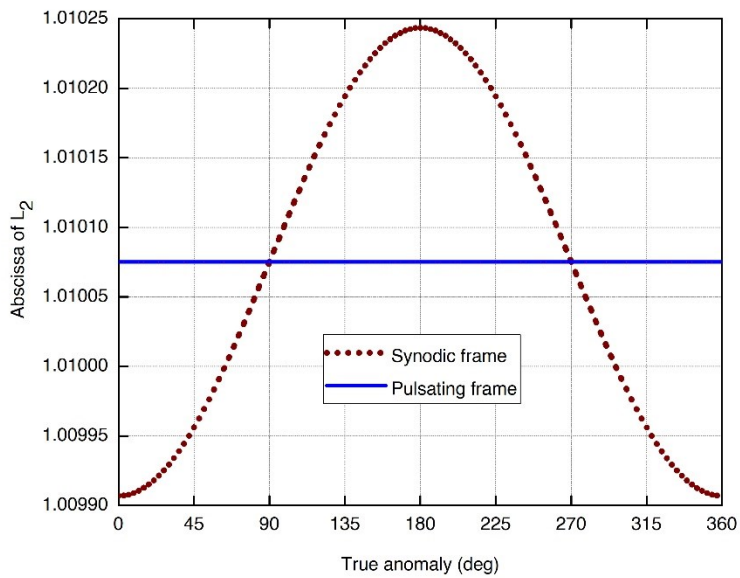


Figure 2.6. Variation of Sun-Earth L_2 with true anomaly of Earth around the Sun

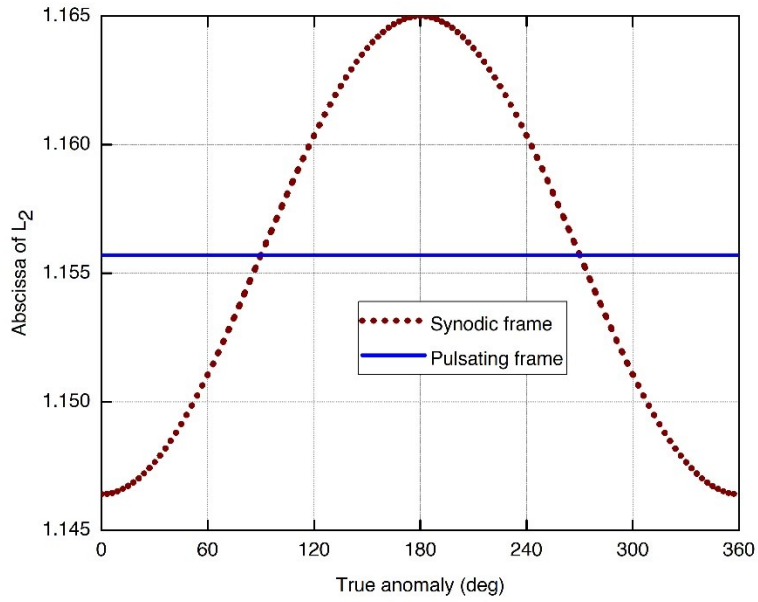


Figure 2.7. Variation of Earth-Moon L_2 with true anomaly of Moon around the Earth

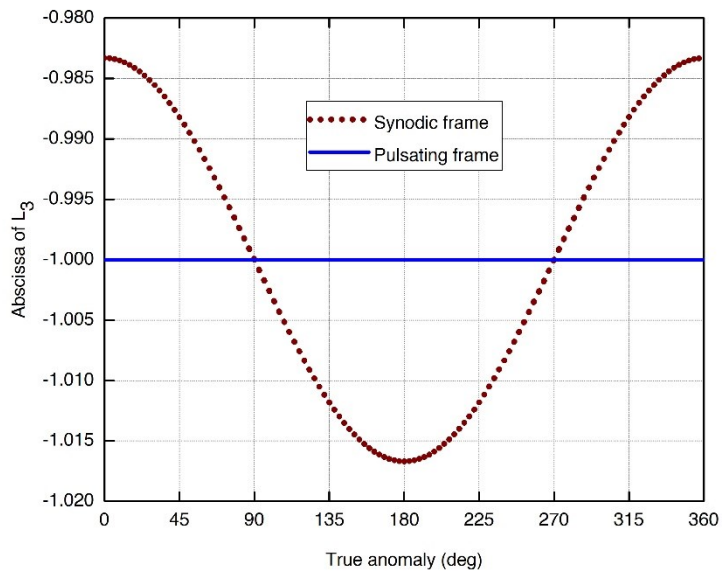


Figure 2.8. Variation of Sun-Earth L_3 with true anomaly of Earth around the Sun

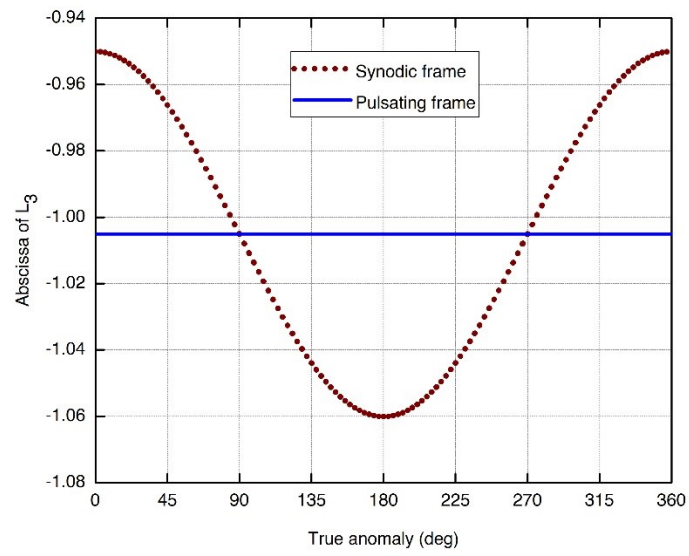


Figure 2.9. Variation of Earth-Moon L_3 with true anomaly of Moon around the Earth

Chapter 3: Preliminary Mission Design in the CRTBP Framework

Chapter Summary

This chapter gives an account of the preliminary Lagrangian point mission design in the CRTBP framework. Two steps of the mission design (halo orbit design and transfer trajectory design) are accomplished under the CRTBP framework. At first, the conventional differential correction (DC) technique is used for the design of halo orbits in the CRTBP framework. The problem formulation using the DC technique renders it highly sensitive to initial conditions and it is found that the differential correction procedure doesn't give the required out of plane amplitude in the first level. The design is refined in a second level numerical procedure such as numerical continuation methods to realize the desired out-of-plane magnitude. In order to overcome these problems, a single level scheme based on Differential Evolution (DE) is employed (Nath and Ramanan, 2016). The differential evolution based algorithm provides precise halo orbit design in a single level procedure and can work with search bounds (avoiding the need for a close initial guess). However, the computational time and effort for the basic differential evolution algorithm (Scheme 1) is found to be very large compared to the differential correction procedure. Two variants of differential evolution which differ in the mutation strategies are employed. It is observed that Scheme 2 performs better than all others in computational time and effort.

The transfer trajectory design to the halo orbit is constructed using a two-impulse technique employing differential evolution and doesn't make use of the manifold theory. The location of insertion into the halo orbit and the components of velocity impulse are treated as unknowns and determined using differential evolution. There is flexibility in terms of selection of closest approach altitude (passed as a part of objective function), unlike in the manifold theory based technique. Also, the method is found to be robust to generate transfers for any desired flight durations. The results are found to be in good agreement with the existing literature results.

3.1 Introduction

A typical mission design to a halo orbit around the Lagrangian points from the Earth involves two steps. In the first step, a halo orbit with prescribed geometrical characteristics is designed

and in the second step, an optimal transfer trajectory to the halo orbit from an Earth parking orbit is generated. As discussed in Chapter 1, both these steps are executed first in a basic force model to generate reference preliminary designs and then refined in the full force ephemeris model. In this chapter, the CRTBP framework (described in Chapter 2) is used to generate the reference designs which serve to initiate the mission design involving higher fidelity ephemeris model. The motivations to generate the preliminary mission design in the CRTBP framework are multi-fold; a) serves as a prelude to the proposed mission design in the ERTBP framework b) serves to explore the ways (if any) to extend the mission design in the CRTBP framework to the ERTBP framework and c) serves to implement and validate the different algorithms (for e.g. differential evolution) etc. The next section presents the design of halo orbits.

3.2 Design of Halo Orbits

3.2.1 Design Methodology

The halo orbits are three dimensional, perfectly periodic orbits around the Lagrangian points in the CRTBP framework. The methodology for the design of halo orbits utilizes the fact that these orbits are perfectly symmetrical about the $x - z$ plane. The design of the halo orbit involves obtaining a suitable initial state that leads to orthogonal crossing of the $x - z$ plane at half period. The initial state and the state at half period are given by $[x_0, 0, z_0, 0, \dot{y}_0, 0]$ and $[x_{T/2}, 0, z_{T/2}, 0, \dot{y}_{T/2}, 0]$, where T is the period. The determination of unknowns is accomplished using Differential Correction (DC) and Differential Evolution (DE) techniques.

3.2.2 Design of Halo Orbits using Differential Correction

The equations of motion governing the motion of the third body in the CRTBP framework are given by Eq. (2.2). These equations can be rewritten as six first order differential equations and linearized relative to a reference solution. The solution to the linear state variational equations is given by:

$$\delta X_t = \Phi(t, t_0) \delta X_0 \quad (3.1)$$

where $\Phi(t, t_0)$ is the State Transition Matrix (STM). It gives the sensitivity of the state at time t to small perturbations in the initial state at time t_0 . The Differential Correction (DC) schemes

use the STM to derive the changes to the initial conditions which nullify the deviations in the final state and lead to the required final conditions. In halo orbit design, this necessitates the numerical integration of 36 differential equations (elements of STM) along with 6 state equations. The methodology for the design of halo orbit using differential correction scheme is as follows (Rausch, 2005):

1. The third order analytical solution for halo orbit design (Richardson, 1980) is used as the initial guess and the trajectory is numerically propagated till it crosses the $x - z$ plane again. The x and z velocity components are computed at this half period. These components are expected to be zeros. The aim of the differential correction procedure is to reduce the deviations in these velocity components to zeros.
2. To accomplish this, the State Transition Matrix $\phi(t, t_0)$ is utilized. The STM is initiated to be an identity matrix and is updated with time using numerical integration of 36 differential equations.
3. Of the six initial state variables, $[x_0, z_0, \dot{y}_0]$ are the three initial non-zero variables in this problem. Setting *the crossing of the $x - z$ plane* as the termination criteria automatically ensures that $y_{T/2} = 0$. Of the remaining components $[x_{T/2}, z_{T/2}, \dot{y}_{T/2}]$ are free, leaving only two variables to be reduced to zeros. The resulting system of two equations has three unknowns and is solved by keeping one of the unknowns fixed. Here, the initial z coordinate is kept unchanged and the following relation is derived:

$$\begin{bmatrix} \delta x_0 \\ \delta \dot{y}_0 \end{bmatrix} = \begin{bmatrix} \phi_{41} - \phi_{21} \frac{\ddot{x}}{\dot{y}} & \phi_{45} - \phi_{25} \frac{\ddot{x}}{\dot{y}} \\ \phi_{61} - \phi_{21} \frac{\ddot{z}}{\dot{y}} & \phi_{65} - \phi_{25} \frac{\ddot{z}}{\dot{y}} \end{bmatrix}^{-1} \begin{bmatrix} -\dot{x}_{T/2} \\ -\dot{z}_{T/2} \end{bmatrix} \quad (3.2)$$

The elements of STM matrix and its variation are included as Appendix A.

4. The initial state is updated using the deviations estimated in Eq. (3.2) and the steps 1-3 are repeated till the deviations become less than a predefined tolerance value.

3.2.2.1 Numerical Results

The halo orbit design around Sun-Earth Lagrangian point L_1 obtained using DC procedure is given in Table 3.1. The results are given in normalized units. The initial conditions correspond to $Az = 120,000$ km.

Table 3.1 Halo orbit initial conditions generated by different methods.

Parameter	3rd order theory	Differential correction
x_0	0.988870881206145	0.988838312653001
y_0	0	0
z_0	0.000884831344456	0.000884831344456
\dot{x}_0	0	0
\dot{y}_0	0.008902883528595	0.008959263969673
\dot{z}_0	0	0
Period (non-dimensional)	3.03131584	3.05842562
Az achieved	117,792.60 km	119,358.42 km

Although the initial conditions are close, the achieved Az amplitude, with DC is different. This happens because the DC procedure requires fixation of one of the design variables. To reinforce this phenomenon, the results for different Az amplitudes are presented in Table 3.2. The computational time is very less. But two points must be kept in mind (i) a close guess is used (ii) the DC procedure requires one more level of refinement to obtain the required Az amplitude. It is well known that if close guess is not used, even divergence is possible in any DC process. A numerical method like pseudo arc length continuation (Paffenroth, 2000) can be used in the second level refinement process to realize the desired Az amplitude.

Table 3.2 Comparison of halo orbit amplitudes obtained from DC procedure.

Az desired (km)	Az Achieved (km)	Computational time (s)	No of iterations
40,000	39,791.43	0.004	5
120,000	119,358.42	0.004	5
400,000	396,995.62	0.004	5
750,000	736,125.19	0.006	5
900,000	874,195.26	0.006	5

3.2.3 Design of Halo Orbits using Differential Evolution

Differential Evolution (DE) is a stochastic direct search method whose idea is to mimic the evolution of living species (Storn and Price, 1997). For a problem of N unknown parameters, respective search domains are to be defined. From these bounds, an initial population of size NP is built randomly, following uniform distribution and the objective function is evaluated for each member of the population. The members of this population are tested for violation of path constraints, if any. A new member is formed using three operations of mutation, crossover and selection. The new member will replace the existing member if the corresponding objective function value is lesser than that of the existing member. The process is repeated till a predefined convergence criterion is met. This basic variant of DE is denoted as Scheme 1.

Halo orbit design using differential evolution (DE) employs the same design philosophy as differential correction, that the initial conditions are to be obtained which lead to orthogonal crossing of the $x - z$ plane at half period. The x and z velocity components at crossing need to be zeros. In order to accomplish this and to meet the requirement of desired Az amplitude, the following objective function ‘ $OBJ1$ ’ is set: (Nath and Ramanan, 2016).

$$OBJ1 = |\dot{x}_{T/2} + \dot{z}_{T/2} + Az_{achieved} - Az_{desired}| \quad (3.3)$$

The iterative numerical algorithm needs to minimize the objective function to a predefined tolerance. Here, a tolerance of $1.0E-15$ ensures that the accuracies in x and z velocity components and the Az amplitude achieved are of the orders of mm/s and mm, respectively.

3.2.3.1 Selection of Bounds for the Search Region

The choice of bounds for the search region in DE for the three unknowns $[x_0, z_0, \dot{y}_0]$ are made on the basis of dynamics involved in the problem. The reasons for the choice are given as follows:

1. The lower limit for x_0 is chosen to be 0.95 units from the Earth because the design is for halo orbits near the L_1 Lagrangian point located at 0.989986 units from the Earth. The upper limit is chosen to be 1 because the halo orbits cannot exceed the x -coordinate of the Earth.
2. The lower limit for z_0 is chosen to be 0 because the z -coordinate of the initial position z_0 is above the $x - y$ plane. For setting the upper limit, the ranges of Az amplitudes expected are explored. For example, the normalized unit for 100,000 km is nearly 0.0006684 and that for 1000,000 km it is 0.0066845. So the upper limit is set as 0.1.
3. The lower limit for \dot{y}_0 is chosen to be 0 because the solution is required to be on the $x - z$ plane with a positive y component of velocity. The L_1 Lagrangian point has a velocity of 0.98998909525 units about the Sun-Earth center of mass. The velocity of spacecraft in the rotating frame has to be very small compared to the velocity of L_1 point in the inertial frame. So, the upper limit is chosen as 0.3.

3.2.3.2 Computational Algorithm

- i. An initial population of size NP (number of members) is built. Each member (row) of the population consists of three unknowns $[x_0, z_0, \dot{y}_0]$ of the current problem, represented by U vector and the value of the objective function. The values for these unknowns are chosen randomly from their respective bounds. To evaluate the objective function $OBJ1$ (Eq. (3.3)), numerical integration of the equations of motion (Eq. (2.2)) is carried out using Runge-Kutta 4th order integrator (RK4) till the half period. Similarly, all the members (rows) of the initial population are generated and the initial population will be a $(NP \times 4)$ matrix.

- ii. A trial member, from the search bounds, is generated for each member of the current population through the processes of mutation, crossover and selection:
 - a. **Mutation:** A mutant member is generated using some randomly selected members from the current population such that they are not the same as the member under testing. A scaling factor denoted by F is used for the mutation process, and the mutant member \mathbf{V} is generated according to the relation $\mathbf{V}_i = \mathbf{U}_{R_1} + F(\mathbf{U}_{R_2} - \mathbf{U}_{R_3})$. Here R_1, R_2 and R_3 are three distinct random integers chosen from $[1, NP]$ and the variable i varies between 1 and NP . These members are chosen such that they are different from the element under testing (i member), that is R_1, R_2 and R_3 must not be equal to i .
 - b. **Crossover:** The member of the current population under testing and the mutant member together generate the trial member. A parameter ‘crossover frequency’ (CR) is used to generate a trial member (Price, Storn and Lampinen, 2005). A random number $rand(j)$ is generated between 0 and 1, for each component of the i^{th} member U for which trial member is to be generated. For each of the component (j), if $rand(j) > CR$, the j^{th} component of the i^{th} member of the current population is retained for the trial vector and if $rand(j) \leq CR$, the component in the trial vector is replaced with the j^{th} component of the mutant vector.
 - c. **Selection:** The objective function $OBJ1$ is evaluated for the trial member and the member under testing is replaced by this trial member if the objective function value is less.
- iii. The generation of trial members and subjecting the trial member to the above three operations are carried out for all the members in the current population and thus, a new population is generated.
- iv. The above mentioned steps are repeated till the convergence criterion is met, i.e., the minimum objective function value in the population is less than a small pre-fixed tolerance value (ϵ).

A synthetic diagram explaining the above algorithm is depicted in Figure 3.1.

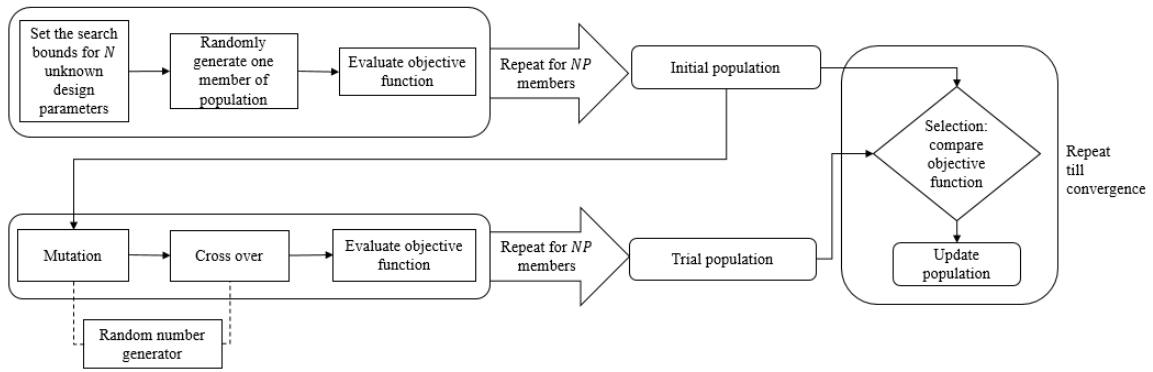


Figure 3.1 A synthetic diagram of the proposed DE-based solution for the design of halo orbit

3.2.3.3 Numerical Results

The halo orbit design around Sun-Earth Lagrangian point L_1 using DE procedure for $Az = 120,000$ km has been generated. The step size used in RK4 integrator is 0.01 in the following tables, unless specified. It is well understood that the DE parameters need to be ‘tuned’ to the specific problem at hand. In other words, a set of DE parameters which work well with a problem, in terms of performance, may not be suitable for a different problem. Towards this goal, extensive trial runs by varying DE parameters such as mutation scale factor F , crossover frequency CR and population size NP are conducted and sample results are given below. The computational time is measured using the ‘time’ command in the Linux operating system during the execution of the FORTRAN code.

Table 3.3 DE performance for different population sizes NP .

Other fixed parameters: $CR = 0.8$, $F = 0.5$

Population size, NP	No. of iterations	Computational time (s)
30	1920	165.812
40	261	69.380
50	279	89.044
60	262	106.836
70	264	126.444

Table 3.3 shows the DE performance for varying population sizes. Based on this result, the population size NP has been fixed to be 40 for further study. Similarly, based on Table 3.4 and Table 3.5, the values for crossover frequency CR and mutation scale factor F have been fixed to be 0.8 and 0.5, respectively. The converged solution up to 14 decimals in all cases with varying DE parameters for $Az = 120,000$ km is:

$x_0 = 0.988838391108559$, $z_0 = 0.000889605690139$ and $y_0 = 0.008960602178616$ and the Az amplitude achieved is 119999.99999999678 km.

Table 3.4 DE performance for varying cross over ratio CR .

Other fixed parameters: $NP = 40, F = 0.5$

Cross over ratio, CR	No. of iterations	Computational time (s)
0.5	846	126.400
0.6	516	93.532
0.7	350	77.900
0.8	261	69.056
0.9	343	75.472

Table 3.5 DE performance for varying mutation factor F .

Other fixed parameters: $NP = 40, CR = 0.8$

Mutation factor, F	No. of iterations	Computational time (s)
0.5	846	126.400
0.6	516	93.532
0.7	350	77.900
0.8	261	69.056
0.9	343	75.472

In order to establish the robustness of the DE procedure, results are generated with different seeds (generating different random number sequences) and different bounds for initial conditions. The performance results are presented in Table 3.6 and Table 3.7, respectively. The DE process converges to the same solution for the narrow bounds, wider bounds and different

seeds. The DE based halo orbit design process doesn't require a good initial guess. However, the bounds for the search region need to be specified logically. The design produced by DE process can be considered global because the same solution was obtained for different bounds for search domains and different seeds for random number generation. This suggests that the solution obtained is globally optimal. Using the initial conditions reported above, the equations of motion Eq. (2.2) are propagated for a full revolution. The halo orbit and its projections onto different planes are plotted for Az amplitude of 120,000 km in Figure 3.2.

Table 3.6 DE performance for varying seeds.

Other fixed parameters: $NP = 40$, $F = 0.5$, $CR = 0.8$

Seed	No of iterations	Function value	Computational time (s)
-65	447	5.56E-16	98.256
-101	361	3.13E-16	106.664
-5055	261	8.09E-16	69.120
-39505	342	9.13E-16	93.512
-844505	279	7.82E-16	80.468

Table 3.7 DE performance for varying search bounds.

Other fixed parameters: $NP = 40$, $F = 0.5$, $CR = 0.8$, seed = -5055

Bounds on $[x_0, z_0, \dot{y}_0]$	No of iterations	Computational time (s)
(0.95, 1), (0, 0.1), (0,0.5)	261	69.120
(0.97, 1), (0, 0.1), (0,0.5)	267	47.488
(0.95, 1), (0, 0.01), (0,0.5)	258	52.856
(0.95, 1), (0, 0.05), (0,0.5)	245	56.940
(0.95, 1), (0, 0.1), (0,0.01)	279	31.436
(0.985, 0.99), (0, 0.001), (0,0.01)	220	20.988
(0.9887, 0.9889), (0.0007, 0.0009), (0.0088,0.009)	199	17.676

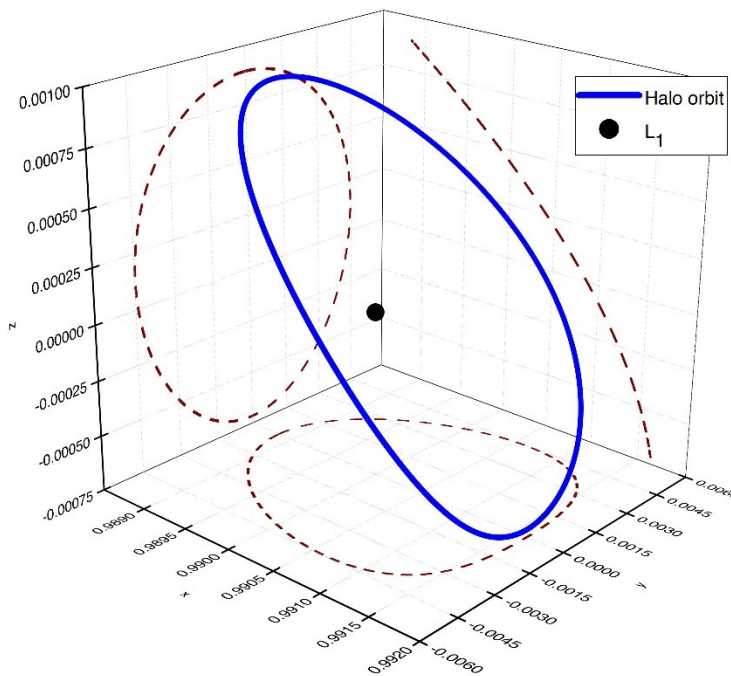


Figure 3.2. Halo orbit with 120,000 km Az amplitude from DE scheme.

3.2.3.4 Halo Orbit Design using Modified Differential Evolution

As observed earlier, the computational time and effort taken by the basic DE process (denoted as Scheme 1) is very large compared to the DC process. To reduce the computational time and get better performance from the DE based process, two variants of DE are employed. The basic idea is to modify the mutation process as follows:

1. Use the vector of lowest cost from the population and four population vectors for mutation (Storn and Price, 1997). Denoted as Scheme 2, the mutation process is carried out as follows:

$$V_{G+1} = x_{best,G} + F(x_{r1,G} + x_{r2,G} - x_{r3,G} - x_{r4,G}) \quad (3.4)$$

2. Use the vector of lowest cost from the population and three population vectors for mutation. Denoted as Scheme 3, the mutation process is carried out as follows:

$$V_{G+1} = x_{r1,G} + F(x_{r2,G} - x_{r3,G}) + F(x_{best,G} - x_{r3,G}) \quad (3.5)$$

In the above equations, V is the trial vector, G is the current generation and $x_{r,G}$ denotes the randomly chosen vectors from the population.

3.2.3.5 Numerical Results

The illustrative results of halo orbit design around Sun-Earth Lagrangian point L_1 using the modified algorithms with Scheme 2 and Scheme 3 are presented below. The bounds on $[x_0, z_0, \dot{y}_0]$ are fixed as (0.95, 1.0), (0.0, 0.1) and (0.0, 0.3), respectively. The values for crossover frequency CR and mutation scale factor F have been fixed to be 0.8 and 0.5, respectively. The converged solution up to 14 decimals with all variants of DE is:

$$x_0 = 0.988838391108559, z_0 = 0.000889605690139 \text{ and } \dot{y}_0 = 0.008960602178616$$

Figure 3.3 and Figure 3.4 show the performance of three variants of DE for varying population sizes. Scheme 2 performs better than Scheme 1 and Scheme 3 in terms of computational time and effort, probably because it generates the trial vector around the vector of lowest cost from the population. It is interesting to note that, although Scheme 3 is supposed to be a better performing algorithm than the basic variant Scheme 1, for the current problem it is not so. An optimization technique/scheme which performs very well in an engineering problem may prove to be futile with another.

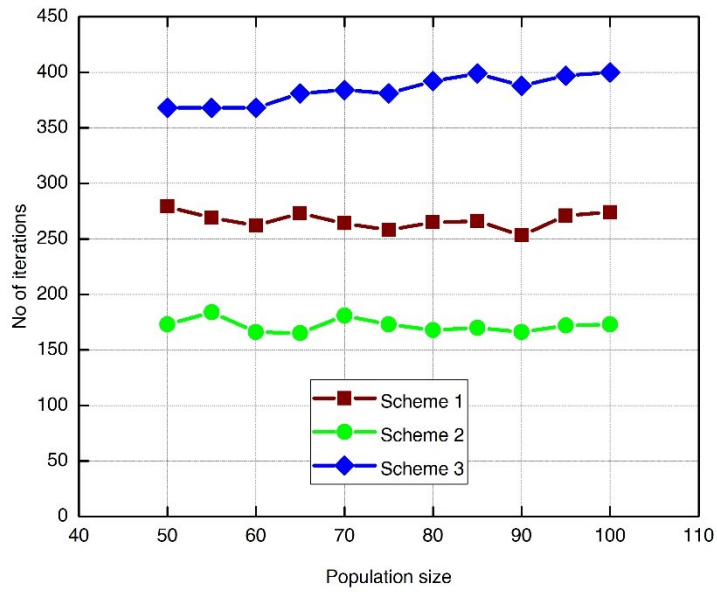


Figure 3.3. Performance of variants of DE in terms of computational effort for halo orbit design around Sun-Earth L_1

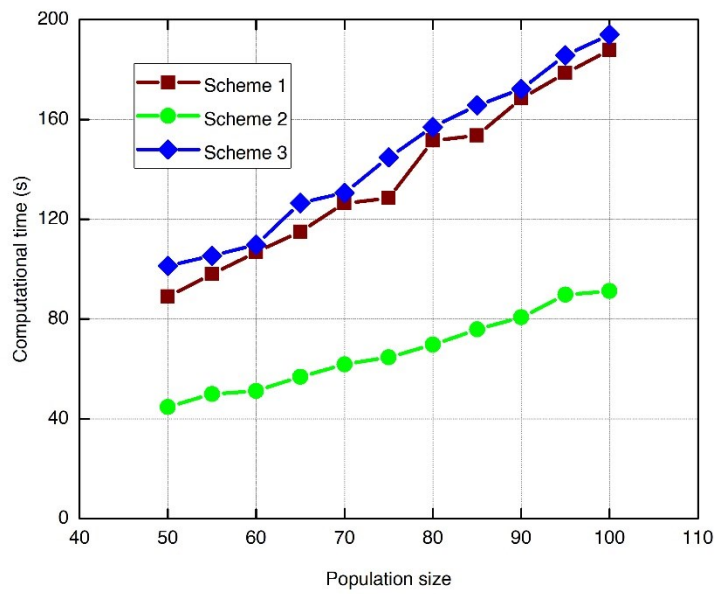


Figure 3.4 Performance of variants of DE in terms of computational time for halo orbit design around Sun-Earth L_1 .

To reinforce these findings, the halo orbit design around Sun-Earth Lagrangian point L_2 for $Az = 500,000$ km using the modified algorithms with Scheme 2 and Scheme 3 is attempted. The motivation is to test the consistency of the results across different dynamical scenarios. The bounds on $[x_0, z_0, \dot{y}_0]$ are fixed as $(1.0, 1.2)$, $(0.0, 0.1)$ and $(0.0, 0.3)$, respectively. The values for crossover frequency CR , population size NP and mutation scale factor F have been fixed to be 0.8, 60 and 0.5, respectively.

Figure 3.5 shows the performance of variants of DE for halo orbit design around Sun-Earth L_2 . Scheme2 performs the best in this scenario as well. The gains in computational time and iterations of Scheme 2 over Scheme 1 are presented in Table 3.8 using the following scheme:

$$Gain = (Value\ in\ Scheme\ 1 - Value\ in\ Scheme\ 2) / Value\ in\ Scheme\ 1 \quad (3.6)$$

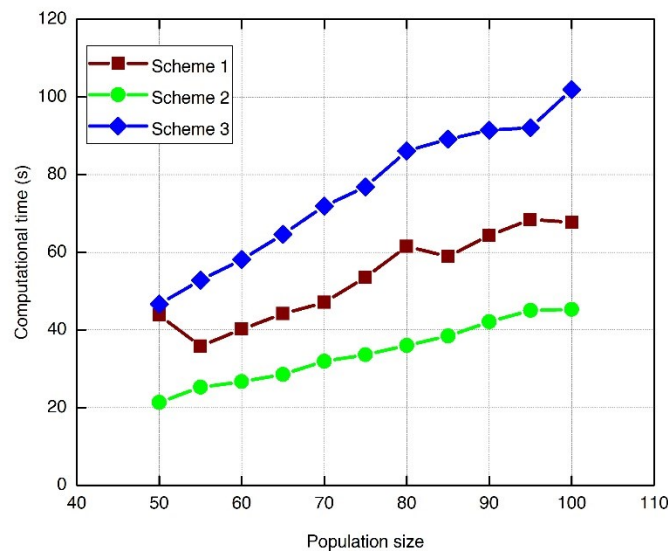


Figure 3.5 Performance of variants of DE in terms of computational time for halo orbit design around Sun-Earth L_2

Table 3.8 Performance of Scheme 2 over Scheme 1.

Az amplitude (km)	Gain in computational time (%)	Gain in iterations (%)
40,000	38.46	35.94
120,000	33.00	32.93
400,000	34.09	34.17
750,000	26.47	25.63
900,000	28.93	27.40

3.3 Transfer Trajectory Design to Halo Orbits

3.3.1 Design Methodology

The optimal transfer trajectories to halo orbits in the CRTBP framework are generated using a differential evolution based methodology (Nath and Ramanan, 2016). In such transfers, the first maneuver (ΔV_{EPO}), known as trans-halo orbit maneuver, is given from Earth Parking Orbit (EPO) such that it injects the space vehicle directly into the transfer trajectory and the space vehicle reaches the quasi-halo orbit around the Lagrangian point. The second impulse $\Delta \vec{V}_{TOI}$ is imparted to insert the space vehicle into the target orbit.

In the design process, the location of the insertion on the target orbit and components of the velocity impulse $\Delta \vec{V}_{TOI} [\Delta \dot{x}, \Delta \dot{y}, \Delta \dot{z}]$ required for target orbit insertion (TOI), $\Delta \vec{V}_{TOI}$ are treated as unknown design parameters and obtained using the DE based procedure. These components are added to the current velocity on the target orbit at the chosen location and backward propagation of N -body equations of motion is carried out. The unknown components are chosen such that, on backward propagation, the desired closest approach altitude CAA from the Earth is achieved. The numerical propagation is ended when CAA is achieved and this CAA

need not be desired value. In order to accomplish the desired *CAA* by minimizing the velocity impulse, an objective function *OBJ2* is set as:

$$OBJ2 = W_h \frac{|CAA_{achieved} - CAA_{desired}|}{S - E \text{ distance}} + W_v |\Delta \vec{V}_{TOI}| \quad (3.7)$$

where

$$|\Delta \vec{V}_{TOI}| = \sqrt{\Delta \dot{x}^2 + \Delta \dot{y}^2 + \Delta \dot{z}^2} \quad (3.8)$$

The objective function is normalized in consistent with the normalized equations of motion and the weights W_h and W_v are introduced to handle the different magnitudes of the terms. The first term is divided by the average Sun-Earth distance ($S - E \text{ distance} = 149597870.7$ km), because the *CAA* is expressed in physical units. After a few trial runs, the weights are chosen as $W_h = 10$, $W_v = 0.1$ for the cases where the trajectories flyby the Earth and $W_h = 1$, $W_v = 10$ where the trajectories pierce through the Earth. To avoid piercing, the velocity components are penalized heavily. The closest approach altitude from the Earth (*CAA*) is assumed to be 200 km for all the transfers and a 200 km circular orbit is assumed for Earth parking orbit for the computation of velocity impulse. These choices facilitate comparison of the results with the existing results in the literature. The numerical process based on DE is ended when the difference between the maximum and minimum of the objective function values of members in the population is less than a small value (1.0E-7). The trans-orbit maneuver (ΔV_{EPO}) is computed as the vectorial difference of geocentric velocity of the spacecraft at *CAA* in the transfer trajectory (on numerical backward propagation) from the velocity of spacecraft in the chosen circular EPO. The total velocity impulse required for the transfer, ΔV_{TOTAL} is computed as the sum of orbit insertion velocity and velocity impulse from EPO.

A step-by-step algorithm is described below, based on the design philosophy outlined above.

3.3.2 Computational Algorithm

1. An initial population of size $NP \times (n + 1)$ is built following the steps (i) - (iv) given below. Each member (row) of the population consists of four unknown design

- parameters $[\nu, \Delta\dot{x}, \Delta\dot{y}, \Delta\dot{z}]$ of the current problem and the value of the objective function. These unknowns are the location of insertion on the orbit (ν) and three components of HOI velocity perturbations ($\Delta\dot{x}, \Delta\dot{y}, \Delta\dot{z}$).
- i. The values of the unknowns are chosen randomly within their respective bounds. In order to search the solution in the whole of search space uniformly, the random number generation is performed using uniform distribution. Different independent random number sequences are used for choosing the initial values for each of the design parameters from their respective search bounds and for generating the trial elements (c.f. step 2).
 - ii. The randomly chosen velocity perturbations are added to the velocity vector at the randomly selected location.
 - iii. To evaluate the objective function (Eq. 3.6), the equations of motion in the CRTBP framework (Eq. 2.5) are numerically integrated backward in time using Runge-Kutta-Fehlberg 7/8 integrator (RKF7/8) till the first closest pass to Earth (*CAA*) is encountered. The absolute and relative tolerances for the Runge-Kutta-Fehlberg 7/8 integrator are set as 1.0E-12.
 - iv. Repeat the steps (i), (ii) and (iii) till an initial population of size $NP \times 5$ is built.
2. Through the three processes of mutation, crossover, and selection, a trial member is formed from the search bounds for each member of the current population.
 - i. Mutation: A mutant member is formed by randomly selecting members from the current population in such a way that they are not equivalent to the member being tested. For the mutation process, a scaling factor represented by F is employed.
 - ii. Crossover: The trial member is created by combining a member of the current population under testing with a mutant member. To construct a trial member, a parameter called ‘crossover frequency’ (CR) is employed.
 - iii. Selection: The objective function is evaluated for the trial member, and if the corresponding function value is less, the member under testing is replaced by this trial member.
 3. Step 2 is performed for all members of the current population, resulting in the generation of a new population.

4. Steps 2-3 are repeated until the convergence criterion is fulfilled, i.e., the difference between the population's maximum and minimum objective function values is smaller than a small pre-defined tolerance value (ϵ).

A FORTRAN95 code is developed and implemented on a machine running Linux OS and equipped with an Intel Core i5 CPU running at 2.5 GHz and 8GB of RAM. The GFORTRAN random number generator RAND is used to generate all of the random numbers. Following several trial runs, the DE parameters are set to $NP = 40$, $F = 0.5$ and $CR = 0.8$ and the weights in $OBJ2$ (Eq.3.6) as $W_h = 10$ and $W_v = 0.5$. An initial step size of $h = 0.01$ is employed for numerical integration to ensure reasonable computational time and accuracy. The tolerance value (ϵ) is fixed at $1.0E-5$.

3.3.3 Numerical Results

The search bounds for each of the velocity components $[\Delta\dot{x}, \Delta\dot{y}, \Delta\dot{z}]$ are set as $[-200, 200]$ m/s and the search bounds for location of insertion as $[0, 177.32428]$ days. The flight duration is restricted to be less than 200 days. After adding the randomly selected velocity perturbations to the state vector at a randomly selected location on the halo orbit, backward numerical propagation of equations of motion in the CRTBP framework is carried out and the propagation is ended when CAA is encountered and the objective function $OBJ2$ is evaluated. The process is repeated till convergence.

The optimal transfer leads to the insertion in a location corresponding to 174.39906 days (the location is represented by the number of days, a third body spends in the halo orbit since initial position on $x - z$ plane) and requires 20.12 m/s for orbit insertion. The corresponding flight duration is 192.36215 days and requires a total velocity impulse of 3280.95 m/s which includes the velocity from EPO (3260.83 m/s). This design matches well with the values (20.3 m/s ($|\Delta\vec{V}_{TOI}|$), 3214.3 m/s (ΔV_{EPO}), 203.75 days) reported by Howell et al. (1994) and the solution (18.0 m/s ($|\Delta\vec{V}_{TOI}|$), 3266 m/s (ΔV_{EPO}), 196 days) of Nath and Ramanan (2016), for a slightly different CAA of 185 km. Rausch (2005) also reports a similar total velocity impulse of 3270.7 m/s (20.5 m/s for TOI) for a flight duration of 205.1 days, for the transfer to the same halo orbit ($Az = 120,000$ km). The results for a shorter flight duration of 122.05 days is also presented in Table 3.9 and the corresponding projections are plotted in Figure 3.6. These results are presented here for benchmarking purposes.

Table 3.9. Optimal transfer in the CRTBP framework to halo orbit

Target orbit and framework	Orbit insertion velocity, $ \Delta\vec{V}_{TOI} $ (m/s)	Velocity impulse from EPO, ΔV_{EPO} (m/s)	Total velocity impulse (m/s)	Orbit insertion location (days)	Flight time (days)
Halo orbit, CRTBP	20.12	3260.83	3280.95	174.39906	192.36215
	26.53	3260.62	3287.16	103.91421	122.05133

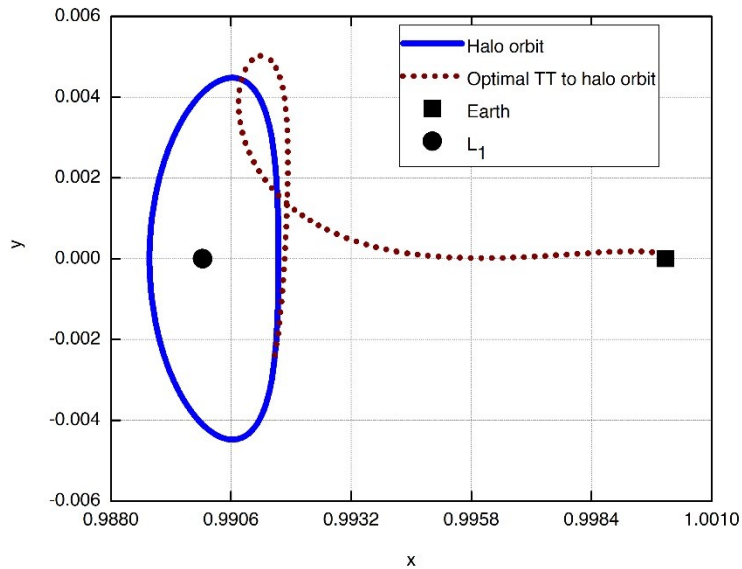


Figure 3.6 $x - y$ projection of optimal transfer trajectory to halo orbit for $Az = 120,000$ km

3.4 Conclusions

Preliminary mission design to Lagrangian points from the Earth is generated under the CRTBP framework. The design of halo orbit around Sun-Earth Lagrangian points is carried out using Differential Correction (Gradient based) and Differential Evolution (Non Gradient based) optimization techniques. It is found that the DC procedure doesn't give the required Az amplitude in a single level scheme. The Az amplitude on convergence is 119,358 km (not

120,000 km as expected). Further refinements to the initial conditions obtained are necessary. The DE based algorithm provides precise design in a single level process. For example, when the required Az amplitude is 120,000 km, the DE based procedure achieves 119,999.99 km. The DE based algorithm works even when the bounds for the design variables are very wide whereas the DC based algorithm requires a very close initial guess. However, the computational time and effort for the basic DE algorithm (Scheme 1) is found to be very large compared to the DC procedure. Two improved variants of DE in terms of mutation strategies have been explored. It is observed that the Scheme 2 performs better than all others in computational time and effort. The implementation of various algorithms has been validated and sets the foundation for the proposed mission design under the ERTBP framework.

Chapter 4: Design of MR Orbits in the Sun-Earth System under the ERTBP Framework

Chapter Summary

This chapter gives an account of the design of Multi-Revolution (MR) orbits around the Lagrangian points in the Sun-Earth system under the ERTBP framework. At first, the concept of perfectly periodic, multi-revolution (MR) halo orbits in the ERTBP framework is explained. In the conventional approach to design an MR orbit, the halo orbit initial conditions (CRTBP) are used with numerical continuation on eccentricity and by dividing the whole orbit into multiple segments. An alternative scheme based on differential evolution is proposed which avoids the continuation on eccentricity and treats the whole trajectory (MR orbit) as a single segment. The design and analysis of different MR orbits in the Sun-Earth system are presented. Unlike in the differential correction based method, the proposed methodology could produce both Lyapunov and halo orbit MR solutions for the same period. Further, it could capture multiple solutions for each of the halo or Lyapunov MR orbits. Multithreading technique is employed to reduce the computational time.

4.1 Introduction

This chapter is the first of the three chapters (4, 5 and 6) describing the mission design to Lagrangian points under the ERTBP framework. In this chapter, the design of Multi-Revolution (MR) orbits around the Lagrangian points in the Sun-Earth system is presented. The MR orbits differ from the halo orbits in the CRTBP framework (Chapter 3) in their geometrical characteristics because the MR orbits make multiple revolutions around the Lagrangian point before repeating its geometry, whereas the halo orbit repeats the geometry after one revolution. The similarities between these orbits are that both the (theoretical) halo orbit and the MR orbit are perfectly periodic in nature and are characterized by their symmetry about the $x - z$ plane. The fact that the MR orbits innately inherit the multi-revolution nature of the *actual* (quasi-periodic) orbits in the ephemeris model is a strong motivation to explore the existence of such orbits in the Sun-Earth system. Furthermore, the existence of MR halo orbits in the Earth-Moon system is reported in the literature (Peng and Xu, 2015a) whereas no

such orbits have been explored in the Sun-Earth system. The proposed design of MR orbits around the Lagrangian point L_1 in the Sun-Earth system utilizing the differential evolution technique is presented in the following sections.

4.2 Design of MR Orbits using Differential Evolution

4.2.1 Terminology and Design Philosophy

The MR orbits are perfectly periodic orbits in the ERTBP framework. Under the ERTBP framework, unlike in the CRTBP framework, these periodic orbits make multiple revolutions around the Lagrangian point before repeating the geometry. The MR orbits generated in this research are represented by the notation $MaNb$. The symbols M and N represent the number of revolutions completed by the third body around the Lagrangian point and by primaries around their barycenter respectively. The symbols a and b are integers which denote the values of M and N respectively. For example, an orbit $M5N2$ means the spacecraft (third body) makes five revolutions around the Lagrangian point while the primaries complete two revolutions around the barycentre. Clearly, these multi revolution orbits are $M:N$ resonant orbits in the ERTBP framework, where $M > 1$. This terminology is same as the one used by Peng and Xu (2015a).

This study deals with two classes of periodic orbits in the ERTBP framework. They are:

1. Three dimensional, multi-revolution halo orbits
2. Planar, multi-revolution Lyapunov orbits.

The periods of MR orbits (T_E) and the halo orbits in CRTBP (T_C) are related by the commensurable constraint (Peng and Xu, 2015a):

$$T_E = MT_C = 2N\pi \quad (4.1)$$

Peng et al. (2017) used halo orbit initial conditions in CRTBP to start the numerical continuation together with a multi-segment optimization method to obtain MR halo orbits in ERTBP. The multiple segments were used to avoid problems associated with numerically integrating the equations of motion for long term. The main problem, as indicated by them (Peng, Bai and Xu, 2017), is non-convergence when a single segment is used. As an alternative method to differential correction, the design of MR orbits is attempted using a differential

evolution based technique. In this method, the whole trajectory is considered as a single segment and the solution is obtained in a single level scheme without numerical continuation on eccentricity.

To generate the design of MR orbits, the equations of motion in the ERTBP framework (c.f. Eq. (2.13)) are numerically integrated for half period with the randomly chosen values for the unknowns. The characteristic of the MR orbits is that they cross the $x - z$ plane orthogonally twice, at $t = 0$ and $t = T/2$ where T is the period (similar to halo orbits in CRTBP). At half-period, the y component must be zero to ensure $x - z$ plane crossing and the velocity components \dot{x} and \dot{z} must be zeros to ensure the orthogonal crossing. Therefore, the initial state and the state at half period are given by $[x_0, 0, z_0, 0, \dot{y}_0, 0]$ and $[x_{T/2}, 0, z_{T/2}, 0, \dot{y}_{T/2}, 0]$ respectively. In order to accomplish the orthogonal crossing of $x - z$ plane, the objective function ‘*OBJ3*’ is set as:

$$OBJ3 = \sqrt{y_{T/2}^2 + \dot{x}_{T/2}^2 + \dot{z}_{T/2}^2} \quad (4.2)$$

The objective function *OBJ3* is evaluated at the half period. The values of the unknowns that drive the objective function to zero, is chosen as the design. The differential evolution technique is used for the selection of suitable values that drives the objective function to zero.

The period of MR orbit, as discussed earlier, is given by $2N\pi$. For the design of an MR halo orbit in ERTBP, the search bounds are chosen around the design obtained in CRTBP. For obtaining the design in CRTBP, the equations of motion of ERTBP are numerically integrated with $e = 0$ till half period and the objective function is evaluated. In CRTBP, the period of the halo orbit is given by $2N\pi/M$ (Eq. (4.1)).

Note that the objective function does not include the Az amplitude of the orbit, as this information is not available for this problem. The period of the orbit which is known, is used to terminate the numerical propagation of equations of motion.

4.2.2 Computational Algorithm

Based on the design philosophy described in the previous sub-section, a step-by-step algorithm is described below.

- i. An initial population of size NP (number of members) is built. Each member (row) of the population consists of three unknowns $[x_0, z_0, \dot{y}_0]$ of the current problem, represented by \mathbf{U} vector and the value of the objective function. The values for these unknowns are chosen randomly from their respective bounds. The bounds are chosen based on relative geometry of Lagrangian point and Earth. To evaluate the objective function (Eq. (4.2)), numerical integration of the equations of motion (c.f. Eq. (2.13)) is carried out using Runge-Kutta-Fehlberg 7/8 integrator (RKF7/8) till the half period (The numerical integrator is changed to RKF7/8 in the place of previously employed RK4 integrator to ensure robustness, numerical stability and to have adaptive step size control). Similarly, all the members (rows) of the initial population are generated and the initial population will be a $(NP \times 4)$ matrix.
- ii. A trial member, from the search bounds, is generated for each member of the current population through the processes of mutation, crossover and selection:
 - a. Mutation: A mutant member is generated using some randomly selected members from the current population such that they are not the same as the member under testing. A scaling factor denoted by F is used for the mutation process, and the mutant member \mathbf{V} is generated according to the relation $\mathbf{V}_i = \mathbf{U}_{R_1} + F(\mathbf{U}_{R_2} - \mathbf{U}_{R_3})$. Here R_1, R_2 and R_3 are three distinct random integers chosen from $[1, NP]$ and the variable i varies between 1 and NP . These members are chosen such that they are different from the element under testing (i member), that is R_1, R_2 and R_3 must not be equal to i .
 - b. Crossover: The member of the current population under testing and the mutant member together generate the trial member. A parameter ‘crossover frequency’ (CR) is used to generate a trial member (Price, Storn and Lampinen, 2005). A random number $rand(j)$ is generated between 0 and 1, for each component of the i^{th} member \mathbf{U} for which trial member is to be generated. For each of the component (j), if $rand(j) > CR$, the j^{th} component of the i^{th} member of the current population is retained for the trial vector and if $rand(j) \leq CR$, the component in the trial vector is replaced with the j^{th} component of the mutant vector.

- c. Selection: The objective function $OBJ1$ is evaluated for the trial member and the member under testing is replaced by this trial member if the objective function value is less.
- iii. The generation of trial member and subjecting the trial member to the above three operations are carried out for all the members in the current population and thus, a new population is generated.
- iv. The above mentioned steps are repeated till the convergence criterion is met, i.e., the minimum objective function value in the population is less than a small pre-fixed tolerance value (ϵ).

A FORTRAN95 code has been developed and implemented in a computer with Linux operating system having Intel Core i7 processor and 8GB RAM. All the random numbers are generated using the GFORTRAN random number generator RAND. After a few trial runs, the DE parameters are chosen as $NP = 40$, $F = 0.5$ and $CR = 0.8$. For numerical integration, an initial step size $h = 0.01$ is chosen which ensures reasonable computational time and accuracy. The value for the small tolerance is fixed at $1.0E-15$.

4.2.3 Results

As pointed out earlier, the position and velocity parameters in the Sun-Earth system are normalized with the mean Sun-Earth distance ($1AU = 149597870.7$ km) and the mean velocity of Earth around Sun (29.78525436 km/s). These constants are obtained from the DE431 ephemeris files.

4.2.3.1 Design of MR Halo Orbit M5N2

For the MR halo orbit M5N2 in the Sun-Earth system, the period of halo orbit in the CRTBP framework is $4\pi/5$ (c.f. Eq. 4.1). The initial conditions in CRTBP corresponding to the halo orbit of period $4\pi/5$ are obtained using the proposed method. They are:

$$x_0 = 0.992441012736910, z_0 = 0.011924534199957 \text{ and } \dot{y}_0 = 0.014880910771653.$$

The bounds for the generation of MR halo orbit M5N2 are chosen around the above mentioned CRTBP initial conditions. They are:

$$x_0 \in [0.990, 0.994], z_0 \in [0.010, 0.013], \dot{y}_0 \in [0.013, 0.016].$$

The converged initial conditions of MR halo orbit M5N2 are obtained using the proposed method. They are:

$$x_0 = 0.99262745046564, z_0 = 0.012236794715286 \text{ and } \dot{y}_0 = 0.014301185117020.$$

The 3D trajectory obtained by propagating the equations of motion with these initial conditions and its projections are depicted in Figure 4.1.

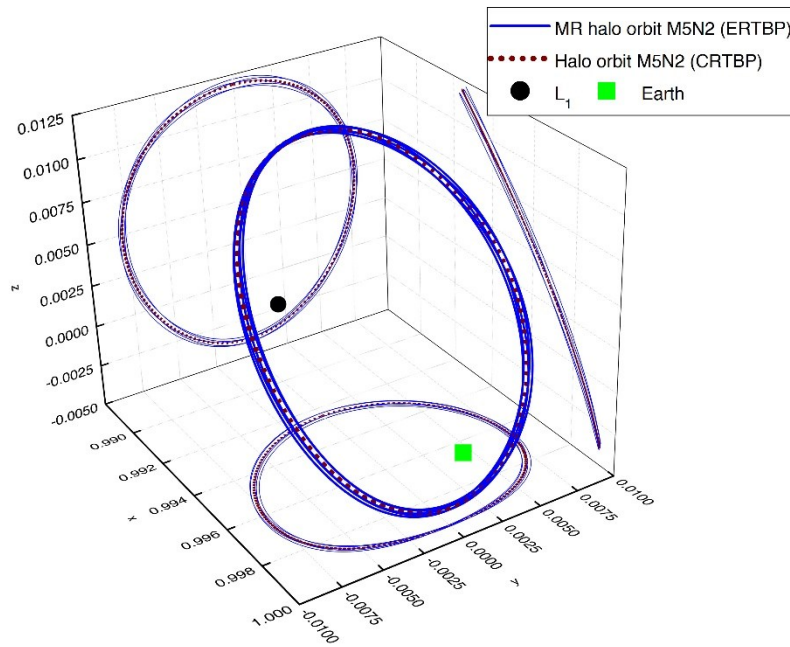


Figure 4.1 Trajectory and projections of MR halo orbit M5N2 around Sun-Earth L₁

4.2.3.2 Reduction in Computational Time using Multithreading

In order to get solutions quickly, parallelisation of the code with multithreading technique is implemented. The evaluation of objective function for the members of the population, which is the most time consuming part, is distributed to multiple threads. To select the number of threads, the designs of M2N1 MR halo orbit and M4N1 MR Lyapunov orbit around the L₁ point of Sun-Earth system are generated for different number of threads. The

performance of the DE based algorithm for different number of threads is presented in Table 4.1. A step size of $h = 0.01$ is used for this analysis.

Table 4.1. Performance of DE with varying no of threads

No. of threads	Computational time for the design of M2N1 MR halo orbit (s)	Computational time for the design of M4N1 MR Lyapunov orbit (s)
1	269.9	266.0
2	139.8	136.2
3	165.4	182.0
4	125.6	123.6

It can be seen from Table 4.1 that the performance with two threads is better compared to the single thread version. More computational time is required for three threads compared to two threads, because for the population size of 40, three threads do not share the workload equally and one thread has to wait for others to complete their part of work (forty is not divisible by 3). The best performance is obtained with four threads, due to optimal workload sharing for this problem with the given parameters. The time taken for computation in this case is only about the half of the time taken by the single thread version. Further increase in number of threads involves more effort of splitting and merging the threads, resulting in more computational time. Although, the trend is presented for two MR orbits, it is found to be same for other MR orbits as well. So, all computations in this study are performed with four threads. The above observations are strictly valid only for the population size of 40.

4.2.3.3 Multiple Options of MR Orbits for the Same Period

For a given period, it is known that multiple options of MR orbits exist (Peng and Xu, 2015a). That means, the third body makes different number of revolutions in the same period. For example, for a period of 4π , in which primaries make two revolutions, the MR orbit can be determined such that the third body makes 4, 5 or 6 revolutions. As mentioned earlier, they are represented as M4N2, M5N2 and M6N2 respectively.

For the generation of initial conditions of these multiple options, the search bounds are chosen around the corresponding CRTBP initial conditions. The CRTBP initial conditions for different periods are given in Table 4.2. In CRTBP framework, a periodic orbit can fall into

either the Lyapunov class or the halo orbit class. For some periods (orbits M2N1 through M3N2 in Table 4.2), Lyapunov class of orbits get generated and for some other periods (orbits M4N2 through M6N2 in Table 4.2), halo orbits get generated. The ERTBP designs obtained using the proposed method are given in Table 4.3. It can be observed from Table 4.3 that the MR orbits obtained in ERTBP by choosing the search bounds around the initial conditions of CRTBP lead to the same class of orbit as in CRTBP. A strategy to generate orbits belonging to both Lyapunov and halo class for a given MR orbit is mentioned in section 4.2.3.5.

Table 4.2. Period and CRTBP initial conditions

MR orbit	Period of orbit in CRTBP	x_0	z_0	\dot{y}_0	Class of orbit
M2N1	$2\pi/2$	0.988467259009926	0.00000000000000039	0.031857770450931	Lyapunov
M3N1	$2\pi/3$	0.991803632165068	0.00000000000000040	0.029520763950809	Lyapunov
M4N1	$2\pi/4$	0.993459441784834	0.00000000000000031	0.029400782805934	Lyapunov
M5N1	$2\pi/5$	0.994482534215127	0.00000000000000001	0.029903541419596	Lyapunov
M3N2	$4\pi/3$	0.984582101371522	0.00000000000000146	0.036618577415171	Lyapunov
M4N2	$4\pi/4$	0.997591408689920	0.01226067968533936	0.005998243864184	Halo
M5N2	$4\pi/5$	0.992441012736910	0.01192453419995794	0.014880910771653	Halo
M6N2	$4\pi/6$	0.994291639269525	0.01236680691237496	0.012606259797867	Halo

Table 4.3 ERTBP initial conditions for different periods

MR orbit	Period of MR orbit	x_0	z_0	\dot{y}_0	Class of orbit
M2N1	2π	0.988251589011885	0.00000000000000014	0.031869005270398	Lyapunov
M3N1	2π	0.988878776129805	0.00000000000000009	0.008864227523245	Lyapunov
M4N1	2π	0.993346765817969	0.00000000000000031	0.029181316689041	Lyapunov
M5N1	2π	0.989397162635537	0.00000000000000031	0.008697000832206	Lyapunov
M3N2	4π	0.984492068876374	0.00000000000000057	0.036589886586495	Lyapunov
M4N2	4π	0.989603642799316	0.00543039495431103	0.030014493911509	Halo
M5N2	4π	0.992627450465642	0.01223679471528681	0.014301185117020	Halo
M6N2	4π	0.992653199985368	0.01186329510869675	0.014870093594936	Halo

The closeness of the solutions brings out the high sensitivity of the problem and the efficiency of the proposed method. The trajectories of M5N2 MR orbit are depicted in Figure 4.1 along with the corresponding halo orbit of CRTBP framework. The relation between period

and A_z amplitude for the halo orbits around L_1 in the Sun-Earth system in CRTBP framework is given in Figure 4.2. It can be observed from Figure 4.2 that the decrease in period when the A_z amplitude increases from the planar Lyapunov orbits to about 800,000 km is not very drastic. With further increase in the A_z amplitude, the period reduces significantly.

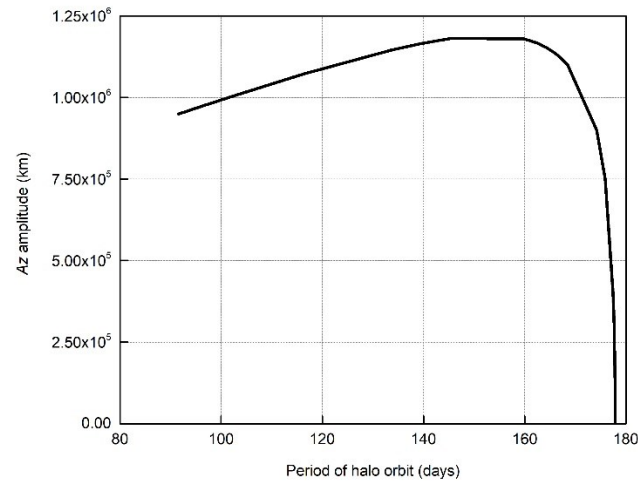


Figure 4.2. Period- A_z amplitude profile for halo orbits around L_1 in the Sun-Earth system

4.2.3.4 Evaluation of Multiple Options of MR Orbits

Two parameters: radial distance from the Earth to the spacecraft and velocity of spacecraft in the orbit are used to analyse the multiple options. The radial distance is an important parameter for communication system. The radial distance and its variation for different MR orbits are presented in Table 4.4 and Figure 4.3.. It can be observed that the variation of radial distance increases as the number of third body revolutions (M) increases for MR halo orbits with same period. However, no such trend has been observed for MR Lyapunov orbits. The magnitude of velocity in the MR halo orbit is a critical parameter in the station keeping aspects of the orbit. The components of velocity of the spacecraft in the MR halo orbit are obtained directly from the numerical integration of equations of motion (c.f. Eq. (2.13)) and are expressed in the inertial J2000 frame. The magnitude of velocity is found as the norm of the three velocity components and its variation is presented in Table 4.4 and Figure 4.4. It can be observed that the variation of velocity in MR halo orbits increases when the number of third body revolutions (M) increases. This is expected because the spacecraft is traversing longer distances in a given time. The MR Lyapunov orbits don't show such a trend. The choice for a

particular design among multiple options is specific to a mission and this analysis is expected to help arrive at trade-offs.

Table 4.4. Variation of radial distance and velocity in MR orbits

MR orbit	Class of MR orbit	Minimum radial distance (km)	Maximum radial distance (km)	Minimum velocity in orbit (m/s)	Maximum velocity in orbit (m/s)
M2N1	Lyapunov	169,339.3	2,330,013.7	652.1	949.2
M3N1	Lyapunov	507,240.7	1,663,256.5	104.0	937.8
M4N1	Lyapunov	961,715.7	1,094,520.4	752.6	882.5
M5N1	Lyapunov	141,519.3	1,585,707.0	94.8	2,234.0
M4N2	Halo	1,740,800.5	2,382,212.8	630.5	954.7
M5N2	Halo	552,237.9	2,136,940.5	425.9	1,108.0
M6N2	Halo	241,141.0	2,087,244.5	302.6	1,763.6

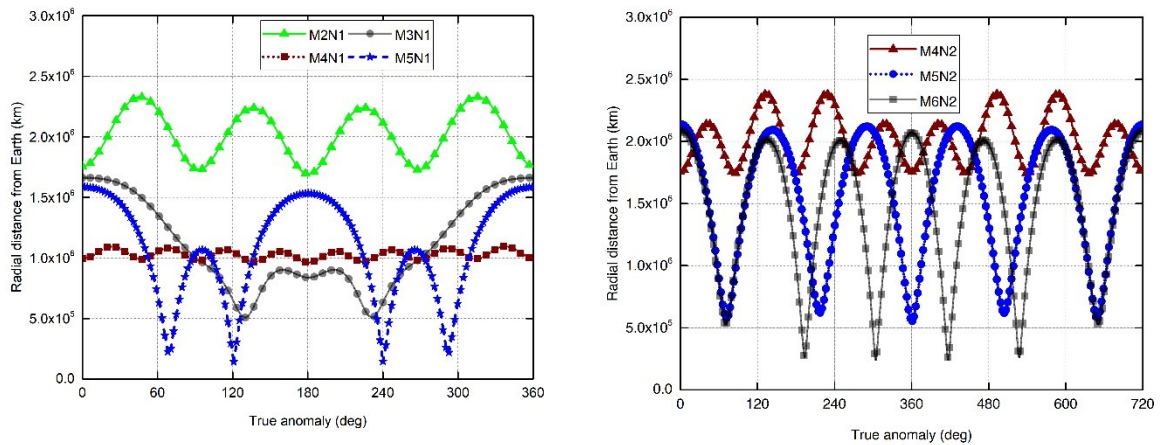


Figure 4.3 Evolution of radial distance from Earth in MR orbits

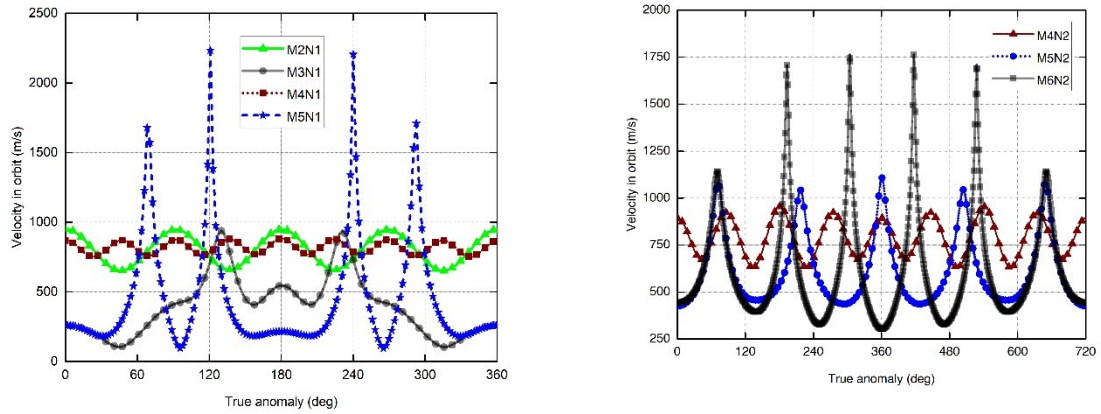


Figure 4.4 Evolution of velocity in MR orbits

4.2.3.5 Halo and Lyapunov Design Solutions for an MR Orbit

The design methodologies based on differential correction produce halo or Lyapunov orbits under the ERTBP framework depending on the class of orbits produced in CRTBP framework. That means if the CRTBP framework produces halo orbit, then ERTBP also will produce halo and if CRTBP produces Lyapunov, then ERTBP also will produce a Lyapunov orbit. But, the proposed methodology based on DE produces both halo and Lyapunov solutions for an MR orbit by suitable choice of the bounds on z component of position in the ERTBP framework.

For example, the initial conditions of the halo orbit in the CRTBP framework which corresponds to the M4N2 orbit are: $[0.99759140868992047773, 0.01226067968533936631, 0.00599824386418409330]$. The MR halo solution, listed in Table 4.3, is obtained by using the bounds as: $[(0.985, 0.998), (0.001, 0.015), (0.002, 0.05)]$, whereas the bounds $[(0.985, 0.998), (0.0, 0.000001), (0.002, 0.05)]$ leads to a Lyapunov solution: $[0.98825158899736526008, 0.00000000033245386642, 0.03186900527425608558]$. In the selection of bounds for Lyapunov solution, the bounds for z_0 are chosen to be very close to zero using the fact that Lyapunov orbits are coplanar with $x - y$ plane. The M4N2 halo and Lyapunov orbits and their projections are plotted in Figure 4.5. Table 4.5 gives both the design solutions for different MR orbits. *These results, to the best knowledge of the authors, have not been reported in the literature.*

Table 4.5 Halo and Lyapunov design solutions for different MR orbits

MR orbit	Class of MR orbit	x_0	z_0	\dot{y}_0
M4N2	Halo	0.989603642799316	0.005430394954311	0.030014493911509
	Lyapunov	0.988251588997365	0.0000000003324538	0.031869005274256
M5N2	Halo	0.992627450465642	0.012236794715286	0.014301185117020
	Lyapunov	0.989815766102827	0.000000000196083	0.007719240171460
M6N2	Halo	0.992653199985368	0.011863295108696	0.014870093594936
	Lyapunov	0.990243834969832	0.000000000010040	0.028817211689774

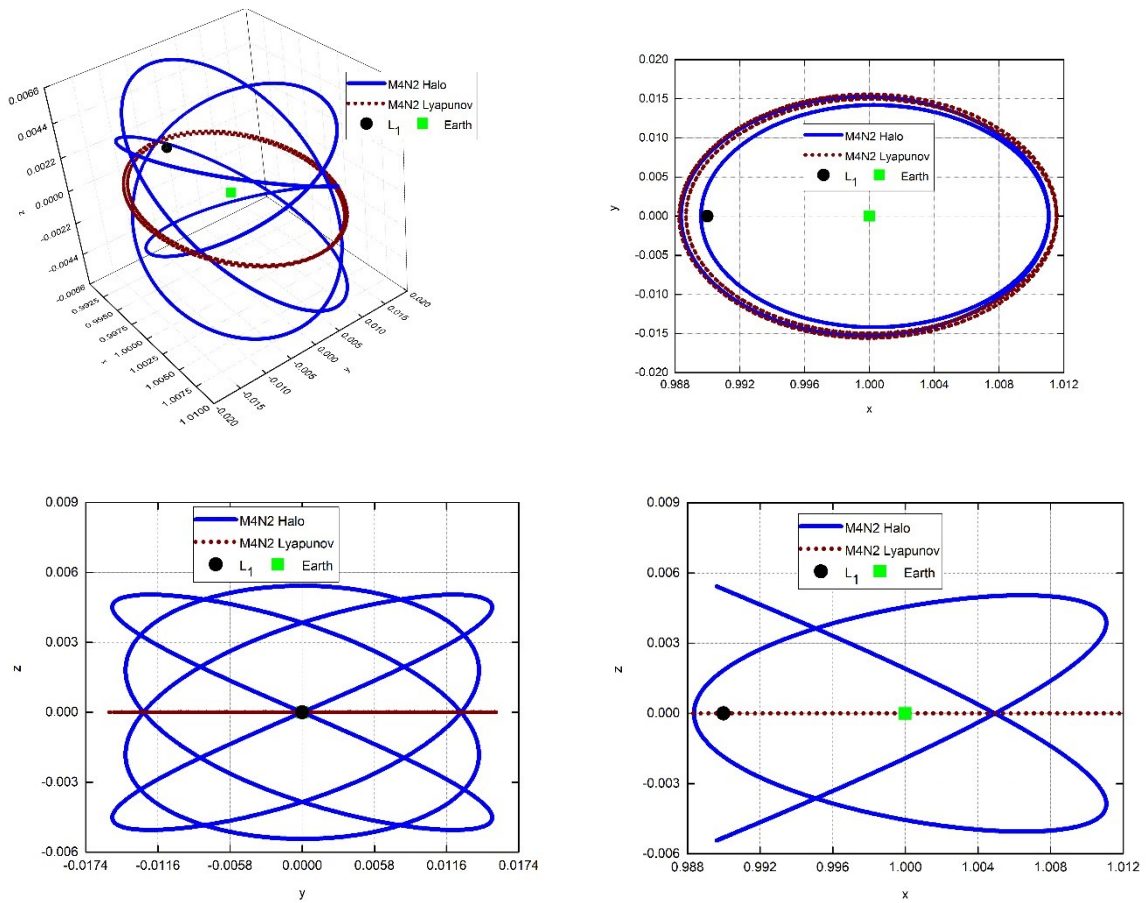


Figure 4.5 Trajectory and projections of M4N2 halo and M4N2 Lyapunov orbits

4.2.3.6 Evaluation of Halo and Lyapunov Design Solutions for an MR Orbit

The evaluation is carried out using the two parameters radial distance and velocity in the orbit, as reported in the earlier section. The variation of radial distance from Earth and the velocity in orbit for the different classes of MR orbits are given in Table 4.6. The difference in radial distance and velocity for the halo and Lyapunov solutions of the M4N2 MR orbit are

comparable while the other orbits show drastic differences. These results can be useful in making a choice among different halo or Lyapunov solutions. If minimum variation in radial distance is desirable for a mission, then M4N2 MR halo orbit is preferable. However, the magnitudes of radial distances are very high. A trade-off study can be conducted using this method to make a choice.

Table 4.6 Variation of radial distance and velocity in MR orbits having period 4π

MR orbit	Minimum radial distance (km)	Maximum radial distance (km)	Minimum velocity in orbit (m/s)	Maximum velocity in orbit (m/s)
M4N2 halo	1,740,800.5	2,382,212.8	630.5	954.7
M4N2 Lyapunov	1,693,393.2	2,330,013.7	652.1	949.2
M5N2 halo	552,237.9	2,136,940.5	425.9	1,108.0
M5N2 Lyapunov	2,05,854.9	1,121,545.9	521.3	1,005.6
M6N2 halo	241,141.0	2,087,244.5	302.6	1,763.6
M6N2 Lyapunov	970,464.6	1,697,809.7	641.9	916.2

4.2.3.7 Multiple Design Solutions for an MR Orbit

For a given MR orbit, independent of whether they belong to the class of halo or Lyapunov, multiple design solutions are identified using the proposed method. That means, for different sets of initial conditions, the third body makes the same number of revolutions in a given period. The proposed methodology could capture multiple initial conditions for the same halo/Lyapunov MR orbits by varying the bounds of the search region and the seed for random number generation. The initial conditions of multiple designs for different MR orbits are listed in Table 4.7. The trajectory and projections corresponding to multiple designs of MR halo orbit M4N2 are plotted in Figure 4.6.

Table 4.7 Multiple design solutions for different MR orbits

MR orbit	x_0	z_0	\dot{y}_0	Multiple design solutions
M3N1 Lyapunov	0.988878776129805	0.00000000000000009	0.008864227523245	Design1
	0.989294923832702	0.00000000000000023	0.005264647607516	Design2
M3N2 Lyapunov	0.984492068876374	0.00000000000000057	0.036589886586495	Design1
	0.985392416949155	0.00000000001488270	0.035796900227535	Design2
M4N2 halo	0.989603642799316	0.00543039495431103	0.030014493911509	Design1
	0.989109963327943	0.00638867729496482	0.029763001049187	Design2
M6N2halo	0.992653199985368	0.01186329510869675	0.014870093594936	Design1
	0.992687386309502	0.00949371754195974	0.011882404547626	Design2

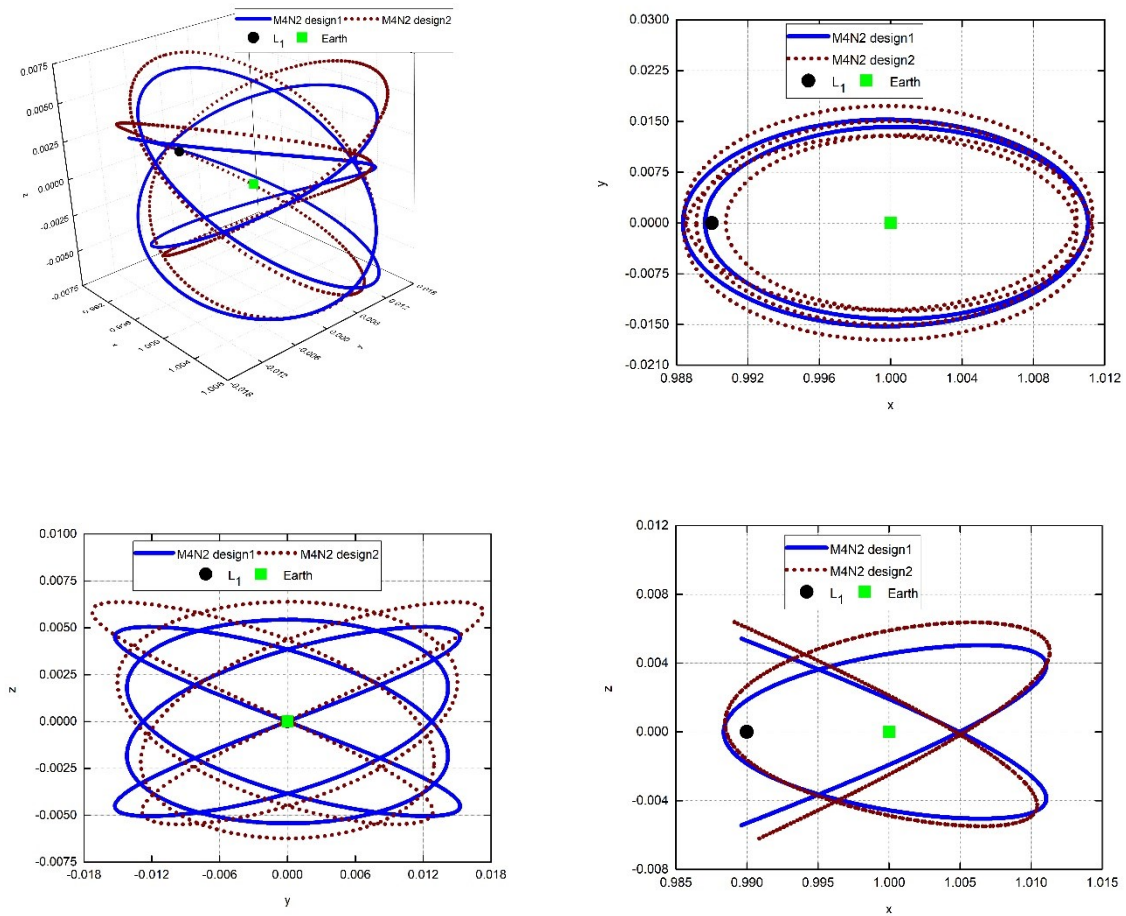


Figure 4.6 Trajectory and projections of MR orbits corresponding to M4N2 design1 and M4N2 design2

The evaluation of multiple solutions is carried out using the two parameters radial distance and velocity in the orbit, as reported in an earlier section. From Table 4.8, it can be

seen that extent of variation of radial distance and velocity are different for multiple design solutions.

Table 4.8 Variation of radial distance and velocity in multiple design solutions for a given MR orbit

MR orbit	Multiple design solutions	Minimum radial distance (km)	Maximum radial distance (km)	Minimum velocity in orbit (m/s)	Maximum velocity in orbit (m/s)
M3N1 Lyapunov	Design1	507,240.7	1,663,256.5	104.0	937.8
	Design2	299,297.6	1,601,001.7	62.6	1392.0
M3N2 Lyapunov	Design1	2,299,284.0	3,513,167.7	650.7	1091.1
	Design2	2,184,808.4	4,053,855.7	625.7	1101.7
M4N2 halo	Design1	1,740,800.5	2,382,212.8	630.5	954.7
	Design2	1,667,265.5	2,731,959.6	584.9	953.5
M6N2 halo	Design1	241,141.0	2,087,244.5	302.6	1763.6
	Design2	263,472.5	1,792,433.0	252.0	1627.3

To further compare these multiple design solutions, the concept of average Az amplitude is introduced for an MR orbit in ERTBP. It is well known that Az amplitude uniquely defines a halo orbit in CRTBP. The Az amplitude of the halo orbit is computed as half of the difference between the z coordinates at $t = 0$ and $t = T/2$ in the orbit. The following procedure is introduced to represent the Az amplitude MR halo orbit: for each revolution, the difference between the z coordinates of the two successive $x - z$ plane crossings is computed; the average of the differences of all revolutions is computed. This average Az amplitude is used to represent MR halo orbit. Table 4.9 presents the average, minimum and maximum Az amplitudes for multiple options. This yardstick can be used for the choice of design from among multiple options. The average Az amplitude of MR halo orbit is nearly equal to the Az amplitude of corresponding halo orbit in CRTBP. This justifies the use of CRTBP as a reasonably good approximation to start the real mission design in ERTBP. The trajectory and projections of MR halo orbit M5N2 and its CRTBP halo orbit (Figure 4.1) also demonstrates the above mentioned argument for average Az amplitude.

Table 4.9 Az amplitudes of multiple designs of MR halo orbits

MR halo orbit	Multiple design solutions	Az amplitudes of different revolutions of MR halo orbit (km)			Az amplitude of halo orbit in CRTBP (km)
		Average	Minimum	Maximum	
M4N2	Design1	490,335.6	279,405.0	696,718.0	490,321.6
	Design2	566,806.9	315,882.6	814,861.0	
M6N2	Design1	1,087,030.6	1,024,833.6	1,159,975.4	1096,394.8
	Design2	669,747.1	92,113.3	1,086,620.8	

4.2.3.8 Northern and Southern Family Solutions for an MR Halo Orbit

In the CRTBP framework, the solution obtained for a northern family generates southern family halo orbits if the sign of z_0 is changed, keeping the values of other two variables same. The same strategy applies to MR halo orbits also. For example, the initial conditions of the MR halo orbit M4N2 (design1) in the northern family are: [0.98960364279931624725, 0, 0.00543039495431103774, 0, 0.03001449391150934837, 0]. The initial conditions of the corresponding MR halo orbit in the southern family will be given by [0.98960364279931624725, 0, -0.00543039495431103774, 0, 0.03001449391150934837, 0]. The trajectory and projections of the MR halo orbit M4N2 belonging to the northern and southern families are plotted in Figure 4.7. Because only the sign of z component of position is different and the magnitude remains same, the $x - y$ projections of both the northern and southern family orbits are the same.

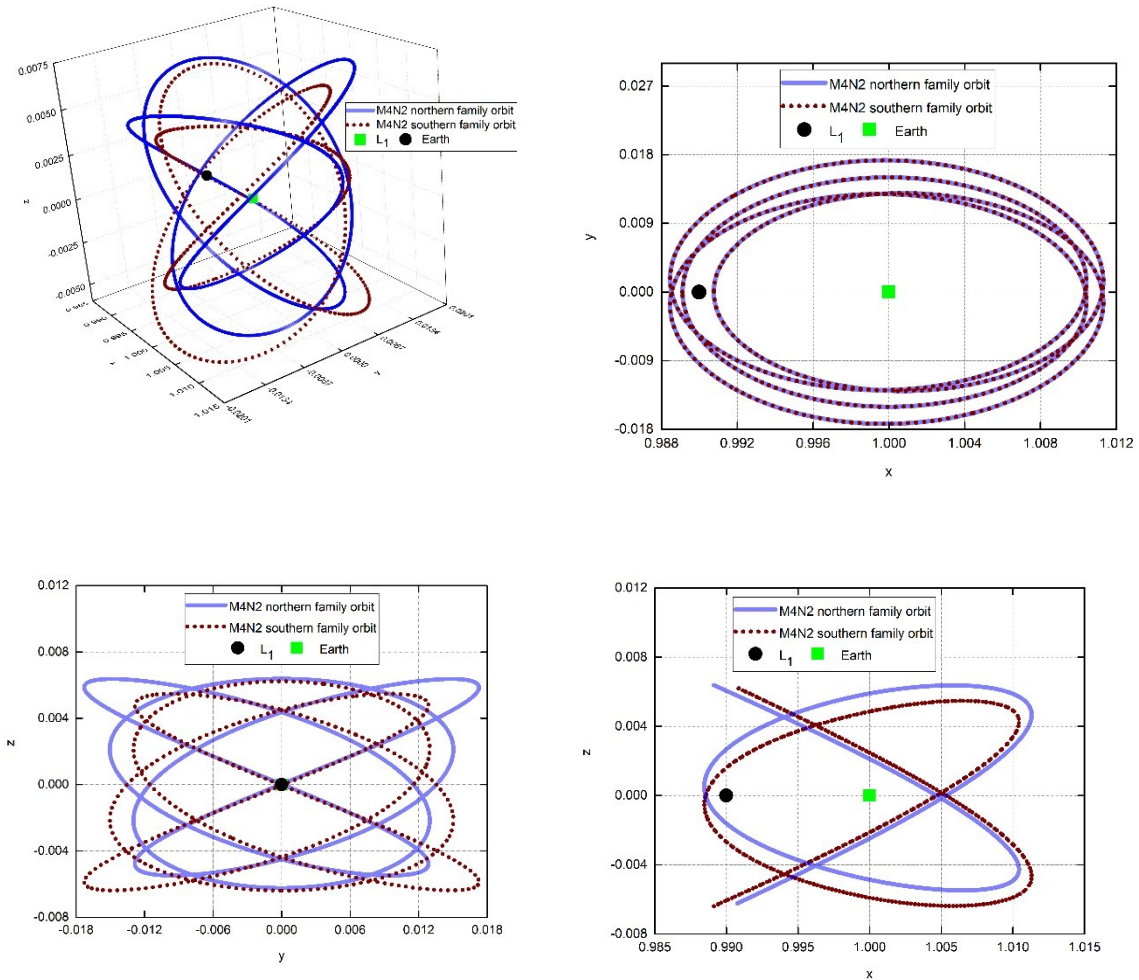


Figure 4.7 Trajectory and projections of MR halo orbit M4N2 belonging to northern and southern families

4.3 Comparison Between Differential Correction and Differential Evolution Methodologies for the Design of MR Orbits

In the CRTBP framework, the design of halo orbit is conventionally carried out using analytical solutions initially (Richardson, 1980) and then refined using a differential correction (DC) scheme (Connor Howell, 1984). Extending the same approach, Peng and Xu produced MR orbits in the ERTBP framework, with numerical continuation methods (Peng and Xu, 2015a). They used multiple segments because of the sensitivity of differential correction to the initial guess. Even with a very good initial guess, differential correction based methodologies for the design of MR halo orbits do not guarantee the solution in a single level scheme. To demonstrate this phenomenon, design of MR halo orbits is carried out using differential

correction with the initial guess based on DE solution (the information on fourth order approximation being unavailable to the author). The methodology for the design of halo orbit using differential correction scheme is as follows:

- i. Using the initial guess, the trajectory is numerically propagated till half period and the x and z velocity components are computed. These components are expected to be zeros. The aim of the differential correction procedure is to reduce the deviations in these velocity components to zeros.
- ii. To achieve this, the State Transition Matrix (STM) $\phi(t, t_0)$ is utilized. The STM is initiated to be an identity matrix and is updated using numerical integration of 36 differential equations (Rausch, 2005). Together with the six state equations, a total of 42 equations are to be integrated numerically.
- iii. $[x_0, z_0, \dot{y}_0]$ are the three initial non-zero variables of this problem. The orthogonal crossing of $x - z$ plane at half period automatically ensures that $y_{T/2} = 0$. Thus, there are only two variables which are to be reduced to zeroes and to assess the sensitivity of the initial variables. This underdetermined system with two equations and three unknowns is solved by fixing the value of one of the three unknowns. Here, the initial z coordinate is kept unchanged and the following relation is obtained (Rausch, 2005):

$$\begin{bmatrix} \delta x_0 \\ \delta \dot{y}_0 \end{bmatrix} = \begin{bmatrix} \phi_{41} - \phi_{21} \frac{\ddot{x}}{\ddot{y}} & \phi_{45} - \phi_{25} \frac{\ddot{x}}{\ddot{y}} \\ \phi_{61} - \phi_{21} \frac{\ddot{z}}{\ddot{y}} & \phi_{65} - \phi_{25} \frac{\ddot{z}}{\ddot{y}} \end{bmatrix}^{-1} \begin{bmatrix} -\dot{x}_{T/2} \\ -\dot{z}_{T/2} \end{bmatrix} \quad (4.3)$$

The state transition matrix ϕ is a (6 x 6) matrix and its variation is given by $\dot{\phi} = A\phi$. The elements of matrix A are given in Appendix B.

- iv. All the above steps are continued till the deviations becomes less than a pre-defined tolerance value.

During this process, starting from the initial guess, the initial values for the unknowns $[x_0, z_0, \dot{y}_0]$ are modified to ensure orthogonal crossing of the orbit at half period ($T/2$). In other words, the x and z velocity components at half period are ensured to be zeros.

Treating the MR halo orbit as a single segment results in divergence in the DC procedure. This is due to the accumulated numerical errors in the long-term propagation. This is demonstrated using the design of MR halo orbit M4N1, obtained using DE process. The initial conditions obtained using DE are: [0.99756513268929190525, 0.01241813059910885289, 0.00595889129677015144]. This design solution is truncated to four decimal places and is used as the initial guess for the DC process. For numerical integration, Runge-Kutta-Fehlberg 7/8 integrator (RKF7/8) is used in both DE and DC based approaches. It is observed that the solution diverges rapidly when propagated till the half period. This trend continues, even when the actual DE solution is truncated to 12 decimal places and used as initial guess. This is attributed to long term numerical integration of equations of motion with a single segment approach by Peng and Xu (2015a).

To overcome this problem, the trajectory is divided into multiple segments. For this, the states of DE solution are used as the target points. The states at some selected true anomalies are used as target states in the DC process and segment wise convergence is attempted. The objective function is modified as follows:

$$\begin{bmatrix} \delta x_0 \\ \delta y_0 \end{bmatrix} = \begin{bmatrix} \emptyset_{41} - \emptyset_{21} \frac{\ddot{x}}{\dot{y}} & \emptyset_{45} - \emptyset_{25} \frac{\ddot{x}}{\dot{y}} \\ \emptyset_{61} - \emptyset_{21} \frac{\ddot{z}}{\dot{y}} & \emptyset_{65} - \emptyset_{25} \frac{\ddot{z}}{\dot{y}} \end{bmatrix}^{-1} \begin{bmatrix} \dot{x}_T - \dot{x}_A \\ \dot{z}_T - \dot{z}_A \end{bmatrix} \quad (4.4)$$

Here, the subscript T represents the target state of the current segment to be achieved and the subscript A represents the corresponding actual state from the DC process. The DC process modifies the initial guess on unknowns to match the target states, by reducing the deviations to zeros. The convergence criterion used is that the deviations must be less than 1.0E-6 or iterations reach the value of 50.

Table 4.10 Performance of DC and DE methodologies for the design of MR orbits

Number of digits of DE solution for initial guess	True anomaly of converged DC solution (deg)	Period corresponding to convergence	Computational time for DC process (s)	Deviation on x_0 (δx_0)	Deviation on \dot{y}_0 ($\delta \dot{y}_0$)	Computational time for DE process (s)
4	23.14	0.064278	78.4	9.641E-10	4.805E-10	794.3
5	66.17	0.183805	193.6	3.252E-7	8.385E-7	170.1
6	67.32	0.187000	228.2	1.062E-7	3.014E-7	61.0
7	82.21	0.228361	232.8	2.748E-7	1.684E-7	60.2
10	89.83	0.249805	306.3	3.439E-7	9.508E-7	57.2
12	94.82	0.263389	327.9	1.835E-7	5.348E-7	56.7

It can be seen from Table 4.10 that in the DC process a closer initial guess guarantees convergence for a larger segment of the orbit. That means, for an initial guess truncated to twelve decimal places, convergence happens till a true anomaly of 94.82° , whereas, for four decimal places convergence happens only till 23.14° . Even with a good initial guess with twelve decimal places, the DC process diverges well before the half period, pointing out the requirement of multiple segments. Also, the computational time for the DC process increases when the initial guess is closer to the actual solution, because the numerical integration proceeds till a higher fraction of the period.

Because the DE process depends only on the bounds for the unknowns, the convergence happens even with single segment. The time taken for DE process varies with the search bounds. The bounds around truncated values of about 12 and 10 decimal places are so good that the process converges in the first generation itself. The time taken for the DE process is larger compared to the DC process for some initial guesses, but the comparison here is made in the context of a single segment DC process. The design approach of Peng and Xu (2015a) is based on numerical continuation on eccentricity even with multiple segments. They report that the average time for one step of continuation in eccentricity ($\delta e = 0.001$) is about 60s for Earth-Moon system. Assuming the same amount of time for the Sun-Earth system, about 1000s will be required for computation whereas DE takes about 800s with a very fine step size ($h = 0.0001$) and with wide search bounds. Thus, it can be concluded that the time taken for DE based process is comparable to that of DC. The main advantage of DC process on computational time is lost because of multi segment approach and numerical continuation. The DE based scheme works with bounds for the unknowns, eliminating the need of a very good

initial guess, multiple segment and numerical continuation methods. The features of both the schemes are summarized in Table 4.11.

Table 4.11 Qualitative comparison of DC and DE processes for the design of MR orbits

	DC based method	DE based method
Nature of technique	Gradient	Non gradient/Evolutionary
Good Initial Guess	Essential	Bounds for the unknowns
Single/Multiple Segments	Multiple segment approach	Single segment approach
Numerical Continuation	On Eccentricity	Single level
Computational time	Large (1000 s for a typical case)	Comparable (800 seconds)

4.4 Conclusions

The design of multi-revolution (MR) periodic orbits under ERTBP framework in the Sun-Earth system has successfully been generated using the proposed differential evolution-based technique. This single level, single segment approach for halo orbit design produces precise MR orbit design, avoiding the need for multilevel continuation methods. In order to reduce the computational time, multithreading technique has been successfully employed. The time taken for computation with four threads is only about half of the time taken by the single thread version. The concept of average Az amplitude is introduced for an MR halo orbit in ERTBP framework. The average Az amplitudes of MR halo orbits are found to be nearly equal to that of corresponding circular halo orbits. For example, Az amplitudes of MR halo orbit M4N2 and the corresponding halo orbit are 490,335 km and 490,321 km respectively. Multiple options of MR orbits for the same period are generated and analyzed. For multiple options of MR halo orbits with same period, it is found that the variation of radial distance from Earth and the variation of velocity in orbit increases as the number of third body revolutions increases. For example, the variation of radial distance from Earth for the MR halo orbit M4N2 is lesser all along the orbit compared to that for the MR halo orbit M5N2. Both halo and Lyapunov design solutions are captured for an MR orbit. Further, for a given halo or Lyapunov orbit, multiple design solutions are also captured. For example, $[0.9896036427, 0, 0.0054303949, 0, 0.0300144939, 0]$ and $[0.9891099633, 0, 0.0063886772, 0, 0.0297630010, 0]$ are the multiple design solutions for the MR halo orbit M4N2. Many of these results have not been reported in the literature. The design of MR orbits using a differential correction based

approach needs multiple segments for DC approach. The computational time for both the methods are found to be comparable.

Chapter 5: Design of Quasi-Halo Orbits and Optimal Transfers in the Sun-Earth system

Chapter Summary

This chapter gives an account of the design of quasi-halo orbits around the Lagrangian points and transfers to them in the Sun-Earth system using the ERTBP framework. The (periodic) MR halo orbits generated in the ERTBP framework in the Sun-Earth system have large in-plane and out-of-plane amplitudes and so, are not suitable for scientific missions like ISEE3. For viable smaller amplitudes, only quasi-halo orbits do exist around the Sun-Earth Lagrangian point L_1 in the ERTBP framework. So, as an alternative to the periodic orbits under the CRTBP and ERTBP frameworks, the quasi-halo orbits under ERTBP framework are designed and used as reference designs to generate ephemeris designs. These quasi-halo orbits are generated using the proposed approach that employs differential evolution technique. Using a similar approach, the quasi-halo orbits are designed in the ephemeris model also. The methodology could generate quasi-halo orbits that do not require any theoretical velocity corrections for about five years (ten revolutions). Further, the generation of quasi-halo orbits for a wide range of average Az amplitudes (120,000 km to 750,000 km) is demonstrated. In the existing literature, the generation of quasi-halo orbits for small amplitudes ($\sim 120,000$ km) is not addressed. The pros and cons of the reference designs in generating ephemeris design are analysed. It is found that the design in ephemeris model is close to both the initial designs in CRTBP and ERTBP frameworks. However, the use of ERTBP design as the reference design does not result in reduction in computational time. Furthermore, optimal two impulse transfers to the quasi-halo orbit from an Earth parking orbit are generated under the ERTBP framework and the ephemeris model. The location of insertion and the components of orbit insertion velocity are treated as unknowns and determined using differential evolution. The transfer cost in the ephemeris model is found to be less compared to transfers in CRTBP and ERTBP frameworks.

5.1 Introduction

This is the second of the three chapters (4, 5 and 6) describing the mission design to Lagrangian points under the ERTBP framework. In this chapter, the design of quasi-halo orbits around the Lagrangian points in the Sun-Earth system is presented. The motivation for the design of quasi-halo orbits is described below.

5.1.1 Amplitudes of MR Halo Orbits and Motivation for the Design of Quasi-Halo orbits

The amplitudes of different revolutions of the MR halo orbit are not the same. So, the average out-of-plane amplitude (Az_{avg}) and average in-plane-amplitudes (Ax_{avg} and Ay_{avg}) are used to represent the orbits. The in-plane and out-of-plane amplitudes of some of the MR halo orbits in the Sun-Earth system and the halo orbit used for the ISEE3 mission are presented in Table 5.1.

Table 5.1 Comparison of amplitudes of MR halo orbits and ISEE3 halo orbit

Orbit	Ax_{avg} (km)	Ay_{avg} (km)	Az_{avg} (km)
MR halo M2N1	1,057,471.8	1,433,130.6	1,197,263.6
MR halo M4N1	183,133.5	372,301.7	920,274.6
MR halo M4N2	1,698,597.8	2,203,839.3	490,335.6
MR halo M5N2	523,089.6	1,167,325.2	1,182,051.0
MR halo M6N2	451,224.9	884,473.0	1,087,030.7
Halo, ISEE3	206,446.8	666,672.0	120,000.0
Halo, SOHO	206,448.0	666,670.0	120,000.0

The amplitudes of the MR halo orbits are large compared to the halo orbits used for scientific missions such as ISEE3 mission. Such large magnitudes of Ax_{avg} and Ay_{avg} violate the requirement for the communication system that the maximum Sun-Earth-Vehicle (SEV) angle should be greater than 3.5deg and less than 30deg (Farquhar et al., 1977). This constraint results from the need to avoid the Solar Exclusion Zone (SEZ). The Solar Exclusion Zone is a zone around L_1 where communication interference will occur due to solar radio noise (Farquhar et al., 1977). Figure 5.1 and Figure 5.2 show the variation of SEV angle for halo orbits of selected Az amplitudes and MR halo orbits in the Sun-Earth system.

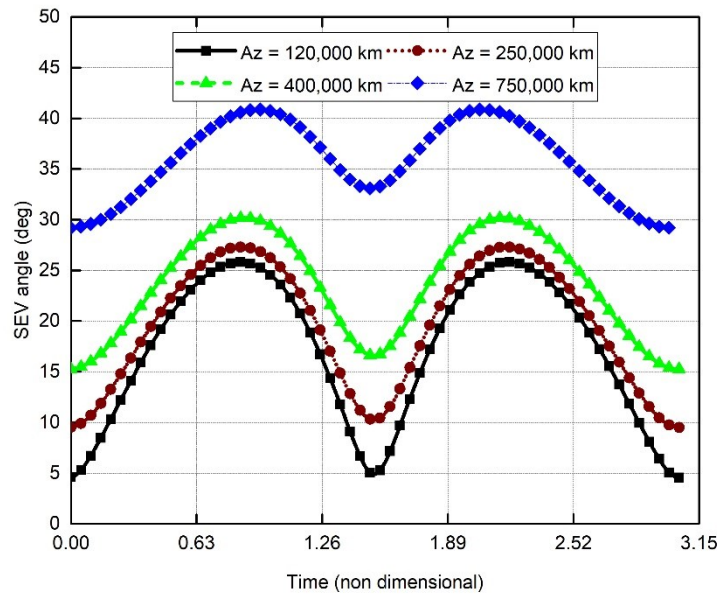


Figure 5.1 Variation of SEV angle along different halo orbits.

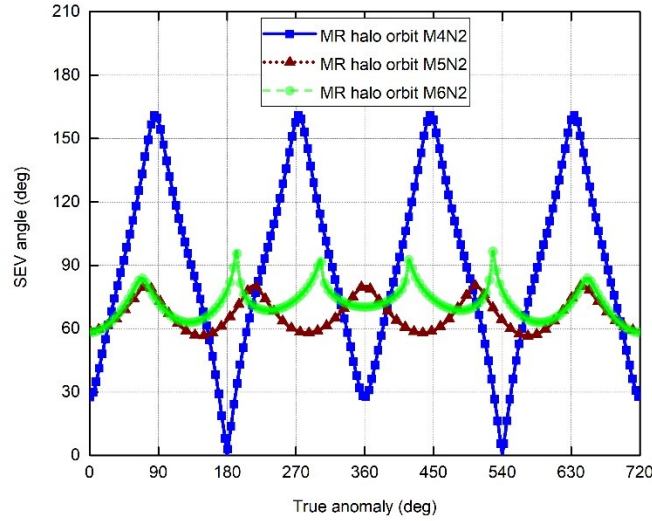


Figure 5.2 Variation of SEV angle along different MR halo orbits

It can be clearly seen from Figure 5.1 and Figure 5.2 that the MR halo orbits (and some of the halo orbits) do not satisfy the constraint on SEV angle. Therefore, it can be concluded that the MR halo orbits in the Sun-Earth system are not suitable for scientific missions. This is because their design is constrained by the commensurability condition. Therefore, the design of quasi-halo orbits of desirable amplitudes, independent of the commensurability constraint, is attempted. The quasi-halo orbit is designed using a differential evolution (DE) based technique and the design process together with numerical results are presented in the next subsection.

5.2 Design of Quasi-Halo Orbits

5.2.1 Design Process for Quasi-Halo Orbit in ERTBP and Optimal Numerical Design

5.2.1.1 Design Process

The proposed design process that uses DE is discussed in this section. The initial conditions of the quasi-halo orbit on the $x - z$ plane $[x_0, z_0, \dot{y}_0]$ are treated as unknowns and are determined using the differential evolution technique. Six equally spaced position vectors from the trajectory of the halo orbit in the CRTBP framework (starting from $t = 0$ and at an interval

of one-sixth the period) are used as the reference points and the deviations from these reference points are evaluated. The numerical propagation of ERTBP equations of motion is carried out until the deviation (D) from any one of the reference points exceeds a predefined value D_{max} . This deviation is evaluated as:

$$D = \sqrt{(x - x_{ref})^2 + (y - y_{ref})^2 + (z - z_{ref})^2} \quad (5.1)$$

where D is the deviation at the current point, $[x, y, z]$ is the position vector on the current design and $[x_{ref}, y_{ref}, z_{ref}]$ is the reference position vector. The smaller the value of D , closer is the generated orbit to the reference trajectory.

The objective function for the DE technique is set as the time till the generated orbit remains close to the reference CRTBP orbit (i.e. time till the deviation exceeds a predefined value). Mathematically, the objective function can be expressed as:

$$\text{Minimize} \quad OBJ1 = 1/(T_{bounded}) \quad (5.2)$$

where $T_{bounded}$ is the time spent in the vicinity of the reference orbit. The DE-based algorithm is terminated when the difference between the maximum and minimum of the objective function values of members in the population is less than a small value (1.0E-7).

5.2.1.2 Optimal Numerical Design

A typical design for $Az \sim 120,000$ km is presented in this section. The search bounds used for the unknown parameters are: $x_0 \in [0.9888, 0.9889]$, $z_0 \in [0.00087, 0.00090]$ and $\dot{y}_0 \in [0.0088, 0.0090]$. The allowed deviation from any reference point is set as $D_{max} = 500,000$ km. The propagation of the trajectory (one member of the population) is terminated when deviation exceeds 500,000 km and the objective function is evaluated. On convergence of the DE based process, the orbit completes nine revolutions. The converged initial conditions of the quasi-halo orbit in the ERTBP framework are:

$$x_0 = 0.988822122557681, z_0 = 0.000875665232609, \dot{y}_0 = 0.008923591446345$$

The trajectory and projections of the quasi-halo orbit are presented in Figure 5.3.

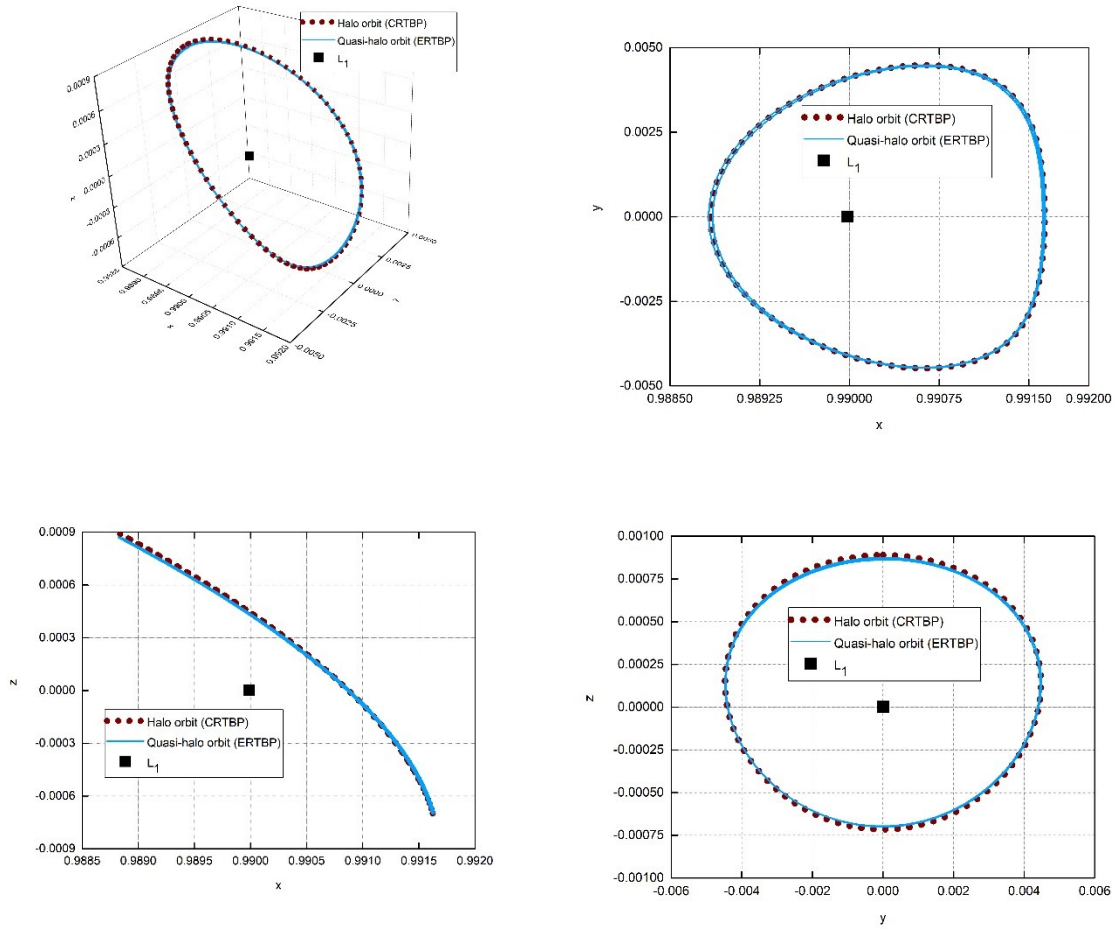


Figure 5.3 Trajectory and projections of the CRTBP halo orbit and nine revolutions of ERTBP quasi-halo orbit ($Az \sim 120,000$ km)

5.2.2 Design Process for Quasi-Halo Orbit in the SEM Ephemeris Model and Optimal Numerical Design

5.2.2.1 Design Process

The initial conditions of the quasi-halo orbit on the $x - z$ plane $[x_0, z_0, \dot{y}_0]$ are treated as unknowns and are determined using the differential evolution technique. These states are in the barycentric rotating frame and they are used after transforming the state vector of the spacecraft to geocentric inertial frame. The ephemeris designs of the quasi-halo orbits based on the CRTBP and ERTBP reference designs are generated. That means, the trajectories of halo orbit in the CRTBP framework and quasi-halo orbit in the ERTBP framework are used as reference

trajectories. For the ephemeris design of quasi-halo orbit based on the CRTBP framework, six equally spaced position vectors from the trajectory of the halo orbit (starting from $t = 0$ and at an interval of one-sixth the period) are used as the reference points and the deviations from these reference points are evaluated. The reference points for all the revolutions of the orbit in the ephemeris model remain the same (because the theoretical halo orbit repeats itself, independent of the time).

For the ephemeris design of quasi-halo orbit based on the ERTBP framework, six equally spaced position vectors from the first revolution of the quasi-halo orbit (starting from $t = 0$ and at an interval of one-sixth the period) are used as the reference points to generate first revolution in ephemeris model and the deviations from these reference points are evaluated. Likewise, to generate the second revolution of ephemeris model, the reference points are drawn from the second revolution of ERTBP model and the deviations from these reference points are evaluated. This process is repeated for all revolutions. The numerical propagation of N – *body* equations of motion is carried out until the deviation (D) from any one of the reference points exceeds a predefined value D_{max} . The DE-based algorithm is terminated when the difference between the maximum and minimum of the objective function values of members in the population is less than a small value (1.0E-7).

5.2.2.2 Optimal Numerical Design

A typical numerical design for $Az \sim 120,000$ km is presented in this section. The search bounds used for the unknown parameters are: $x_0 \in [0.9888, 0.9889]$, $z_0 \in [0.00085, 0.00090]$ and $\dot{y}_0 \in [0.0088, 0.0092]$. The initial epoch (at the $x - z$ plane crossing) is chosen as 01 January 2020, 00:00:00 TDB. This choice facilitates comparison of the results with the existing results in the literature. The allowed deviation from any reference point is set as $D_{max} = 500,000$ km. The propagation of the design in the DE-based process is terminated when the deviation exceeds 500,000 km. On convergence (when the maximum objective function value and minimum objective function value do not differ more than a very small value), the orbit is found to complete ten revolutions (specified in terms of $T_{bounded}$). The converged initial conditions of the quasi-halo orbits in the SEM ephemeris model are summarised in Table 5.2.

Table 5.2 Initial conditions of quasi-halo orbits in different frameworks

Orbit, Framework	x_0	z_0	\dot{y}_0
Halo orbit, CRTBP	0.988838391007297	0.000889601600193	0.008960601048476
Quasi-halo orbit, ERTBP	0.988822122557681	0.000875665232609	0.008923591446345
Quasi-halo orbit in ephemeris model (ref. design: CRTBP)	0.988841753673017	0.000867356410729	0.008951085008246
Quasi-halo orbit in ephemeris model (ref. design: ERTBP)	0.988824123167407	0.000861156195236	0.009098786677194

From Table 5.2, it can be found that the initial conditions of different orbits are very close and brings out the sensitivity of the dynamics. The trajectory and projections of the quasi-halo orbits in the ephemeris model based on the CRTBP and ERTBP frameworks are presented in Figure 5.4 and Figure 5.5 respectively.

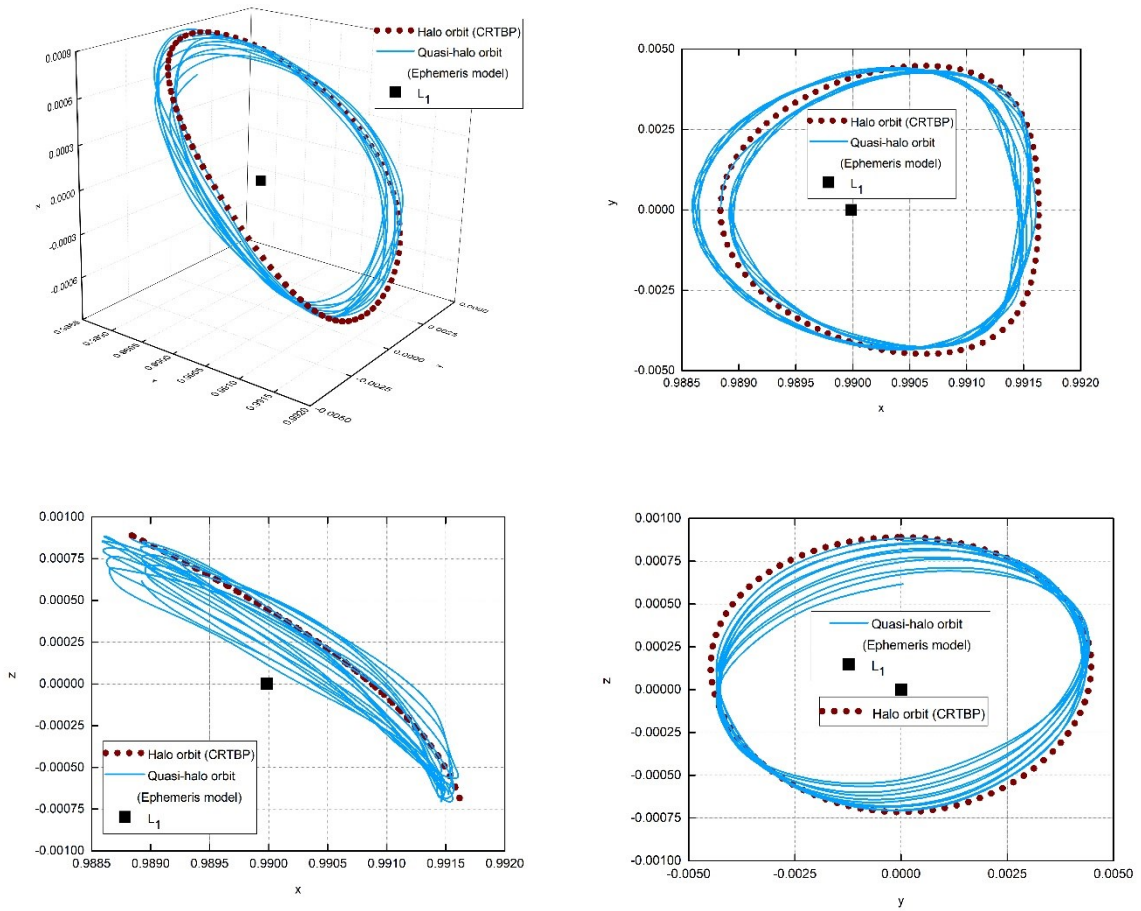


Figure 5.4 Trajectory and projections of the CRTBP halo orbit and ephemeris quasi-halo orbit ($Az \sim 120,000$ km)

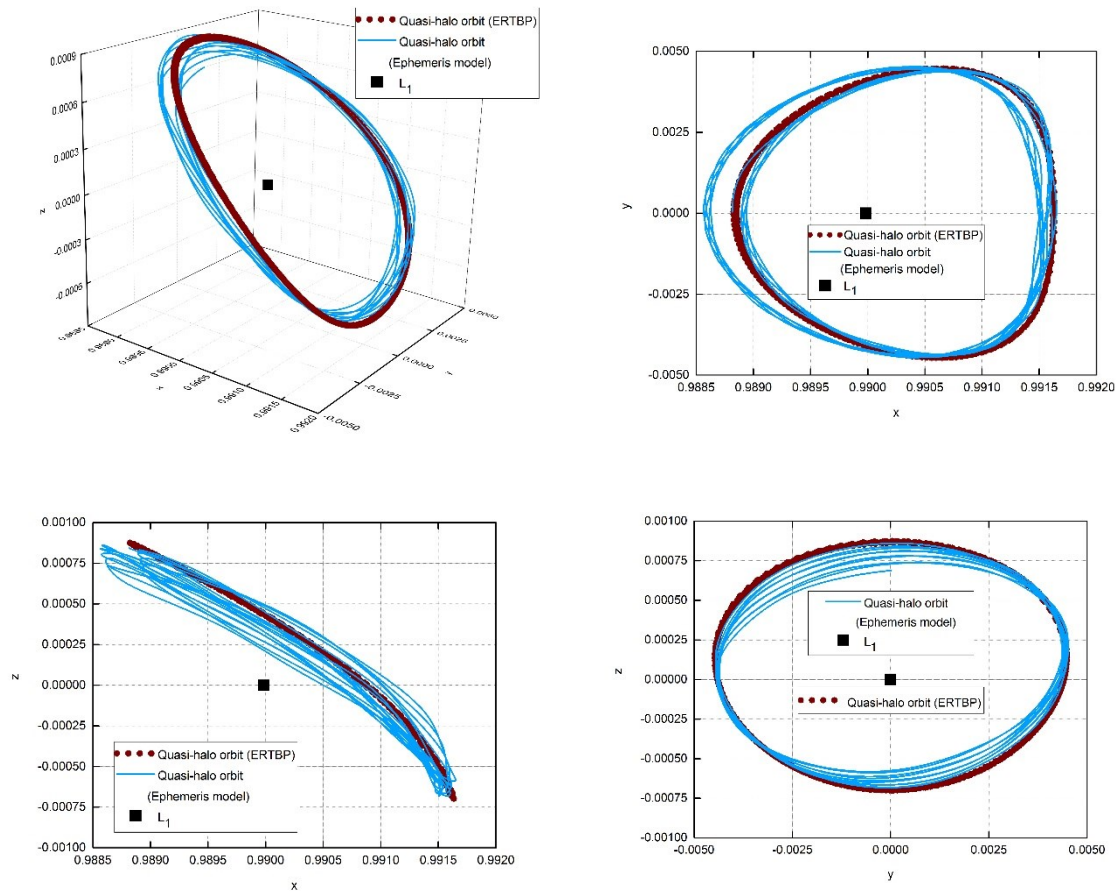


Figure 5.5 Trajectory and projections of the ERTBP quasi-halo orbit and ephemeris quasi-halo orbit ($Az \sim 120,000$ km)

The comparison of average Az amplitudes and computational effort for the design of quasi-halo orbits in the SEM ephemeris model based on CRTBP halo and ERTBP quasi-halo reference trajectories is presented in Table 5.3.

Table 5.3 Comparison of ephemeris designs of quasi-halo orbits

Reference framework/Orbit	Average Az amplitude (km)	No of generations in DE for convergence (10 revolutions of orbit)	Computational time (minutes)
CRTBP, halo	107,378.4	492	41.59
ERTBP, quasi-halo	107,695.3	453	40.32

The computation time is marginally less for the second row but it must be kept in mind that the ERTBP quasi halo orbit generation needs CRTBP orbit as the reference which needs some computer time. So, from the computational time point of view, using CRTBP halo orbit as the reference is beneficial. Further the average amplitude is also nearly same and there is no significant difference in the initial conditions of the orbits (c.f. Table 5.2). *Therefore, it can be concluded that the CRTBP framework captures the major dynamics of the SEM ephemeris model well and that the use of ERTBP framework for the design of orbits doesn't result in any significant advantage over the CRTBP framework.*

5.2.3 Evolution of Radial Distance and Velocity in Quasi-Halo Orbit.

Two parameters: radial distance from the Earth to the spacecraft and velocity of spacecraft in the quasi-halo orbit in the SEM ephemeris model are analysed (similar to the analysis of MR halo orbits, c.f. Section 4.2.3.4). The radial distance is an important parameter for communication system and the velocity in the quasi-halo orbit is an important parameter for the orbit maintenance aspects. The evolution of radial distance is presented in Figure 5.6 and the evolution of velocity is presented in Figure 5.7.

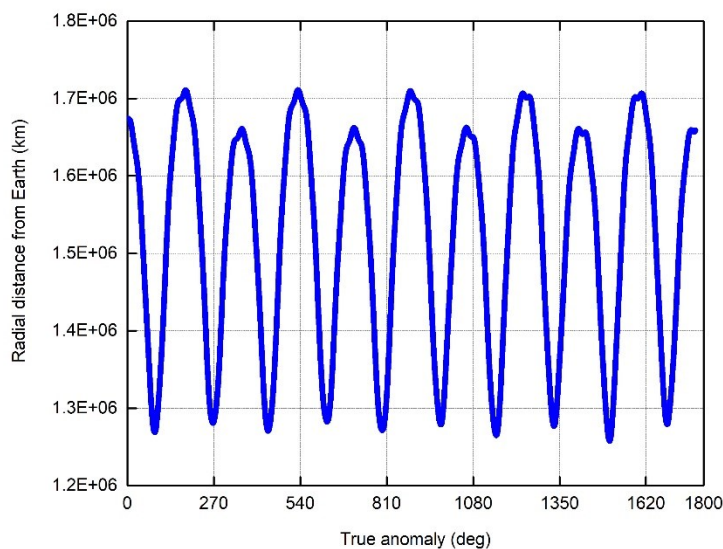


Figure 5.6 Evolution of radial distance from the Earth in quasi-halo orbit ($A_z \sim 120,000$ km)

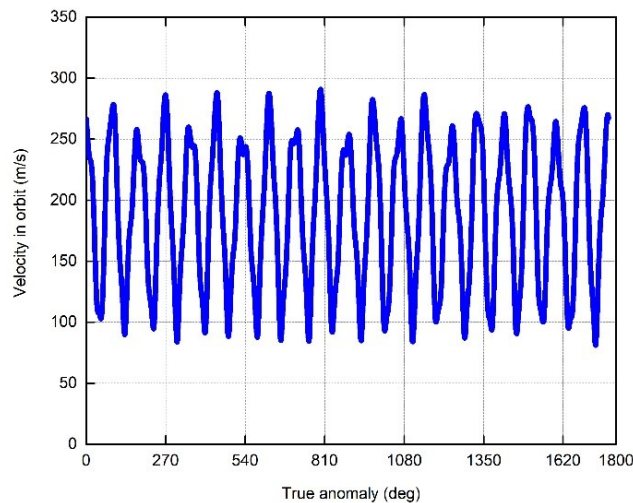


Figure 5.7 Evolution of velocity in quasi-halo orbit ($Az \sim 120,000$ km)

From Figure 5.6 and Figure 5.7, it can be observed that the evolutions of both radial distance and velocity are periodic with multiple revolutions of the quasi-halo orbit. The maximum radial distance from the Earth is 1,711,274.52 km and the minimum is 1,257,882.08 km. The variation is about 26.5% and these numbers can be helpful in arriving at some of the communication system requirements. The maximum velocity in the quasi-halo orbit is 290.74 m/s and the minimum is 81.10 m/s. This amounts to a larger variation (compared to the variation in radial distance) of about 72.10%. The larger variation in the velocity in quasi-halo orbit implies that the planning of orbit maintenance strategies should be done meticulously.

5.2.4 Design of Quasi-Halo Orbits for Different Az Amplitudes

Using the design methodology proposed in Section 5.2.2, multi-revolution quasi-halo orbits in the SEM ephemeris model are generated for different average Az amplitudes. The initial conditions are presented in Table 5.4. The CRTBP orbit is used as reference model.

Table 5.4 Design of quasi-halo orbits in SEM ephemeris model for different Az amplitudes

Az amplitude (km)	x_0	z_0	\dot{y}_0
120,000	0.988824123167407	0.000861156195236	0.009098786677194
280,000	0.988869895229647	0.001988630840825	0.009461133780860
400,000	0.988963693988393	0.003286463805709	0.010249067905969
750,000	0.989271005017044	0.005807748533241	0.012843041555238

Wu et. al (2019) report a five revolution quasi-halo orbit without any maneuver having Az amplitude around 280,000 km. Further, they mention that extension to a ten revolution orbit requires a one-time maneuver of magnitude 8.77897 m/s. The proposed design methodology based on DE generates a ten revolution quasi-halo orbit without *any* maneuvers and has demonstrated that generation of orbits for a wide range of Az amplitudes is possible.

5.2.5 Validation of the Design of the Orbit in the SEM Ephemeris Model

The design of the quasi-halo orbit in the SEM ephemeris model (based on CRTBP halo orbit) is simulated using the GMAT software (NASA, 2016. General Mission Analysis Tool (GMAT) v.R2016a) for validation purposes. The force model in GMAT is chosen to be consistent with the design force model (the Earth as the primary body, the Sun and the Moon as the perturbing bodies and using spherical gravity model for the Earth) and the values of the constants (such as mass ratio, eccentricity etc.) in GMAT are used for generating the design simulation. From the available options, Prince Dormand 7/8 is selected as the numerical integrator in the GMAT software. Because of the different numerical integrator, the two trajectories under comparison are expected to deviate if propagated for a long duration. Therefore, only the first revolution of the quasi-halo orbit, in two segments, is simulated using GMAT for validation purposes. The first segment consists of the part of the trajectory of the quasi-halo orbit from the initial point ($t = 0$) to the second $x - z$ plane crossing on the other side of the Lagrangian point. The second segment starts from the second $x - z$ plane crossing to the third $x - z$ plane crossing near the initial point.

The initial conditions of the first segment of the designed orbit in the SEM ephemeris model expressed in the geocentric inertial J2000 frame are:

$$\begin{aligned}x &= -284277.2999961 \text{ km}, y = 1457512.46619951 \text{ km}, \\z &= 773181.11479972 \text{ km}, \dot{x} = -0.076084145355360 \text{ km/s}, \\ \dot{y} &= -0.011707959109131 \text{ km/s}, \dot{z} = -0.005451745053657 \text{ km/s}.\end{aligned}$$

The initial epoch is 1st January 2020, 00:00:00 TDB. The numerical integration is carried out till the crossing of the $x - z$ plane. The step size used for GMAT simulation is same as the one used in the design generation.

The simulation in the GMAT software closely matches with the simulation of this study. The differences between the position and velocity vectors of this study and the GMAT simulation at the first $x - z$ plane crossing are 8017.28 km (0.63%) and 4.31 m/s (0.82%) respectively.

The initial conditions of the second segment of the designed orbit in the SEM ephemeris model expressed in the geocentric inertial J2000 frame are:

$$\begin{aligned}x &= -1247474.749542988 \text{ km}, y = -153169.4647721561 \text{ km}, \\z &= -181289.6994107395 \text{ km}, \dot{x} = 0.072036605231812 \text{ km/s}, \\ \dot{y} &= -0.477808620353184 \text{ km/s}, \dot{z} = -0.207084071645437 \text{ km/s}.\end{aligned}$$

The epoch at the beginning of the second segment is 29th March 2020, 15:37:52 TDB. The numerical integration is carried out till the crossing of the $x - z$ plane.

The differences between the position and velocity vectors of this study and the GMAT simulation evaluated at the second $x - z$ plane crossing are 6506.57 km (0.38%) and 2.88 m/s (3.06%) respectively. The small differences in these simulations can be attributed to the simulation using a different numerical integrator in GMAT (Prince Dormand 7/8) compared to that used for the generation of the design (Runge-Kutta-Fehlberg 7/8). A reasonably good match is obtained which validates the design process and transformations. The $x - y$ projections of the design trajectory and GMAT simulation in the inertial J2000 frame are presented in Figure 5.8.

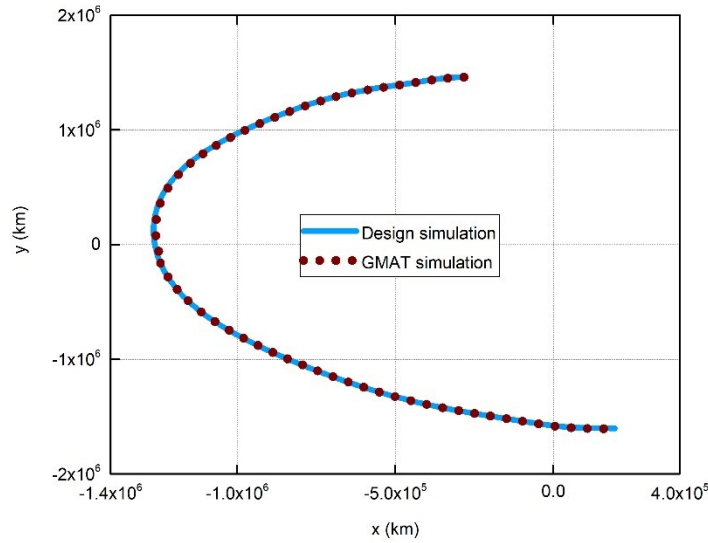


Figure 5.8 Comparison of design simulation and GMAT simulation of the first revolution of quasi-halo orbit.

5.3 Design of Optimal Transfers to Quasi-Halo Orbits

5.3.1 Design Philosophy

The optimal transfer trajectories to multi revolution quasi-halo orbits in the SEM ephemeris model are generated. In such transfers, the first maneuver (ΔV_{EPO}), known as trans-halo orbit maneuver, is given from Earth Parking Orbit (EPO) such that it injects the space vehicle directly into the single segment transfer trajectory and the space vehicle reaches the quasi-halo orbit around the Lagrangian point. The second impulse $\Delta \vec{V}_{TOI}$ is imparted to insert the space vehicle into the target orbit. In the design process, the location of the insertion on the target orbit and components of the velocity impulse $[\Delta \dot{x}, \Delta \dot{y}, \Delta \dot{z}]$ required for target orbit insertion (TOI), $\Delta \vec{V}_{TOI}$ are treated as unknown design parameters and obtained using the DE based procedure. These components are added to the current velocity on the target orbit at the chosen location and backward propagation of N -body equations of motion is carried out. The unknown components are chosen such that, on backward propagation, the desired closest approach altitude CAA from the Earth is achieved. The numerical propagation is ended when CAA is

achieved and this CAA need not be desired value. In order to accomplish the desired CAA by minimizing the velocity impulse, an objective function $OBJ2$ is set as:

$$OBJ2 = W_h \frac{|CAA_{achieved} - CAA_{desired}|}{S - E \text{ distance}} + W_v |\Delta \vec{V}_{TOI}| \quad (5.3)$$

where

$$|\Delta \vec{V}_{TOI}| = \sqrt{\Delta \dot{x}^2 + \Delta \dot{y}^2 + \Delta \dot{z}^2} \quad (5.4)$$

The objective function is normalized in consistent with the normalized equations of motion and the weights W_h and W_v are introduced to handle the different magnitudes of the terms. The first term is divided by the average Sun-Earth distance ($S - E \text{ distance} = 149597870.7$ km), because the CAA is expressed in physical units. After a few trial runs, the weights are chosen as $W_h = 10$, $W_v = 0.1$ for the cases where the trajectories flyby the Earth and $W_h = 1$, $W_v = 10$ where the trajectories pierce through the Earth. To avoid piercing, the velocity components are penalized heavily. The closest approach altitude from the Earth (CAA) is assumed to be 200 km for all the transfers and a 200 km circular orbit is assumed for Earth parking orbit for the computation of velocity impulse. These choices facilitate comparison of the results with the existing results in the literature. The numerical process based on DE is ended when the difference between the maximum and minimum of the objective function values of members in the population is less than a small value ($1.0E-7$). The trans-orbit maneuver (ΔV_{EPO}) is computed as the vectorial difference of geocentric velocity of the spacecraft at CAA in the transfer trajectory (on numerical backward propagation) from the velocity of spacecraft in the chosen circular EPO. The total velocity impulse required for the transfer, ΔV_{TOTAL} is computed as the sum of orbit insertion velocity and velocity impulse from EPO.

5.3.2 Optimal Two Impulse Transfer to Quasi-Halo Orbit in the ERTBP Framework

The search bounds for the unknown velocity components $[\Delta \dot{x}, \Delta \dot{y}, \Delta \dot{z}]$ are set as $[-200, 200]$ m/s. The location of insertion is constrained to lie in the first revolution $[(0, 177.885)$ days] of the quasi-halo orbit to maximise the time spent in the orbit. The flight duration is restricted to be less than 200 days. After adding the randomly selected velocity perturbations to the state vector at a randomly selected location on the target orbit, backward numerical propagation of

equations of motion in the ERTBP framework is carried out and stopped when the *CAA* is reached and the objective function *OBJ2* is evaluated. This process is repeated till convergence.

The optimal transfer that minimizes the velocity impulse while achieving the desired *CAA* leads to the insertion in a location corresponding to 104.85587 days and requires 26.99 m/s for target orbit insertion. The corresponding flight duration is 122.92261 days. This optimal transfer requires a total velocity impulse of 3334.81 m/s. Figure 5.9 depicts the $x - y$ projections of the optimal transfer trajectories from 200 km circular EPO to the quasi-halo orbit.

Table 5.5 Optimal transfer in the ERTBP framework

Target orbit and framework	Orbit insertion velocity, $ \Delta\vec{V}_{TOI} $ (m/s)	Velocity impulse from EPO, ΔV_{EPO} (m/s)	Total velocity impulse (m/s)	Orbit insertion location (days)	Flight time (days)
Quasi halo orbit, ERTBP	26.99	3307.82	3334.81	104.8556	122.9226

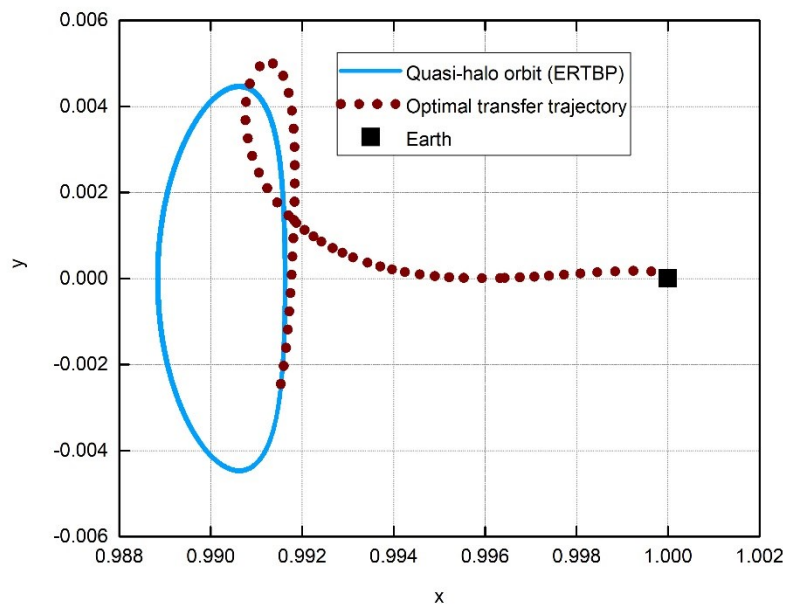


Figure 5.9 $x - y$ projection of the optimal transfer trajectory to the quasi-halo orbit.

5.3.3 Optimal Transfers in the SEM Ephemeris Model

The optimal transfer to the quasi-halo orbit in the SEM ephemeris model is generated. The quasi-halo orbit in the ephemeris model generated using the CRTBP halo orbit is used as the target orbit. The randomly selected velocity perturbations are added to the velocity vector at a randomly selected location on the target orbit. The initial epoch at the orbit insertion point corresponding to $t = 0$ is 1st January 2020, 00:00:00 TDB (c.f. section 5.2.2.2). The state vector of the spacecraft in the barycentric rotating frame is transformed to the geocentric inertial J2000 frame and backward numerical propagation of N -body equations of motion is carried out till the CAA is reached and the objective function $OBJ2$ is evaluated. This process is repeated till convergence. The location of insertion is constrained to lie in the first revolution $[(0, 177.885)$ days] of the quasi-halo orbit to maximise the time spent in the orbit. The search bounds for the unknown velocity components $[\Delta\dot{x}, \Delta\dot{y}, \Delta\dot{z}]$ are set as $[-200, 200]$ m/s. The flight duration is restricted to be less than 200 days.

Table 5.6 presents the optimal transfer to the quasi-halo orbit in the ephemeris model. The epoch at the orbit insertion is 06 September 2019, 16:32:28 TDB (obtained by backward propagation from the epoch at initial state of the orbit). The $x - y$ projections of the optimal transfer trajectories to the quasi-halo orbit based on CRTBP is depicted in Figure 5.10.

Table 5.6 Optimal transfer in the SEM Ephemeris model

Target orbit and framework	Quasi-halo orbit insertion velocity, $ \Delta\vec{V}_{TOI} $ (m/s)	Velocity impulse from EPO, ΔV_{EPO} (m/s)	Total velocity impulse (m/s)	Orbit insertion location (days)	Flight time (days)
Quasi-halo, ephemeris model	32.28	3197.09	3229.36	95.12989	116.30058

From Table 5.6, it can be observed that the cost of transfer in the ephemeris model (3229 m/s) is less compared to the corresponding transfers (3280 m/s) in the CRTBP framework. This confirms the intuitive understanding that the designs in CRTBP framework are conservative in nature and that the least transfer cost is obtained when the complete design is constructed in the ephemeris model. Further, although there is a slight advantage in constructing transfer to

the quasi-halo orbit based on ERTBP framework, the impulse velocity difference is not very significant (the difference is only about 14 m/s). *Therefore, it can be concluded that there is no significant advantage of using ERTBP framework over the CRTBP framework to construct optimal transfers to target orbits.*

The closeness of the initial approximations using CRTBP and ERTBP frameworks for the two design aspects (design of orbit around Lagrangian point and optimal transfer to the orbit) are found to be nearly same. Hence it can be inferred that the CRTBP framework is sufficient to capture the major dynamics near the Sun-Earth Lagrangian points.

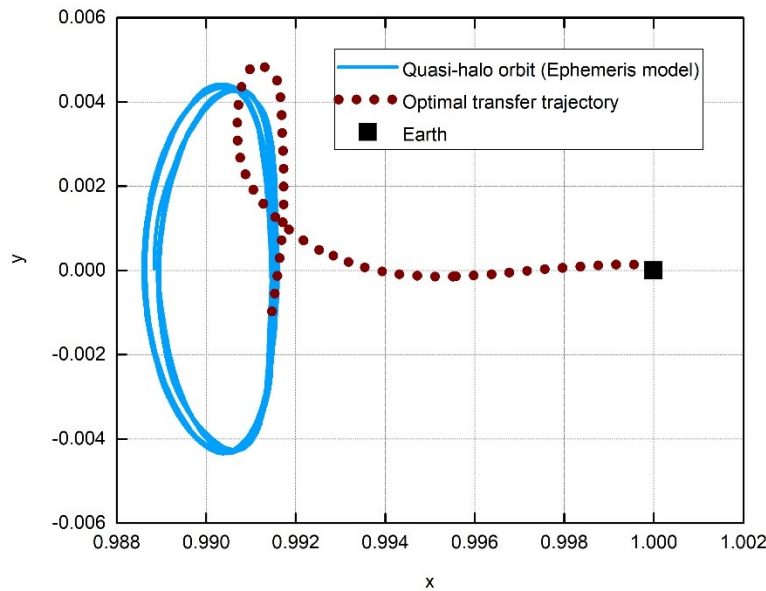


Figure 5.10 $x - y$ projection of the optimal transfer trajectory to the quasi-halo orbit based on CRTBP framework.

5.3.4 Validation of the Design of the Transfer Trajectory in the SEM Ephemeris Model

The design of the transfer trajectory in the SEM ephemeris model is simulated using the GMAT software for validation purposes. The transfer presented in Table 5.6 is considered for validation. For the transfer trajectory that has flight duration of 116.3 days, the state vector at the orbit insertion point, expressed in the geocentric inertial J2000 frame is: [-1097925.3220657, -629549.3439829, -374581.825637, 0.211254520517545, -0.451707694085133, -0.179827258794694] at the epoch 31 August 2019, 14:09:58 TDB. The

units are km and km/s for position and velocity components respectively. For reasons mentioned in Section 5.2.5, the design transfer trajectory is also simulated using GMAT in two segments. On backward propagation for flight duration from the insertion point, the transfer trajectory simulated in GMAT approaches the Earth with a *CAA* of 1670.26 km (design *CAA* is 200 km). The trajectory remains in the neighbourhood of simulation of the ephemeris design, as depicted in Figure 5.11. A reasonably good match is obtained which validates the design process and transformations. A perfect match did not happen because the numerical integrator is different (Prince Dormand 7/8 in GMAT and Runge-Kutta-Fehlberg 7/8 for design generation). It is well known that the designs under complex dynamics are extremely sensitive to numerical integrator and step size.

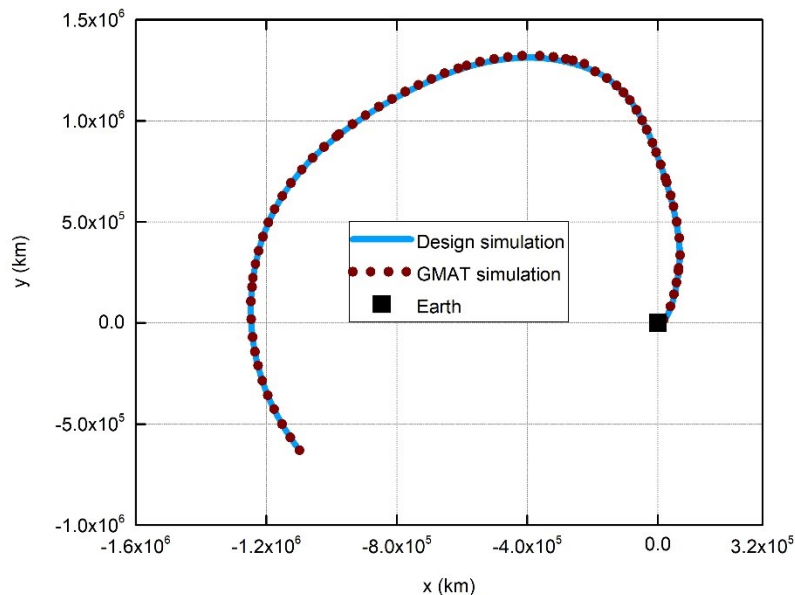


Figure 5.11 GMAT simulation of design of transfer trajectory in the SEM ephemeris model

5.3.5 Sensitivity of the Transfer Trajectory Design

The sensitivity of the transfer trajectory design in the SEM ephemeris model to the changes in the initial conditions is analysed. This is done by introducing some small *additional* perturbations (in addition to the perturbation velocity components $\Delta\vec{V}_{TOI}$) to the converged initial conditions of the optimal velocity vector at the quasi-halo insertion point and the backward propagation of numerical integration of SEM ephemeris equations of motion is carried out till the first close approach to the Earth. The *additional* perturbations are added only

to the velocity vector (*and not the position vector*) to simulate the actual thrusting scenario and are added one component at a time (that means to x , y or z component at a time). The resulting close approach is compared to the optimal close approach in terms of the flight duration and the closest approach distance, CAA . The characteristics of the optimal transfer mentioned in Section 5.3.3 are as follows:

- Optimal quasi-halo orbit insertion velocity components, $\Delta\vec{V}_{TOI}$: [-24.1166, -21.2575, -2.9861] m/s magnitude = 32.2864 m/s.
- CAA achieved: 200.6854 km
- Flight duration: 116.30058 days

The magnitude of *additional* perturbation velocity is varied from 0.1 m/s to 0.5 m/s and amounts to the following: 0.4146% to 2.0732% of x component of optimal velocity component $\Delta\vec{V}_{TOI}$, 0.4704% to 2.3521% of y component of optimal velocity component $\Delta\vec{V}_{TOI}$ and 3.3488% to 16.7442% of z component of optimal velocity component $\Delta\vec{V}_{TOI}$. The results of the sensitivity analysis are presented in Table 5.7.

Table 5.7 Sensitivity analysis of transfer trajectory design in SEM ephemeris model

Magnitude of additional perturbation (m/s)	Sign of perturbation	Perturbed in which component:	Resulting CAA (km)	Resulting flight duration (days)
0.1	+ / -	x	778.92 / 962.11	116.53341 / 116.10821
	+ / -	y	3149.13 / 1918.05	116.03867 / 116.54086
	+ / -	z	732.91 / 3126.82	116.40069 / 116.15692
0.2	+ / -	x	5227.98 / 1157.70	116.47590 / 115.96304
	+ / -	y	3671.47 / 2510.82	116.19373 / 116.51401
	+ / -	z	4075.45 / 2796.54	116.46136 / 116.41309
0.5	+ / -	x	15275.94 / 1154.27	117.41178 / 115.65454
	+ / -	y	820.02 / 12038.29	115.74909 / 117.22702
	+ / -	z	1863.76 / 4285.05	116.45488 / 116.07808

From Table 5.7, it can be inferred that the closest approach altitude CAA aspect of transfer trajectory design is highly sensitive with velocity components, but the flight duration is not. There is no visible common trend with increasing additional perturbation velocity

magnitude. With respect to the optimal transfer ($CAA = 200.6854$ km), the additional perturbed transfer results in 289.46% to 7537.97% when perturbed in x component, 310.01% to 5919.14% in y component and 266.45% to 2042.52% in z component for the above mentioned perturbation velocities. The flight duration varies only by 0.225% (lesser) and 0.955% (more) compared to the optimal transfer. These results emphasize the importance of ensuring precise injection into the quasi-halo orbit.

5.4 Conclusions

It is found that the periodic MR halo orbits around the Lagrangian point in the Sun-Earth system are not feasible for scientific missions like ISEE3 because of large amplitudes. As an alternative, quasi-halo orbits are designed. The proposed design process which uses differential evolution technique, produces a quasi-halo orbit of any desirable out-of-plane amplitude under ERTBP framework independent of system period. This quasi-halo orbit and the CRTBP orbit are used as reference designs and the quasi-halo orbit design is obtained in the higher fidelity SEM ephemeris model. The design methodology based on DE generates a ten revolution quasi-halo orbit (previously reported is five) without *any* maneuvers and has demonstrated that generation of orbits for a wide range of Az amplitudes is possible. Both the CRTBP and ERTBP reference designs generate the ephemeris design and there is no noticeable advantage of considering ERTBP reference design. Transfers under three frameworks (CRTBP, ERTBP and ephemeris) were executed and the total cost for transfer under ERTBP framework is the highest (3334 m/s) and the total cost under the ephemeris framework is 3229 m/s. The transfer cost under CRTBP framework (3290 m/s) lies in between these two costs and more close to ERTBP cost. The closest approach distance to the Earth in the transfer trajectory design is found to be very sensitive to velocity perturbations.

Chapter 6: Mission Design in the Earth-Moon System under the ERTBP framework

Chapter Summary

This chapter gives an account of the preliminary Lagrangian point mission design in the Earth-Moon system under the ERTBP framework. The two steps of mission design (halo orbit design and transfer trajectory design) are accomplished under the ERTBP framework. The success of Differential Evolution (DE) in the Sun-Earth system is the motivation to try DE in the Earth-Moon system. The existing literature uses a differential correction (DC) based technique for the design of MR halo orbits. In this methodology, the MR halo orbit is divided into multiple segments and numerical continuation on eccentricity is performed to arrive at the final design the MR halo orbit. The problem formulation using the DC technique also renders it highly sensitive to initial conditions. An alternative scheme based on differential evolution is proposed which avoids the continuation on eccentricity and treats the MR halo orbit as a single segment. Multithreading technique is employed to reduce the computational time. The design and analysis of different MR halo orbits in the Earth-Moon system are presented. It is found that, the Az amplitude of MR orbit Earth-Moon system under the ERTBP framework is comparable with that of under CRTBP framework and so, can be used for scientific missions.

For the design of transfer trajectories to MR halo orbits in the Earth-Moon system, the manifolds theory is popularly used in the existing literature. Because the manifolds in the Earth-Moon system do not pass close to the Earth, the transfers leveraging manifolds theory involves a bridge maneuver that transfers the space vehicle from the trans-halo trajectory to the stable manifold originating from the halo orbit making the number of maneuvers three. Alternately, a technique that generates two impulse transfer trajectories to MR halo orbits employing differential evolution is proposed. Unlike in the other transfer techniques which divide the transfer trajectory into multiple segments, the proposed technique designs the transfer trajectory in a single segment. In the proposed technique, the location of insertion into the MR halo orbit and the components of the insertion velocity are treated as unknowns and obtained using differential evolution. The optimal solutions indicate that there exist trajectories with

lower cost and for significantly lower time of flight than those reported in the literature for similar problems.

6.1 Introduction

This chapter is the third of the three chapters (4, 5 and 6) describing the mission design to Lagrangian points under the ERTBP framework. In this chapter, the preliminary mission design around the Lagrangian points in the Earth-Moon system is presented. The two steps of mission design (halo orbit design and transfer trajectory design) are accomplished under the ERTBP framework. The success of design of these two steps utilizing Differential Evolution (DE) in the Sun-Earth system is the motivation to try DE in the Earth-Moon system. The existing literature (Peng and Xu, 2015a) uses a differential correction (DC) based technique for the design of MR halo orbits. In this methodology, the MR halo orbit is divided into multiple segments and numerical continuation on eccentricity is performed to arrive at the final design the MR halo orbit. The problem formulation using the DC technique also renders it highly sensitive to initial conditions. An alternative scheme based on DE is proposed which avoids the continuation on eccentricity and treats the MR halo orbit as a single segment.

For the design of transfer trajectory in the Earth-Moon system, the manifold theory is popularly used in the literature. Because the manifolds in the Earth-Moon system do not pass close to the Earth (the minimum CAA is around 3000 km for halo orbits of Az amplitude around 15,000km), the transfers leveraging manifolds theory involves a bridge maneuver that transfers the space vehicle from the trans-halo trajectory to the stable manifold originating from the halo orbit making the number of maneuvers three. Alternately, a technique that generates two impulse transfer trajectories to MR halo orbits employing differential evolution is proposed. Unlike in the other transfer techniques which divide the transfer trajectory into multiple segments, the proposed technique designs the transfer trajectory in a single segment and identifies many optimal solutions not reported in the literature.

The next section describes the design of MR halo orbits in the Earth-Moon system employing a DE-based methodology.

6.2 Design of MR Halo Orbits

6.2.1 Terminology and Design Philosophy

The terminology and design philosophy are described in Chapter 4. For completeness sake, some salient features are repeated in this chapter. The MR halo orbits are three dimensional, perfectly periodic orbits in the ERTBP framework. Under the ERTBP framework, unlike in the CRTBP framework, these periodic orbits make multiple revolutions around the Lagrangian point before repeating the geometry. The MR halo orbits generated in this research are represented by the notation $MaNb$ where a and b are integers which denote the values of M and N respectively. In these periodic orbits, the third body completes M revolutions around the Lagrangian point while the primaries complete N revolutions around the barycentre. For example, an orbit $M5N2$ means the spacecraft makes five revolutions around the Lagrangian point while the primaries complete two revolutions around the barycentre. Clearly, these multi revolution orbits are $M:N$ resonant orbits in the ERTBP framework, where $M > 1$. This terminology is same as the one used by Peng and Xu (2015a). The periods of MR orbits (T_E) and the halo orbits in CRTBP (T_C) are related by the commensurable constraint (Peng and Xu, 2015a):

$$T_E = MT_C = 2N\pi \quad (6.1)$$

Peng et al. (2017) used halo orbit initial conditions in CRTBP to start the numerical continuation together with a multi-segment optimization method to obtain MR halo orbits in ERTBP. The multiple segments were used to avoid problems associated with numerically integrating the equations of motion for long term. The main problem, as indicated by them (Peng, Bai and Xu, 2017), is non-convergence when a single segment is used. As an alternative method, the design of MR orbits is attempted using a differential evolution based technique. In this method, the whole trajectory is considered as a single segment and the solution is obtained in a single level scheme without numerical continuation on eccentricity.

To generate the design of MR orbits, the equations of motion (c.f. (2.13)) are numerically integrated for half period with the randomly chosen values for the unknowns. The characteristic of the MR orbits is that they cross the $x - z$ plane orthogonally twice, at $t = 0$ and $t = T/2$ where T is the period (similar to halo orbits in CRTBP). At half-period, the y component must

be zero to ensure $x - z$ plane crossing and the velocity components \dot{x} and \dot{z} must be zeros to ensure the orthogonal crossing. Therefore, the initial state and the state at half period are given by $[x_0, 0, z_0, 0, \dot{y}_0, 0]$ and $[x_{T/2}, 0, z_{T/2}, 0, \dot{y}_{T/2}, 0]$ respectively. In order to accomplish the orthogonal crossing of $x - z$ plane, the objective function ‘OBJ4’ is set as:

$$OBJ4 = \sqrt{y_{T/2}^2 + \dot{x}_{T/2}^2 + \dot{z}_{T/2}^2} \quad (6.2)$$

The objective function is evaluated at the half period. The values of the unknowns that drive the objective function to zero, is chosen as the design. The differential evolution technique is used for the selection of suitable values that drives the objective function to zero.

The period of MR orbit, as discussed earlier, is given by $2N\pi$. For the design of an MR halo orbit in ERTBP, the search bounds are chosen around the design obtained in CRTBP. For obtaining the design in CRTBP, the equations of motion of ERTBP are numerically integrated with $e = 0$ till half period and the objective function is evaluated. In CRTBP, the period of the halo orbit is given by $2N\pi/M$ (c.f. Eq. (6.1)).

Note that the objective function does not include the Az amplitude of the orbit, as this information is not available for this problem. The period of the orbit which is known, is used to terminate the numerical propagation of equations of motion.

6.2.2 Computational Algorithm

Based on the design philosophy described in the previous sub-section, a step-by- step algorithm is described below.

- i. An initial population of size NP (number of members) is built. Each member (row) of the population consists of three unknowns $[x_0, z_0, \dot{y}_0]$ of the current problem, represented by \mathbf{U} vector and the value of the objective function. The values for these unknowns are chosen randomly from their respective bounds. The bounds are chosen based on relative geometry of Lagrangian point and Earth. To evaluate the objective function (c.f. Eq. (6.2), numerical integration of the equations of motion in the ERTBP framework (c.f. Eq. (2.13)) is carried out using Runge-Kutta-Fehlberg 7/8 integrator (RKF7/8) till the half period. Similarly, all the members (rows) of the initial population are generated and the initial population will be a $(NP \times 4)$ matrix.

- ii. A trial member, from the search bounds, is generated for each member of the current population through the processes of mutation, crossover and selection:
 - d. Mutation: A mutant member is generated using some randomly selected members from the current population such that they are not the same as the member under testing. A scaling factor denoted by F is used for the mutation process, and the mutant member \mathbf{V} is generated according to the relation $\mathbf{V}_i = \mathbf{U}_{R_1} + F(\mathbf{U}_{R_2} - \mathbf{U}_{R_3})$. Here R_1, R_2 and R_3 are three distinct random integers chosen from $[1, NP]$ and the variable i varies between 1 and NP . These members are chosen such that they are different from the element under testing (i member), that is R_1, R_2 and R_3 must not be equal to i .
 - e. Crossover: The member of the current population under testing and the mutant member together generate the trial member. A parameter ‘crossover frequency’ (CR) is used to generate a trial member (Price, Storn and Lampinen, 2005). A random number $rand(j)$ is generated between 0 and 1, for each component of the i^{th} member U for which trial member is to be generated. For each of the component (j), if $rand(j) > CR$, the j^{th} component of the i^{th} member of the current population is retained for the trial vector and if $rand(j) \leq CR$, the component in the trial vector is replaced with the j^{th} component of the mutant vector.
 - f. Selection: The objective function $OBJ1$ is evaluated for the trial member and the member under testing is replaced by this trial member if the objective function value is less.
- iii. The generation of trial member and subjecting the trial member to the above three operations are carried out for all the members in the current population and thus, a new population is generated.
- iv. The above mentioned steps are repeated till the convergence criterion is met, i.e., the minimum objective function value in the population is less than a pre-fixed small tolerance value (ϵ).

6.2.3 Results

6.2.3.1 Validation

For the MR halo orbit M5N2 in the Earth-Moon system, the period of halo orbit in the CRTBP framework will be $4\pi/5$. The initial conditions in CRTBP corresponding to the halo orbit of period $4\pi/5$ are obtained using the proposed method. They are:

$$x_0 = 0.852350553614168, z_0 = 0.178467743252220 \text{ and } \dot{y}_0 = 0.261607202654027.$$

The bounds for the generation of MR halo orbit M5N2 were chosen around the above mentioned CRTBP initial conditions. They are:

$$x_0 \in [0.851, 0.853], z_0 \in [0.175, 0.184], \dot{y}_0 \in [0.258, 0.263].$$

The initial conditions of MR halo orbit M5N2 are obtained using the proposed method. They are:

$$x_0 = 0.851666641652152, z_0 = 0.183285539178136 \text{ and } \dot{y}_0 = 0.258289722252683.$$

These values compare well with those reported by Peng and Xu (2015a) up to 8 decimal places. The 3D trajectory obtained by propagating the equations of motion with these initial conditions and its projections are depicted in Figure 6.1.

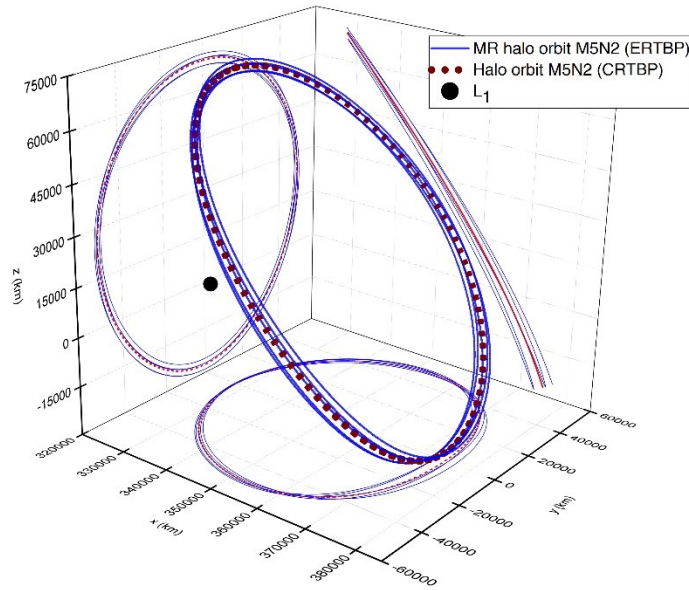


Figure 6.1. Trajectory and projections of MR halo orbit M5N2 around Earth-Moon L_1

6.2.3.2 Reduction in Computational Time using Multithreading

The computational time for the design of M5N2 orbit with the basic serial version of the code is around 702s. In order to get faster results, parallelisation of the code with multithreading technique is carried out. The multithreading implementation is done utilizing the OpenMP FORTRAN APIs (Miguel Hermanns, 2002). The workload of objective function evaluation, which is the most time consuming part, is distributed to multiple threads, employing a shared memory architecture. In this implementation, there is granular control over the number of threads and the division of workload of objective function evaluation. For example, if the number of threads is two, the objective function evaluation of 1-20 members (out of 40) of the current population is assigned to be handled by the first thread and the rest (21-40) members are handled by the second thread. All the computations are carried out in double precision. The performance results are shown in Table 6.1. Performance of DE with varying no of threads.

Table 6.1. Performance of DE with varying no of threads

No of threads	Computational Time (s)
1	702
2	377
3	439
4	343
5	397
6	448

The computational time is found to be varying with the number of threads used in parallel mode, as expected. The performance of the parallel codes is found to be better than the serial code in all cases. The performance with two threads is better compared to the serial version. The objective function evaluation of population size 40 being split up across the threads, three threads do not share the workload equally and one thread has to wait for others to complete their part of work. This is the reason attributed to more computational time for three threads compared to two threads. The best performance is obtained with four threads, possibly due to optimal workload sharing for this problem with the given parameters. The time taken for computation in this case is only about half of the serial version. Further increase in number of threads involves more effort of splitting and merging the threads, resulting in more computational time. Hence all further computations are performed with four threads.

6.2.3.3 Az Amplitudes of Halo Orbits and MR Halo Orbits

The Az amplitude of the halo orbits in the CRTBP framework is computed as half of the difference between the z coordinates at $t = 0$ and $t = T/2$ in the orbit. **The following procedure is introduced to represent the Az amplitude MR halo orbit: for each revolution, the difference between the z coordinates of the two successive x – z plane crossings is computed; the average of the differences of all revolutions is computed.** This average Az amplitude is used to represent MR halo orbit. For different MR halo orbits, the average along with minimum and maximum Az amplitudes are given in Table 6.2.

Table 6.2 *Az* amplitudes of MR halo orbits

MR halo orbit	<i>Az</i> amplitudes of MR halo orbit (km)			<i>Az</i> amplitude of halo orbit (km)
	Average	Maximum	Minimum	
M3N1	44163.02	47359.11	41155.45	44951.52
M5N2	47912.42	48999.70	46863.16	47957.10
M6N2	44145.71	47361.59	41137.68	44951.52

It is well known that *Az* amplitude uniquely defines a halo orbit in CRTBP. It can be seen from Table 6.2 that the average *Az* amplitude of MR halo orbit is nearly equal to the *Az* amplitude of corresponding circular halo orbit. This justifies the use of CRTBP as a reasonably good approximation to start the real mission design in ERTBP. Figure 6.1 shows the trajectory and projections of circular halo orbit also which demonstrates the above mentioned justification. In Figure 6.1, the coordinates are normalised with average Earth-Moon distance of 384,400 km.

6.2.3.4 Multiple Options of MR Halo Orbits with the Same Period

For the same period of the MR halo orbit, multiple options exist. That means, the third body makes different number of revolutions in the same period. For example, for a period of 4π , in which primaries make two revolutions, the MR halo orbit can be determined such that the third body makes 4,5 or 6 revolutions. They are represented as M4N2, M5N2 and M6N2 respectively. For the generation of initial condition of these multiple options, the search bounds are chosen around the corresponding CRTBP initial conditions. The CRTBP initial conditions along with the period used is given in Table 6.3. The ERTBP initial conditions along with the period used is given in Table 6.4.

Table 6.3. CRTBP initial conditions and period

MR halo orbit	x_0	z_0	\dot{y}_0	Period of halo orbit
M2N1	0.804887977215000	0.0000000000000000232	0.3186086654433988	π
M3N1	0.882568854469073	0.194545137496083547	0.2190398008015624	$2\pi/3$
M4N2	0.804887977215000	0.0000000000000000232	0.3186086654433988	π
M5N2	0.852350553614168	0.178467743252220692	0.2616072026540278	$4\pi/5$
M6N2	0.882568854469073	0.194545137496083547	0.2190398008015624	$2\pi/3$

Table 6.4 ERTBP initial conditions and period

MR halo orbit	x_0	z_0	\dot{y}_0	Period of MR halo orbit
M2N1	0.80412515695617723	0.0000000000000000029	0.31182413982453571	2π
M3N1	0.87540405286766474	0.20162065346824166	0.21551063837955558	2π
M4N2	0.80450465962601267	0.000000000000000020	0.31826866733409664	4π
M5N2	0.85166664165215278	0.18328553917813651	0.25828972225268384	4π
M6N2	0.87540405286604528	0.20162065346638729	0.21551063838292425	4π

6.2.3.5 Radial Distances of MR Halo Orbits from the Earth

The radial distance from the Earth to a spacecraft in MR halo orbit is an important parameter because it is a major design driver in the communication system. The radial distance, in effect, is the communication distance to the spacecraft from Earth and its variation for different orbits are presented in Figure 6.2 and Table 6.5. It can be observed that the variation in radial distance decreases as the number of third body revolutions (M) increases for orbits with same period. *Unlike in the Sun-Earth system, there is no drastic variation in the radial distance that helps the design of communication system.*

Table 6.5 Variation of radial distance and velocity in MR halo orbits

MR halo orbit	Maximum radial distance (km)	Minimum radial distance (km)	Maximum velocity in orbit (m/s)	Minimum velocity in orbit (m/s)
M2N1	3.9989e+05	3.0442e+05	509.2602	45.9498
M3N1	3.7766e+05	3.4075e+05	884.9211	219.0713
M4N2	3.4520e+05	3.0456e+05	387.4592	107.3186
M5N2	3.7294e+05	3.2990e+05	557.1879	262.5572
M6N2	3.7766e+05	3.4075e+05	884.9211	219.0713

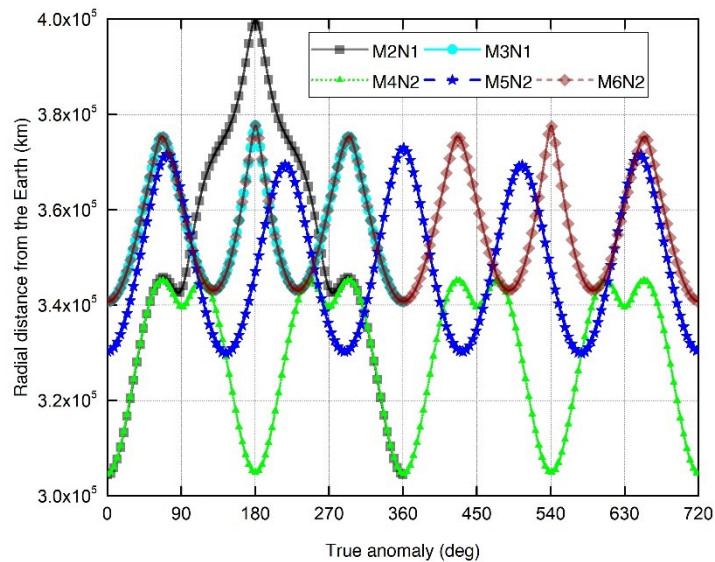


Figure 6.2 Evolution of radial distance from the Earth in MR halo orbits

6.2.3.6 Evolution of Velocity in MR Halo Orbits

The magnitude of velocity in the MR halo orbit is a critical parameter in the station keeping aspects of the orbit. The variation of magnitude of velocity at each point in the ME halo orbits is presented in Figure 6.3 and Table 6.5. It can be observed that the velocity in orbit increase when the number of third body revolutions increase (M). This is expected because the spacecraft is traversing longer distances in a given time. These results are useful in making choices among these multiple options.

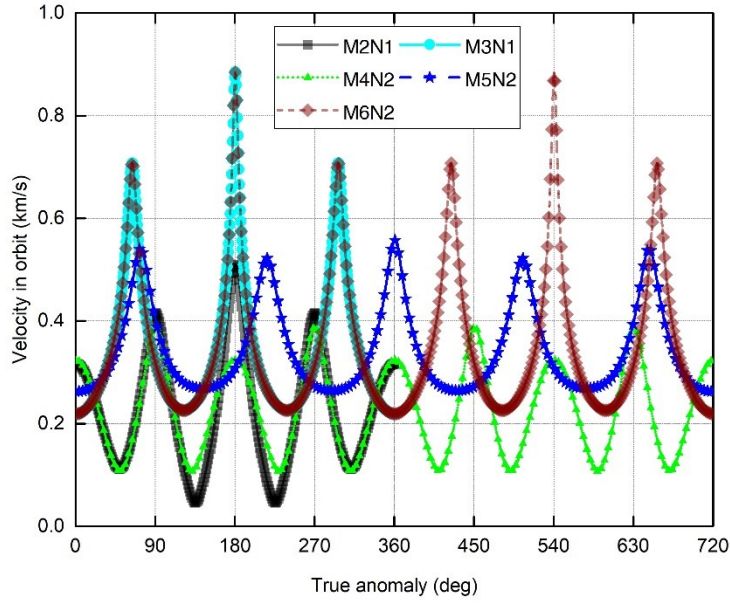


Figure 6.3. Evolution of velocity in MR halo orbits

6.3 Design of Two Impulse Transfers to MR Halo Orbits

In the proposed approach, the transfer trajectory in the Earth-Moon system is generated without involving manifolds. This approach involves only one segment (transfer trajectory) and two maneuvers. The first maneuver (ΔV_{EPO}) injects the space vehicle directly into the single segment transfer trajectory and the space vehicle reaches the MR halo orbit. The second impulse (ΔV_{HOI}) is imparted to insert the space vehicle into the MR halo orbit. The optimal transfer trajectory design to MR halo orbits in ERTBP framework that involves finding the components of maneuvers is generated using differential evolution (DE).

6.3.1 Design Philosophy

In the design process, the location on the MR orbit and the components of maneuver (ΔV_{HOI}) are chosen and after applying this maneuver, backward propagation from this location is carried out to check whether the trajectory reaches close to Earth. At the closest approach altitude, the velocity impulse required to push the spacecraft into transfer trajectory from a chosen parking orbit (ΔV_{EPO}) is computed. The magnitude the halo orbit insertion maneuver is minimized to achieve the desired closest approach distance from the Earth on backward

propagation. The DE technique is used for the selection of (i) suitable precise insertion location on the MR halo orbit (ν) and (ii) the magnitude and the direction of the perturbations to velocity $[\Delta\dot{x}, \Delta\dot{y}, \Delta\dot{z}]$ that minimise the halo orbit insertion cost (ΔV_{HOI}) while fulfilling the required closest approach altitude (CAA) from the Earth. These components are chosen from their respective bounds such that, after imparting the velocity perturbations and on numerical backward propagation, the trajectory achieves the desired CAA . In order to accomplish this, the objective function $OBJ2$ is set as:

$$OBJ2 = W_h \frac{|CAA_{achieved} - CAA_{desired}|}{E - M \text{ distance}} + W_v |\Delta V_{HOI}| \quad (6.3)$$

where

$$\Delta V_{HOI} = \sqrt{\Delta\dot{x}^2 + \Delta\dot{y}^2 + \Delta\dot{z}^2} \quad (6.4)$$

The objective function is normalised in order to conform to the normalised equations of motion and the weights W_h and W_v are introduced because the terms have different magnitudes. The first term is divided by the average Earth-Moon distance ($E - M \text{ distance} = 384,400.0 \text{ km}$), because the CAA is expressed in physical units.

The next sub-section describes a step-by-step algorithm based on the design philosophy outlined above.

6.3.2 Computational Algorithm

1. An initial population of size $NP \times (n + 1)$ is built following the steps (i) - (iv) given below. Each member (row) of the population consists of four unknown design parameters $[\nu, \Delta\dot{x}, \Delta\dot{y}, \Delta\dot{z}]$ of the current problem and the value of the objective function. These unknowns are the location of insertion on the orbit (ν) and three components of HOI velocity perturbations ($\Delta\dot{x}, \Delta\dot{y}, \Delta\dot{z}$). The location on MR halo orbit is represented by the true anomaly of Moon around Earth at that time (Peng and Xu, 2015a).
 - i. The values of the unknowns are chosen randomly within their respective bounds. In order to search the solution space uniformly, the random number generation is performed using uniform distribution. Different random number sequences are used for choosing the initial design parameters from the search bounds and for generating the trial elements (c.f. step 2).
 - ii. The randomly chosen velocity perturbations are added to the velocity vector at the randomly selected location.
 - iii. To evaluate the objective function $OBJ2$ (c.f. Eq. (6.3), the equations of motion Eq. (2.13) are numerically integrated backward in time using Runge-Kutta-Fehlberg 7/8 integrator (RKF7/8) till the first closest pass to Earth (CAA) is encountered. The absolute and relative tolerances for the Runge-Kutta-Fehlberg 7/8 integrator are set as $1.0E-12$.
 - iv. Repeat the steps (i), (ii) and (iii) till an initial population of size $NP \times 5$ is built.
2. Through the three processes of mutation, crossover, and selection, a trial member is formed from the search bounds for each member of the current population.
 - iv. Mutation: A mutant member is formed by randomly selecting members from the current population in such a way that they are not equivalent to the member being tested. For the mutation process, a scaling factor represented by F is employed.
 - v. Crossover: The trial member is created by combining a member of the current population under testing with a mutant member. To construct a

trial member, a parameter called ‘crossover frequency’ (CR) is employed.

- vi. Selection: The objective function is evaluated for the trial member, and if the corresponding function value is less, the member under testing is replaced by this trial member.
3. Step 2 is performed for all members of the current population, resulting in the generation of a new population.
 4. Steps 2-3 are repeated until the convergence criterion is fulfilled, i.e., the difference between the population's maximum and minimum objective function values is smaller than a small pre-defined tolerance value (ϵ).

A FORTRAN95 code is developed and implemented on a machine running Linux OS and equipped with an Intel Core i5 CPU running at 2.5 GHz and 8GB of RAM (Although this hardware configuration is different from that mentioned in Section 4.2, the inferences and comparisons made there are independent of the those made in this section). The GFORTRAN random number generator RAND is used to generate all of the random numbers. Following several trial runs, the DE parameters are set to $NP = 40$, $F = 0.5$ and $CR = 0.8$ and the weights in $OBJ2$ (Eq.4.3) as $W_h = 10$ and $W_v = 0.5$. An initial step size of $h = 0.01$ is employed for numerical integration to ensure reasonable computational time and accuracy. The tolerance value (ϵ) is fixed at $1.0E-5$.

6.3.3 Results

The transfer trajectory design to the MR halo orbit M5N2 (i.e. primaries complete two revolutions around the barycentre while space vehicle completes five revolutions in the MR halo orbit around Lagrangian point) is considered for design analysis purposes. The CAA altitude around Earth is assumed to be 185 km and a 185 km circular orbit assumed for Earth parking orbit for the computation of velocity impulse (trans-halo injection). These choices facilitate ease of comparison of the results with the existing results in literature.

6.3.3.1 Optimal Two Impulse Transfer

The search for the optimal transfer is conducted by treating the location on the halo orbit (v) and the HOI velocity components $[\Delta\dot{x}, \Delta\dot{y}, \Delta\dot{z}]$ as unknowns. The search bounds for the velocity components are set as $[-3000 \text{ m/s}, 3000 \text{ m/s}]$. The optimal transfer to MR halo orbit M5N2 requires a total velocity impulse of 3.2802 km/s (of which 0.4882 km/s is for MR halo

orbit insertion) for a flight duration 4.92426 days. This optimal transfer leads to insertion into a location of MR halo orbit that corresponds to Moon’s true anomaly of 359.82 deg (the location corresponds to the apogee of the third revolution by the spacecraft). The optimal total velocity impulse obtained using the proposed technique is about 107 m/s lower than the lowest value (3.388 km/s) reported in Peng and Xu (2015b). *It is to be noted that the transfers reported by Peng and Xu (2015b) need flight durations between 56 and 71 days, whereas the optimal transfer using the proposed approach requires a flight duration of about 5 days only.* Figure 6.4 depicts the $x - y$ projection of optimal trajectory from 185 km circular Earth parking orbit to the MR halo orbit M5N2.

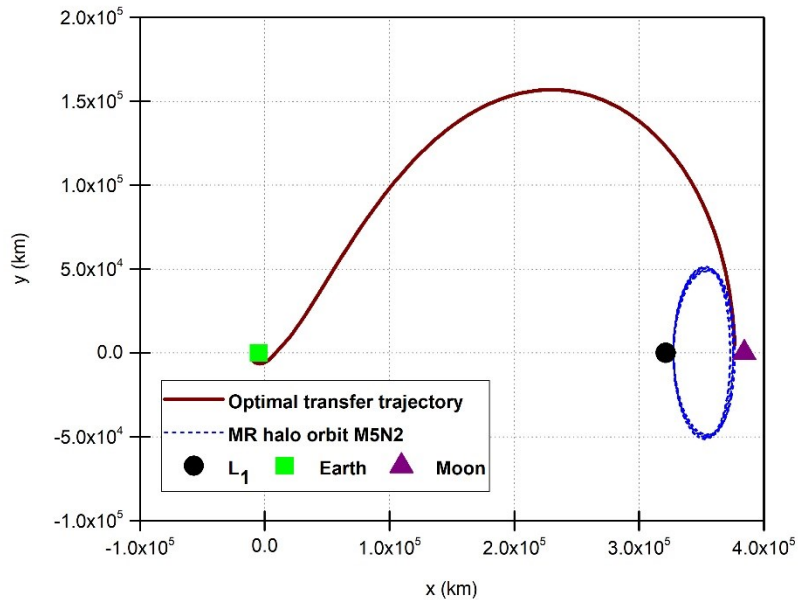


Figure 6.4 $x - y$ projection of the optimal transfer trajectory to MR halo orbit M5N2

To compare the transfers, an optimal transfer to the halo orbit having Az amplitude of 47924 km under the CRTBP framework has been generated. This Az amplitude is the average Az amplitude of the MR halo orbit M5N2 used for the transfer under the ERTBP framework. The initial conditions of the halo orbit design are: [0.845272317414636, 0.0, 0.170480760011887, 0.0, 0.265160667222108, 0.0] and the period is 11.459994 days. The optimal transfer obtained using the proposed approach requires a total velocity impulse of 3.4270 km/s (of which 0.4678 km/s is for halo orbit insertion) and the location of insertion corresponds to the apogee of the orbit. The corresponding flight duration is 4.79290 days. As

reported earlier, the total velocity impulse required for the optimal transfer in the ERTBP framework (i.e. to the MR halo orbit M5N2) is 3.2802 km/s (for a flight duration of 4.92426 days) which is less by about 147 m/s compared to the optimal transfer in the CRTBP framework obtained in this study. This difference is attributed to the inclusion of effect of eccentricity in the dynamics of the system.

6.3.3.2 Performance and Robustness of the DE Based Algorithm

To establish the robustness of the DE based algorithm, the optimal transfer trajectory design to the MR halo orbit M5N2 is generated with different search bounds for the velocity components and different seeds for random number generation. The HOI insertion location is constrained to lie in the third revolution of the spacecraft around the Lagrangian point L_1 . The initial step size for all these computations is set as $h = 0.01$. The speed of convergence depends on the values of weights for the terms of the objective function. A sensitivity analysis on these weights is carried out (c.f. Table 6.6) and the weights (W_h, W_v) in Eq. (6.3) are selected as (10, 0.5). The performance of the DE based algorithm for different search bounds for velocity components (seed = -5055 and weights (10, 0.5)) and different seeds (search bounds for velocity components = [-3000 m/s, 3000 m/s] and weights (10, 0.5)) are presented in Table 6.7 and Table 6.8 respectively.

Table 6.6 Performance of the DE based algorithm with different weights in objective function

Weights (W_h, W_v) in Eq. (6.3)	CAA obtained (km)	ΔV_{HOI} (km/s)	No of iterations for convergence	Computational time (s)
(10, 0.1)	184.967	0.48824	406	1645
(10, 0.2)	185.062	0.48823	333	1387
(10, 0.5)	185.019	0.48823	187	905
(10, 1.0)	185.157	0.48822	172	702
(10, 2.0)	186.373	0.48822	198	946

Table 6.7 Performance of the DE based algorithm with different search bounds for velocity components

Search bounds for velocity components (m/s)	HOI location (deg)	ΔV_{HOI} (km/s)	No of iterations for convergence	Computational time (s)
[-3000, 3000]	359.82	0.48822	187	905
[-2000, 2000]	362.14	0.48826	171	767
[-1000, 1000]	362.17	0.48821	355	702

Table 6.8 Performance of the DE based algorithm with different seeds for random number generation

Seed	HOI location (deg)	ΔV_{HOI} (km/s)	No of iterations for convergence	Computational time (s)
-5055	359.82	0.48822	187	905
-258410	362.20	0.49322	189	954
- 8545523	362.17	0.49124	179	925

It can be observed from Table 6.7 and Table 6.8 that the DE based algorithm converges to nearly the same solution irrespective of the search bounds for velocity components and seeds for random number generation. This establishes the robustness of the DE based algorithm and the global optimality of the solution obtained.

6.3.3.3 Transfers to Different MR Halo Orbit Locations

The transfer trajectories to different MR halo orbit insertion locations (v) are studied. The unknowns for this problem are the components of HOI velocity $[\Delta\dot{x}, \Delta\dot{y}, \Delta\dot{z}]$ and are determined using the proposed technique. The flight duration for these transfers is constrained to be less than 10 days. Figure 6.5 and Figure 6.6 present the velocity impulses and flight durations for different MR halo orbit insertion locations.

The five peaks in Figure 6.5 and Figure 6.6 correspond to the periodicity of five revolutions of the M5N2 orbit. The velocity impulse required to leave EPO (ΔV_{EPO}) varies between 2.758 km/s and 2.877 km/s and the velocity impulse for HOI varies between 0.488

km/s 1.1 km/s. The variation in the total velocity impulse is largely due to the velocity impulse required for halo orbit insertion (ΔV_{HOI}). Note that the total velocity impulse varies between 3.280 km/s and 3.747 km/s. *So, if the mission is capable of handling a margin of about 470 m/s, the flexibility of reaching any location with slight variation in flight duration is possible.* Although transfers to different manifold injection points of halo orbits in CRTBP can be achieved using the manifold approach (Rausch (2005)), the corresponding cost aspects are not discussed therein.

Peng and Xu constructed transfers to MR halo orbit M5N2 using the manifold approach (Peng and Xu, 2015b). They report that the total velocity cost varies between 3.388 km/s to 3.934 km/s for transfers to different locations. With the proposed technique, the transfer cost varies between 3.28 km/s and 3.747 km/s. Also, the flight durations obtained in this study using the proposed technique vary between 3.92 days and 5.75 days, *whereas the transfers reported by Peng and Xu (2015b) need flight durations between 56 and 71 days.* It can be concluded that the proposed direct technique without involving manifold theory is able to capture optimal transfers with lower cost even for significantly lower flight durations.

For a direct comparison between the optimal transfers to the MR halo orbit M5N2 using the proposed approach and the manifold theory (Peng and Xu, 2015b), the transfer trajectory design to the insertion location $v = 126.648$ deg (derived from the Figure 10 of Peng and Xu (2015b)) having a flight duration of 57.42011 days is generated. The optimal transfer obtained using the proposed approach requires a total velocity impulse of 3.8215 km/s whereas the manifold approach (Peng and Xu, 2015b) requires 4.6121 km/s which means that the transfer using the proposed technique requires less by about 787 m/s.

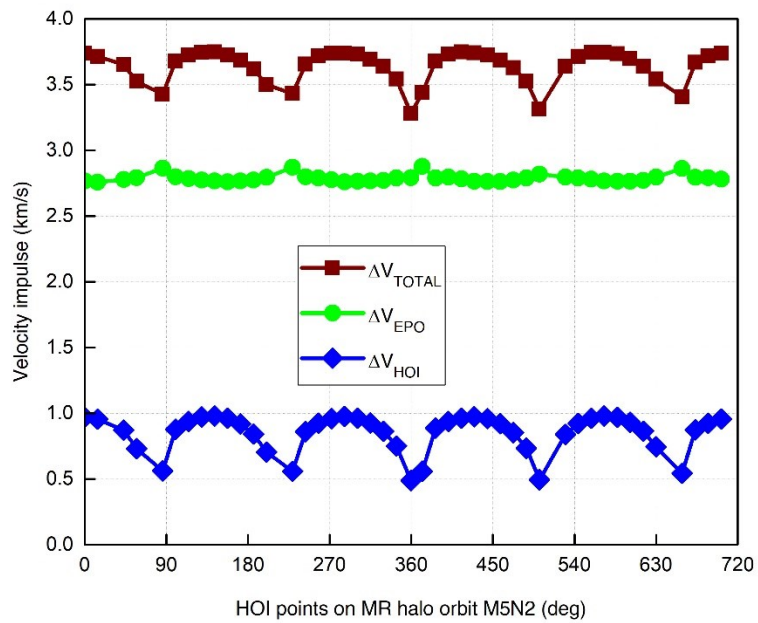


Figure 6.5 Velocity impulses for optimal transfers to different locations on the MR halo orbit M5N2

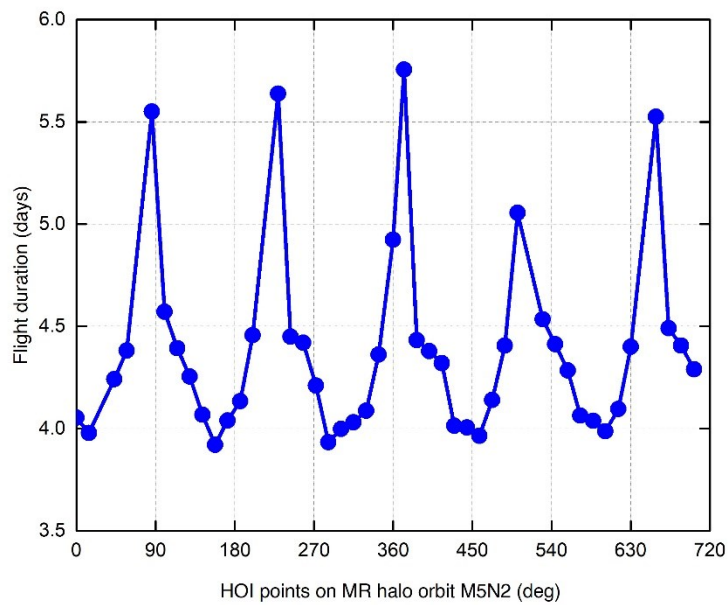


Figure 6.6 Flight durations for optimal transfers to different locations on the MR halo orbit M5N2

6.3.3.4 Optimal Transfers to Different Locations on MR Halo Orbit with Fixed Flight Duration

The transfers to different locations on the MR orbit are analyzed by fixing flight durations. The transfer trajectory designs are generated for two flight durations (i) 4 days (ii) 5 days. The locations are varied at intervals of 30deg and is a known variable. The unknowns for this problem are the HOI velocity components $[\Delta\dot{x}, \Delta\dot{y}, \Delta\dot{z}]$ and are determined using the proposed technique. After adding the velocity perturbations to the state vector at a location on the MR halo orbit, the backward numerical propagation of equations of motion is carried out and stopped when the required flight duration is reached to evaluate the objective function. The required optimal velocity impulses are presented in Figure 6.7.

Again, the five peaks of ΔV_{HOI} and ΔV_{TOTAL} in Figure 6.7 correspond to the periodicity of five revolutions of the M5N2 orbit. The velocity impulse from the EPO (ΔV_{EPO}) remains nearly constant for both the fixed flight durations. The differences between the minimum and maximum HOI velocity impulses are 445.4 m/s and 640.4 m/s for flight durations of 4 and 5 days respectively. The maximum difference in ΔV_{TOTAL} requirement for flight durations 4 and 5 days is about 192 m/s. If the mission is capable of handling a margin of 200 m/s, then the flexibility of reaching any location with slight variation in flight duration is possible.

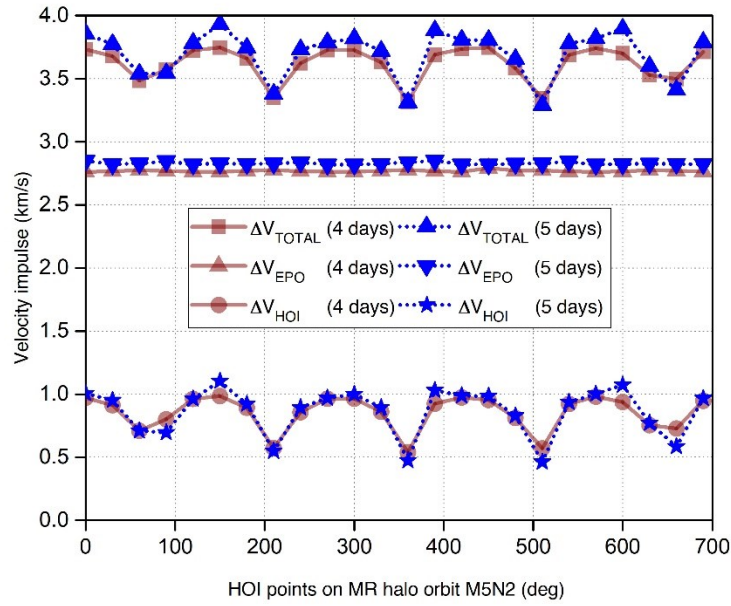


Figure 6.7 Velocity impulses for optimal transfer to different locations on MR halo orbit M5N2

6.3.3.5 Optimal Transfer for Different Flight Durations

The transfer trajectories for the MR halo orbit M5N2 are generated for different flight durations. The unknowns for this problem are the location on the halo orbit (v) and the HOI velocity components $[\Delta\dot{x}, \Delta\dot{y}, \Delta\dot{z}]$ and are determined using the proposed technique. After adding the velocity perturbations to the state vector at a randomly selected location on the MR halo orbit, backward numerical propagation of equations of motion is stopped when the required flight duration is reached and the objective function is evaluated. The CAA for all these transfers is kept as 185 km. Figure 6.8 presents the velocity impulses for the transfers with different flight durations. The maximum total velocity impulse (ΔV_{TOTAL}) is about 4.90 km/s for a flight duration of 15 days. A cyclic trend is observed with respect to the flight durations in this study. For transfers using manifold approach, Peng and Xu (2015b) observe that the total velocity cost comes down with increasing flight durations. However, they restricted their analysis for flight durations between 56-71 days and in the neighbourhood of manifold perigee. The above mentioned trend is not observed with the proposed technique.

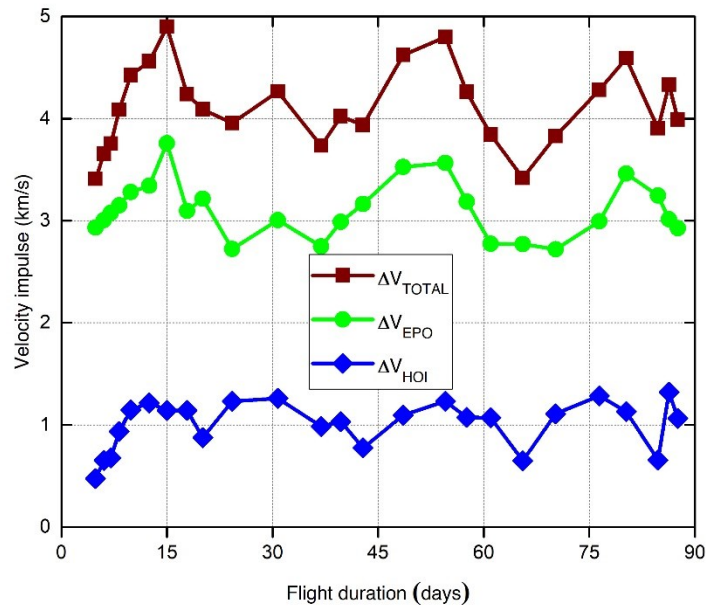


Figure 6.8 Optimal velocity impulses for different flight durations for the MR halo orbit M5N2

The $x - y$ projections of optimal transfers obtained using the proposed technique for some flight durations are depicted in Figure 6.9. The characteristics of the transfers in Figure 6.9 are summarized in Table 6.9

Table 6.9 Characteristics of transfers identified in Figure 6.8 and Figure 6.9.

Orbit	Flight duration (days)	ΔV_{TOTAL} (km/s)	Number of close passes to Earth	Difference between each close pass (days)	CAA of each close pass (km)
a	6.0	3.6566	1	-	185
b	15.0	4.900	2	8.41	185, 3982
c	36.9	3.955	5	8.27, 8.74, 7.67, 8.17	185, 616, 764, 5862, 1465
d	54.5	3.4183	7	8.23, 7.29, 7.93, 9.72, 8.28, 8.48	185, 955, 2550, 1008, 3852, 11732, 14242

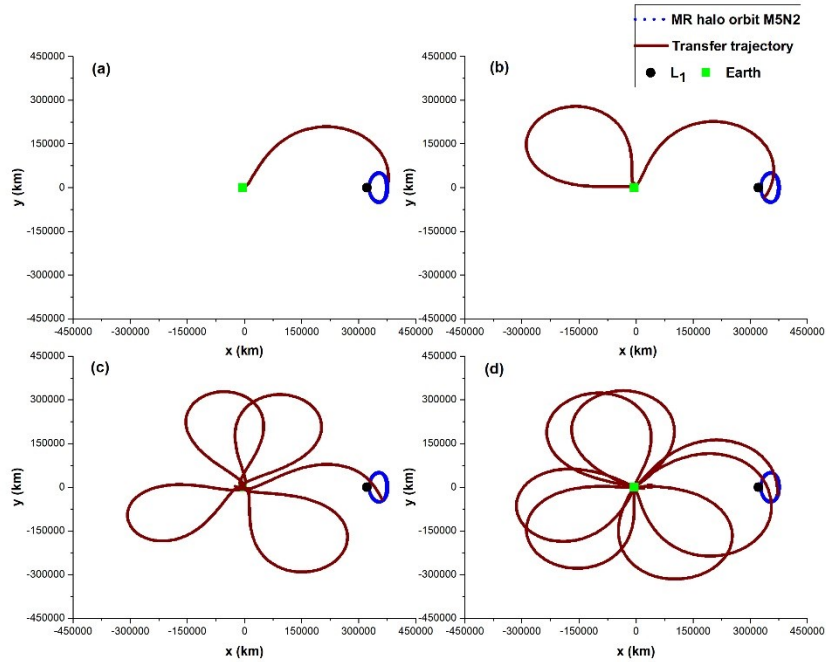


Figure 6.9 $x - y$ projections of transfers for different flight durations for the MR halo orbit M5N2

The transfer trajectory for flight duration of 6 days directly reaches the halo orbit. The geometries of trajectories shown in Figure 6.9 are completely different from those obtained using the manifold approach. In the CRTBP framework, Parker and Born (2008) report transfers having similar flight durations, where the spacecraft spends most of the flight duration around the Lagrangian point (in the manifold segment). *In contrast, the trajectories depicted in Figure 6.9 are in the neighborhood of Earth for most of the flight duration.* The structure of these trajectories is similar to those obtained for the transfers from a low Earth orbit to a low Moon orbit under the CRTBP framework by Lei et al. (2013). The variation of radial distance from Earth for these transfers is presented in Figure 6.10.

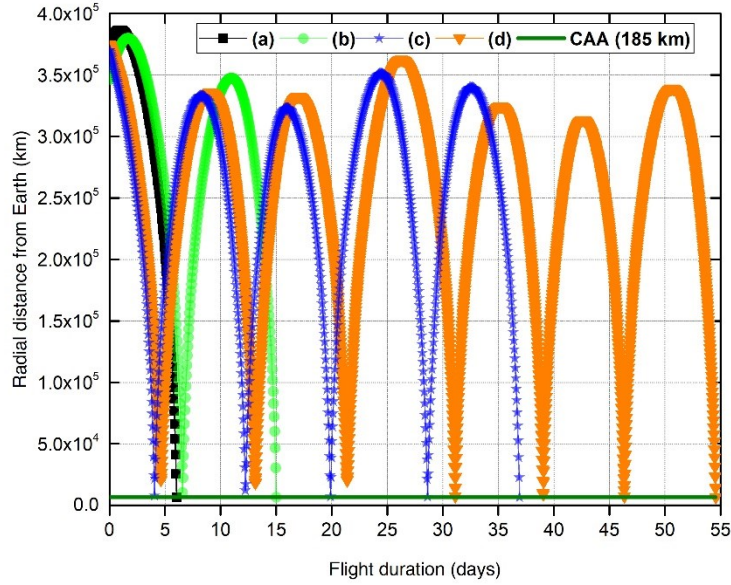


Figure 6.10 Variation of geocentric radial distance for different flight durations

It can be observed from Figure 6.10 that the close passes to Earth in all these trajectories repeat at an interval of 7-10 days. The spacecraft reaches up to a maximum distance of 60 Earth radii.

6.3.3.6 Optimal Transfers to Different MR Halo Orbit Revolutions

As mentioned earlier, a spacecraft in the MR halo orbit M5N2 makes five revolutions around the Lagrangian point while the primaries make two revolutions around the barycentre. The MR halo orbit is not a simple repetition of the halo orbit in CRTBP and therefore, the transfer trajectories from different revolutions in the same MR halo orbit are analysed. The period of each revolution in the MR halo orbit M5N2 is approximately $4\pi/5$. So, the search bounds for the HOI location point for different revolutions are chosen as multiples of $4\pi/5$. For example, the search bounds for the HOI location point in the first revolution is $v \in \left[0, \frac{4\pi}{5}\right]$, for the second revolution is $v \in \left[\frac{4\pi}{5}, \frac{8\pi}{5}\right]$ and so on. The unknowns for this problem are the location on the halo orbit (v) and the HOI velocity components $[\Delta\dot{x}, \Delta\dot{y}, \Delta\dot{z}]$ and are determined using the proposed technique. The results for the transfer to different revolutions

of MR halo orbit M5N2 are presented in Table 6.10. The *CAA* for all these transfers is kept as 185 km.

From Table 6.10, it can be observed that the HOI velocity for revolutions 2 and 4 are nearly the same, but different from those for revolutions 1, 3 and 5. The difference between the maximum and minimum HOI velocities is about 50 m/s. Note that there is only a marginal difference in flight duration. For each revolution, the location of minimum HOI velocity impulse corresponds to the farthest radial distance from Earth (apogee of each revolution). Further, these locations correspond to the closest distance from Earth-Moon Lagrangian point L_1 . These are demonstrated in Figure 6.11 and Figure 6.12 respectively. The Y-axes of Figure 6.11 and Figure 6.12 are the distances of locations on the M5N2 halo orbit from Earth and from L_1 respectively. It is restated that the location of insertion on the MR halo orbit is represented by the true anomaly of Moon around Earth (X-axes of Figure 6.11 and Figure 6.12)

Table 6.10 Optimal transfer trajectory to different revolutions of MR halo orbit M5N2

Revolution number	HOI point in terms of true anomaly (deg)	ΔV_{HOI} (km/s)	ΔV_{EPO} (km/s)	ΔV_{TOTAL} (km/s)	Flight duration (days)
1	71.960	0.50566	2.8304	3.3360	5.1476253
2	217.342	0.46744	2.8273	3.2947	4.8984034
3	359.820	0.48828	2.7917	3.2802	4.9241521
4	506.894	0.46785	2.8206	3.2885	5.1687698
5	648.561	0.45535	2.8293	3.2847	4.9714350

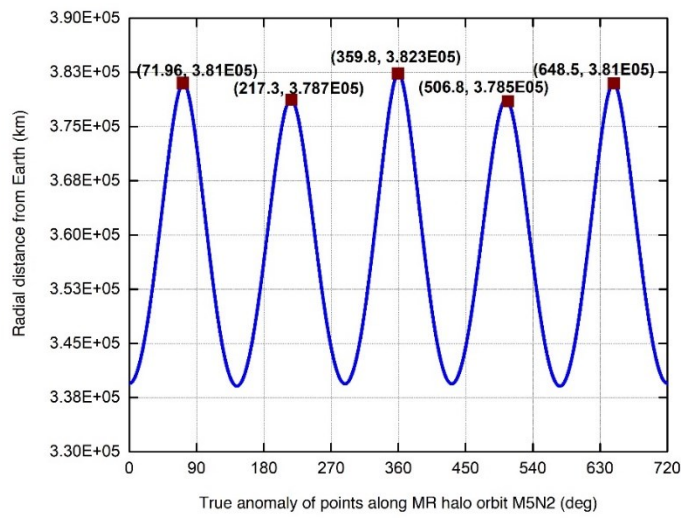


Figure 6.11 Locations of minimum HOI velocity impulse for different revolutions as a function of radial distance from the Earth

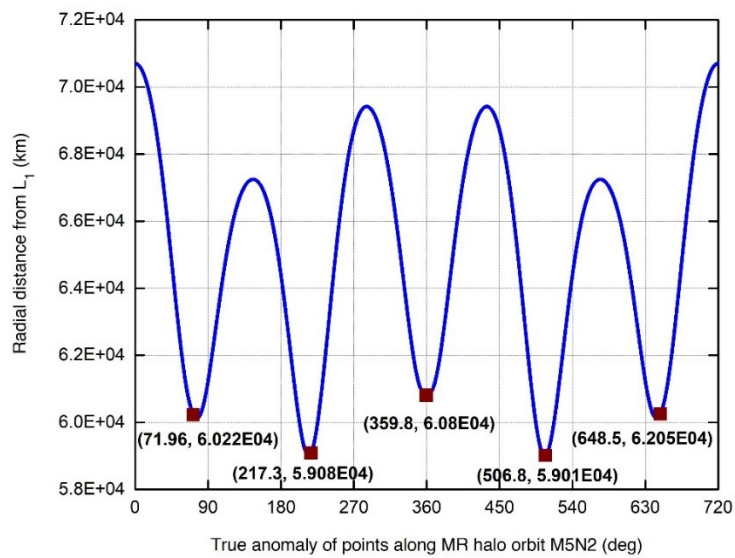


Figure 6.12. Locations of minimum HOI velocity impulse for different revolutions as a function of radial distance from L_1 .

Although the results in Figure 6.11 and Locations of minimum HOI velocity impulse for different revolutions as a function of radial distance from L_1 . Figure 6.12 are presented for the MR halo orbit M5N2, the trend is found to be same for other orbits as well. The trajectory and projections of optimum transfers from different revolutions of MR halo orbit M5N2 are presented in Figure 6.13, wherein TT represents transfer trajectory.

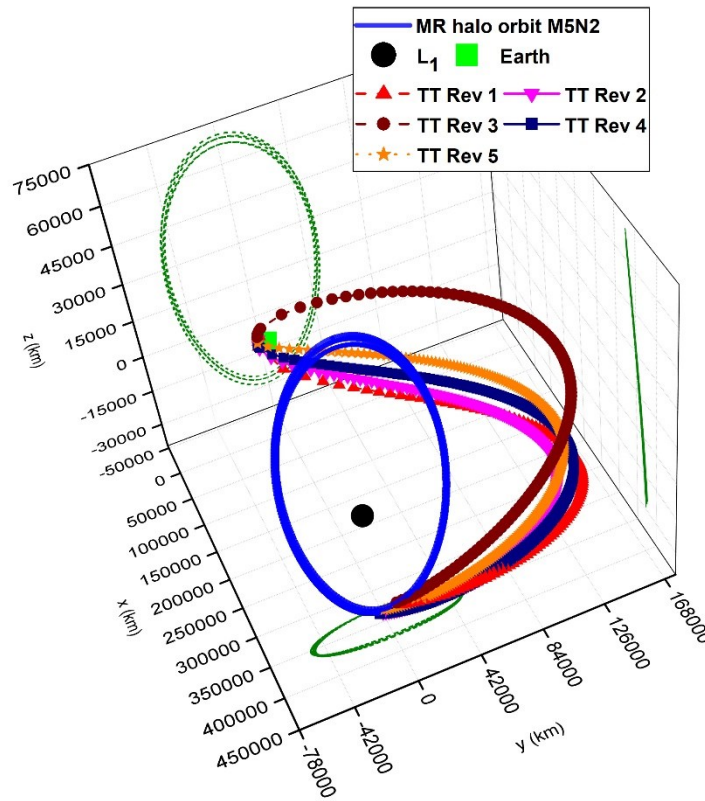


Figure 6.13. Trajectory and projections of optimal transfers to different revolutions of MR halo orbit M5N2

6.3.3.7 Optimal Transfers from Different Closest Approach Altitudes

The transfer trajectories for the MR halo orbit M5N2 are generated for different closest approach altitudes. The unknowns for this problem are the location on the halo orbit (v) and the HOI velocity components $[\Delta\dot{x}, \Delta\dot{y}, \Delta\dot{z}]$ and are determined using the proposed technique. After adding the velocity perturbations to the state vector at a randomly selected location on the MR halo orbit, the backward numerical propagation of equations of motion is stopped when the required CAA is reached and the objective function is evaluated. The flight duration is

constrained between 2 and 10 days. The results for transfers with various closest approach altitudes are presented in Table 6.11.

From Table 6.11, it can be observed that the ΔV_{HOI} 's for all these *CAA*'s are between 400 m/s and 490 m/s which implies that there is no significant variation in the HOI velocity impulse depending on *CAA*. Also, $\Delta V_{HOI}, \Delta V_{EPO}$ and total velocity impulse decrease with increasing *CAA*.

Table 6.11. Transfer trajectory designs for different *CAA*'s.

<i>CAA</i> (km)	HOI point in terms of true anomaly (deg)	ΔV_{HOI} (km/s)	ΔV_{EPO} (km/s)	ΔV_{TOTAL} (km/s)	Flight duration (days)	Velocity at <i>CAA</i> (km/s)
185	359.82	0.48822	2.7917	3.2802	4.924152	10.7373
200	73.947	0.45451	2.8171	3.2716	4.976615	10.7225
500	75.620	0.44524	2.5840	3.0292	5.094445	10.4894
1000	505.705	0.43795	2.2062	2.6441	4.937150	10.1113
2000	506.808	0.42438	1.5753	1.9997	5.040203	9.4808
3000	506.798	0.41456	1.0431	1.4576	5.031087	8.9484
4000	649.421	0.40764	0.5895	0.9972	5.055669	8.4945

6.3.3.8 Optimal Transfers to Different MR Orbits in the Earth-Moon System

The transfer trajectory designs to different MR orbits around the Lagrangian point L_1 in the Earth-Moon system are generated using the proposed technique. The *CAA* for all these transfers is kept as 185 km. The flight duration is constrained between 2 and 10 days. The unknowns for this problem are the location on the halo orbit (v) and the HOI velocity components $[\Delta\dot{x}, \Delta\dot{y}, \Delta\dot{z}]$ and are determined using the proposed technique. The initial conditions and period of the target MR orbits in this study are presented in Table 6.12 and the optimal transfer trajectory designs are presented in Table 6.13.

As mentioned earlier, in these orbits, N denotes the number of revolutions of primaries around the barycentre. From Table 6.13, it can be observed that the MR halo orbit M3N1 is preferable over the MR Lyapunov orbit M2N1 because the total velocity impulse required for

transfer is less. Also, among orbits with $N = 2$, the MR Lyapunov orbit M4N2 has the least ΔV_{TOTAL} for transfer.

Table 6.12 Initial conditions and period of target MR orbits

MR orbit and class	x_0	z_0	\dot{y}_0	Period
M2N1 Lyapunov	0.804125156956177	0.000000000000000029	0.31182413982453	2π
M3N1 halo	0.875404052867664	0.201620653468241	0.21551063837955	2π
M4N2 Lyapunov	0.804504659626012	0.000000000000000020	0.31826866733409	4π
M4N2 halo	0.895820897947402	0.194415672884192	0.34702042423622	4π
M5N2 halo	0.851666641652152	0.183285539178136	0.25828972225268	4π

Table 6.13 Transfer trajectory designs for different MR orbits.

MR orbit and class	HOI point in terms of true anomaly (deg)	ΔV_{HOI} (km/s)	ΔV_{EPO} (km/s)	ΔV_{TOTAL} (km/s)	Flight duration (days)	Velocity at CAA (km/s)
M2N1 Lyapunov	91.056	0.44931	2.7858	3.2351	4.3708185	10.6910
M3N1 halo	66.025	0.39580	2.8377	3.2335	5.0100358	10.7422
M4N2 Lyapunov	88.504	0.42921	2.7840	3.2132	4.2512113	10.6895
M4N2 halo	237.636	0.60700	2.7953	3.4023	5.2342646	10.7465
M5N2 halo	359.820	0.48828	2.7917	3.2802	4.9241521	10.7373

6.4 Conclusions

Preliminary Lagrangian point mission design in the Earth-Moon system is accomplished under the ERTBP framework. Motivated by the success of application of Differential Evolution (DE)-based design methodology for the mission design in the Sun-Earth

system, the methodology is extended to the Earth-Moon system for the design of MR halo orbits and transfer trajectory design to MR halo orbits.

The design of MR halo orbits using DE is a single level, single segment approach for halo orbit design and produces precise MR halo orbit design, avoiding the need for multilevel continuation methods. In order to reduce the computational time, multithreading technique is successfully employed. Numerical results for different MR halo orbits in Earth-Moon system are presented. It is found that, the average Az amplitude of MR orbit Earth-Moon system under the ERTBP framework is comparable with that of under CRTBP framework and so, can be used for scientific missions. For example, the average the Az amplitude of MR orbit M5N2 is 47912.42 km whereas the Az amplitude of corresponding halo orbit in CRTBP is 47957.10 km. Multiple options of MR halo orbits for the same period are generated and analyzed. For multiple options of MR halo orbits with same period, it is found that the variation in radial distance from Earth decreases and the velocity in orbit increases as the number of third body revolutions increases.

For the transfer trajectory design to MR halo orbits, it is established that the use of manifold theory is not necessary. The proposed technique using DE is a unified approach to generate optimal transfer trajectory design to halo orbits under CRTBP framework and to MR halo orbits under ERTBP framework. The minimum total velocity impulse required for transfer to the MR halo orbit M5N2 is 3.2802 km/s for a flight duration of 4.92426 days, which are lower than the values reported in the existing literature (3.388 km/s and 65 days respectively). The geometry of the transfer trajectory is entirely different from the one obtained using manifold approach. The trajectories are in the neighborhood of Earth for the most part of the flight duration whereas the transfer trajectory of manifold approach is in the neighborhood of the Lagrangian point L_1 . The proposed approach is used to analyse various mission scenarios with different flight durations, different insertion locations, different Earth parking orbit altitudes and different target MR orbits. A cyclic trend is observed for transfers with different flight durations. There is no significant variation in the HOI velocity impulse (the variation is only 80 m/s for CAAs of 4000 km to 185 km) even for higher CAAs. Any location on MR halo orbit can be reached with a flight duration between 4 and 6 days. Transfers to different revolutions of a given MR halo orbit are analysed and the locations of minimum halo orbit insertion velocity impulse are found to be the apogees of each revolution.

Chapter 7: Summary and Conclusions

The current research aims at generating mission design to Lagrangian points of the Sun-Earth and Earth-Moon restricted three body systems. Extending the state-of-the-art in the literature (preliminary mission design using the Circular Restricted Three Body Problem (CRTBP) Framework), the current research *explored the use of Elliptic Restricted Three Body Problem (ERTBP) framework* for the two steps in preliminary design, i.e. halo orbit design and transfer trajectory design. The designs generated under the ERTBP framework are used as reference designs to initiate the designs in high fidelity SEM ephemeris model, which considers the influence of the three major celestial bodies (the Sun, the Earth and the Moon) on a spacecraft near the Sun-Earth and Earth-Moon Lagrangian points. It is found that the use of the ERTBP framework for preliminary mission design in the Sun-Earth system does not provide significant advantages over the CRTBP framework. Differential Evolution (DE), an evolutionary optimization technique is employed for the numerical solution process and is found to be a very versatile tool for solving Lagrangian point mission design. It is demonstrated that the FORTRAN 95 codes developed based on the proposed techniques can be used as mission design and analysis tools for exploring various mission scenarios. The important contributions of the current research and the inferences derived are summarized as follows.

1. *Explored the use of the ERTBP framework for complete preliminary mission design to Lagrangian points in the Sun-Earth and Earth-Moon systems.* Multi-Revolution (MR) orbits, which are perfectly periodic orbits in the ERTBP framework, are designed in the Sun-Earth and Earth-Moon systems utilizing a differential evolution-based methodology. It is found that the MR halo orbits in the Sun-Earth system have very large amplitudes and cannot be used for a scientific mission like ISEE3 due to communication system related constraints. As an alternative, quasi-halo orbits in the Sun-Earth system which doesn't require any theoretical design maneuvers for about five years are generated. Two impulse transfer trajectories to the MR orbits and quasi-halo orbits are generated. *It is substantively concluded that the use of ERTBP framework for the preliminary mission design to Lagrangian points in the Sun-Earth system does not provide any significant advantage over the CRTBP framework. In other words, the CRTBP framework captures the major dynamics of the problem well and is sufficient for preliminary design analysis purposes. This inference is*

applicable to the Lagrangian point mission design in the Sun-Earth system only and is attributed to the small eccentricity of the system (average eccentricity ~ 0.0167).

2. ***Successfully employed differential evolution technique for the two steps of the preliminary mission design;*** the design of halo orbits and the design of transfer trajectory. The DE-based formulation of the problem poses advantages such as no need of a close reference design, flexibility in the formulation of objective function etc. and renders the technique suitable for Lagrangian point mission design compared to the conventional DC based technique. Further, many complexities associated with the differential correction based technique (such as divergence when numerically integrating the equations of motion for a long time, inability to converge with a single segment etc.) are avoided. ***Therefore, the differential evolution technique is found to be very versatile in solving Lagrangian point mission design problems.***
3. ***Proposed a unified methodology for the design of Lagrangian point missions applicable to different dynamical systems*** (Sun-Earth, Earth-Moon etc.). The proposed methodology based on differential evolution is robust, versatile and is flexible to incorporate different design requirements through suitable formulation of objective functions and choice of parameters (like mass ratio, eccentricity etc.). The designs of halo orbits in CRTBP, MR halo orbits in ERTBP and quasi-halo orbits in ERTBP and ephemeris model are generated using a common problem formulation scheme. For the design of transfer trajectory, because the proposed two-impulse technique does not make use of the manifold theory, the common scheme is used to generate transfers to halo orbits in Sun-Earth and Earth-Moon systems (avoiding the need for bridge segment in the latter). ***Therefore, the proposed unified methodology can be used to generate Lagrangian point mission design to any restricted three body systems like Sun-Earth, Earth-Moon, Sun-Mars, Earth-Asteroid etc.***
4. ***Successfully avoided possible inter-dependence of the two steps of preliminary mission design (design of halo orbit and design of transfer trajectory) through the problem formulation using differential evolution technique.*** That means, the possible modification of the target halo orbits to quasi-halo orbits while generating transfer trajectory due to the patching of multiple segments in the conventional differential correction and multiple shooting techniques is avoided. This results in better exploration and analysis of independent mission scenarios and for conducting trade-off studies.

The major observations and highlights derived from various aspects of the current research are summarized as follows:

1. The design of perfectly periodic Multi-Revolution (MR) orbits in the Sun-Earth system is successfully generated under the ERTBP framework and reported for the first time in the literature (to the best knowledge of the author). The proposed methodology utilizing differential evolution is a single level, single segment approach and produces precise MR orbit design, avoiding the need for multilevel continuation methods. In this research:
 - a. The concept of average Az amplitude is introduced for an MR halo orbit in ERTBP framework and the average Az amplitudes of MR halo orbits are found to be nearly equal to that of corresponding circular halo orbits. For example, Az amplitudes of MR halo orbit M4N2 and the corresponding halo orbit are 490,335 km and 490,321 km respectively.
 - b. Multiple options of MR orbits for the same period are generated and analyzed. It is found that the variation of radial distance from Earth and the variation of velocity in orbit increases as the number of third body revolutions increases. For example, the variation of radial distance from Earth for the MR halo orbit M4N2 is lesser all along the orbit compared to that for the MR halo orbit M5N2.
 - c. Both halo and Lyapunov design solutions are captured for an MR orbit. Further, for a given halo or Lyapunov orbit, multiple design solutions are also captured. For example, $[0.9896036427, 0, 0.0054303949, 0, 0.0300144939, 0]$ and $[0.9891099633, 0, 0.0063886772, 0, 0.0297630010, 0]$ are the multiple design solutions for the MR halo orbit M4N2.
2. It is found that the periodic MR halo orbits around the Lagrangian point in the Sun-Earth system are not feasible for scientific missions like ISEE3 ($Az = 120,000$ km) because of large amplitudes. For example, the minimum Az amplitude of an MR halo orbit in the Sun-Earth system is 490,335 km (MR halo orbit M4N2). Such large amplitudes violate the requirement for the communication system which results from the need to avoid pointing at the solar disk (solar exclusion zone). For viable smaller amplitudes, it is found that only quasi-halo orbits are feasible and that the design process needs to be independent of the commensurability constraint which relates the period of the halo orbit to the system period 2π .

3. A design methodology for the design of quasi-halo orbits around the Lagrangian points and transfers to them in the Sun-Earth system under the ERTBP framework and SEM ephemeris model, based on the differential evolution technique is proposed. In this research:
 - a. Quasi-halo orbits of small amplitudes ($Az \sim 120,000$ km) are successfully generated in the ERTBP framework and SEM ephemeris model (the current state-of-the-art in the literature restricts to *large* amplitude, $Az > 280,000$ km). **The generated orbits don't require any theoretical design maneuvers for about five years (*about twice the duration reported in the literature*).**
 - b. It is demonstrated that the proposed methodology could generate quasi-halo orbits for a wide range of Az amplitudes ($\sim 120,000$ km to $750,000$ km).
 - c. ***It is found that both the CRTBP and ERTBP reference designs generate the ephemeris design and there is no noticeable advantage of considering ERTBP reference design.*** The initial conditions of both the halo orbit in the CRTBP framework and quasi-halo orbit in ERTBP framework are found to be very close to the initial conditions of the quasi-halo orbit in the SEM ephemeris model.
 - d. Optimal two-impulse transfers to the halo orbit in the CRTBP framework and quasi-halo orbits in the ERTBP framework and SEM ephemeris model are generated using a unified design methodology based on differential evolution. ***It is found that designs in both CRTBP framework and ERTBP framework provide conservative estimates of total velocity impulse required for the transfer compared to the SEM ephemeris model. In other words, the least cost for transfer is obtained in the SEM ephemeris model.*** For example, the total velocity impulse required for generating transfer to a quasi-halo orbit ($Az \sim 120,000$ km) in the SEM ephemeris model is around 3229 m/s and the corresponding costs in CRTBP and ERTBP frameworks are 3290 m/s and 3334 m/s respectively.
 - e. ***The closest approach distance to the Earth in the transfer trajectory design is found to be very sensitive to velocity perturbations.*** For example, when an additional perturbation of magnitude 0.4146% to 2.0732% of x component of optimal velocity component $\Delta \vec{V}_{TOI}$ results in 289.46% to 7537.97% of closest approach distance.

4. Motivated by the success of application of Differential Evolution for the design of MR orbits in the Sun-Earth system, the analysis is extended to the design of MR halo orbits in the Earth-Moon system. The design of MR halo orbits and the design of transfer trajectory to MR halo orbits are executed under the ERTBP framework. In this research:
 - a. The MR halo orbits in the Earth-Moon system are found to be nearly similar in size to the halo orbits and hence, are suitable for scientific missions. For example, the Az amplitude of the MR halo orbit M5N2 is 47912.42 km whereas the Az amplitude of corresponding halo orbit in CRTBP is 47957.10 km. ***This inference is different from the Sun-Earth system where the large amplitudes don't permit application in a scientific mission.***
 - b. ***For the transfer trajectory design to MR halo orbits in the Earth-Moon system, it is established that the use of manifold theory is not necessary.*** The proposed technique using DE is a unified approach to generate optimal transfer trajectory design to halo orbits under CRTBP framework and to MR halo orbits under ERTBP framework.
 - i. The minimum total velocity impulse required for transfer to the MR halo orbit M5N2 is 3.2802 km/s for a flight duration of 4.92426 days, which are lower than the values reported in the existing literature (3.388 km/s and 65 days respectively). The difference in flight durations is very drastic (4.9 days compared to 65 days) and is obtained by a better search of the solution space (because of independence from the manifold theory).
 - ii. It is found that there is no significant variation in the HOI velocity impulse (the variation is only 80 m/s for CAAs of 4000 km to 185 km) even for higher CAAs. Any location on MR halo orbit can be reached with a flight duration between 4 and 6 days.
 - iii. Transfers to different revolutions of a given MR halo orbit are analyzed and the locations of minimum halo orbit insertion velocity impulse are found to be the apogees of each revolution.

Scope for Future Work

1. The current research focused on the extension of the preliminary Lagrangian point mission in the Sun-Earth-spacecraft restricted three body problem to higher fidelity SEM ephemeris model. The analysis of mission design to MR halo orbits in the Earth-Moon system can be investigated in future. Further, the existence of MR orbits in other physical systems like Sun-Mercury, Sun-Mars etc. could be explored.
2. The current research investigated the Lagrangian point mission design to a physical system (Sun-Earth-spacecraft restricted three body problem) characterized by a small eccentricity (average eccentricity ~ 0.0167). The applicability of the inference that the CRTBP framework captures the major dynamics of the system well, can be investigated with a larger eccentric system like Sun-Mercury-spacecraft (average eccentricity ~ 0.2076) or Sun-Mars-spacecraft (average eccentricity ~ 0.0935) restricted three body systems.
3. The current research considered the three major gravitational forces (due to the Sun, the Earth and the Moon) acting on a spacecraft in the vicinity of Sun-Earth and Earth-Moon Lagrangian points. A future investigation could incorporate the influence of other celestial bodies in the solar system as well as model the solar radiation pressure on the spacecraft. Further, the exploration of other modelling frameworks like bi-circular restricted three body problem or restricted four body problem etc. could be investigated.
4. The current research can be extended to incorporate the orbit maintenance aspects of the quasi-halo orbits. That means, the quasi-halo orbit generated in the SEM ephemeris model can be used as the nominal orbit and the cost required to maintain the spacecraft in close proximity of the nominal orbit to enable the scientific objectives can be investigated.
5. Although the current research focused on the generation of periodic/quasi-periodic orbits and the design of optimal transfer trajectory, the perspectives of launch vehicle trajectory could be incorporated into the preliminary design. For example, the specifics of the desired Right Ascension of Ascending Node (RAAN) and inclination of the Earth Parking Orbit (EPO) could be explored. The robust design process based on differential evolution offers this flexibility to include these aspects in the objective function.

Appendix A – State Transition Matrix in CRTBP

The state transition matrix is a 6 X 6 matrix denoted by Φ and its variation is given by $\dot{\Phi} = A\Phi$ (Nath and Ramanan, 2016) where

$$A = \begin{bmatrix} 0 & 0 & 0 & 1 & 0 & 0 \\ 0 & 0 & 0 & 0 & 1 & 0 \\ 0 & 0 & 0 & 0 & 0 & 1 \\ C_{11} & C_{12} & C_{13} & 0 & 2 & 0 \\ C_{21} & C_{22} & C_{23} & -2 & 0 & 0 \\ C_{31} & C_{32} & C_{33} & 0 & 0 & 0 \end{bmatrix}$$

$$C_{11} = \frac{\partial \ddot{x}}{\partial x} = 1 - \frac{1-\mu}{r_1^3} \left(1 - \frac{3(x+\mu)^2}{r_1^2} \right) - \frac{\mu}{r_2^3} \left(1 - \frac{3(x-(1-\mu))^2}{r_2^2} \right)$$

$$C_{22} = \frac{\partial \ddot{y}}{\partial y} = 1 - \frac{1-\mu}{r_1^3} \left(1 - \frac{3y^2}{r_1^2} \right) - \frac{\mu}{r_2^3} \left(1 - \frac{3y^2}{r_2^2} \right)$$

$$C_{33} = \frac{\partial \ddot{z}}{\partial z} = -\frac{1-\mu}{r_1^3} \left(1 - \frac{3z^2}{r_1^2} \right) - \frac{\mu}{r_2^3} \left(1 - \frac{3z^2}{r_2^2} \right)$$

$$C_{12} = \frac{\partial \ddot{x}}{\partial y} = 3y(1-\mu) \frac{(x+\mu)}{r_1^5} + 3\mu y \frac{(x-(1-\mu))}{r_2^5} = C_{21} = \frac{\partial \ddot{y}}{\partial x}$$

$$C_{13} = \frac{\partial \ddot{x}}{\partial z} = 3z(1-\mu) \frac{(x+\mu)}{r_1^5} + 3\mu z \frac{(x-(1-\mu))}{r_2^5} = C_{31} = \frac{\partial \ddot{z}}{\partial x}$$

$$C_{23} = \frac{\partial \ddot{y}}{\partial z} = 3z(1-\mu) \frac{y}{r_1^5} + 3\mu z \frac{y}{r_2^5} = C_{32} = \frac{\partial \ddot{z}}{\partial y}$$

$$\dot{\Phi}_{11} = \Phi_{41} ; \dot{\Phi}_{12} = \Phi_{42} ; \dot{\Phi}_{13} = \Phi_{43} ; \dot{\Phi}_{14} = \Phi_{44} ; \dot{\Phi}_{15} = \Phi_{45} ; \dot{\Phi}_{16} = \Phi_{46}$$

$$\dot{\Phi}_{21} = \Phi_{51} ; \dot{\Phi}_{22} = \Phi_{52} ; \dot{\Phi}_{23} = \Phi_{53} ; \dot{\Phi}_{24} = \Phi_{54} ; \dot{\Phi}_{25} = \Phi_{55} ; \dot{\Phi}_{26} = \Phi_{56}$$

$$\dot{\Phi}_{31} = \Phi_{61} ; \dot{\Phi}_{32} = \Phi_{62} ; \dot{\Phi}_{33} = \Phi_{63} ; \dot{\Phi}_{34} = \Phi_{64} ; \dot{\Phi}_{35} = \Phi_{65} ; \dot{\Phi}_{36} = \Phi_{66}$$

$$\dot{\Phi}_{41} = C_{11}\Phi_{11} + C_{12}\Phi_{21} + C_{13}\Phi_{31} + 2\Phi_{51} ,$$

$$\dot{\Phi}_{42} = C_{11}\Phi_{12} + C_{12}\Phi_{22} + C_{13}\Phi_{32} + 2\Phi_{52} ,$$

$$\dot{\emptyset}_{43} = C_{11}\emptyset_{13} + C_{12}\emptyset_{23} + C_{13}\emptyset_{33} + 2\emptyset_{53} ,$$

$$\dot{\emptyset}_{44} = C_{11}\emptyset_{14} + C_{12}\emptyset_{24} + C_{13}\emptyset_{34} + 2\emptyset_{54} ,$$

$$\dot{\emptyset}_{45} = C_{11}\emptyset_{15} + C_{12}\emptyset_{25} + C_{13}\emptyset_{35} + 2\emptyset_{55} ,$$

$$\dot{\emptyset}_{46} = C_{11}\emptyset_{16} + C_{12}\emptyset_{26} + C_{13}\emptyset_{36} + 2\emptyset_{56} ,$$

$$\dot{\emptyset}_{51} = C_{21}\emptyset_{11} + C_{22}\emptyset_{21} + C_{23}\emptyset_{31} - 2\emptyset_{41} ,$$

$$\dot{\emptyset}_{52} = C_{21}\emptyset_{12} + C_{22}\emptyset_{22} + C_{23}\emptyset_{32} - 2\emptyset_{42} ,$$

$$\dot{\emptyset}_{53} = C_{21}\emptyset_{13} + C_{22}\emptyset_{23} + C_{23}\emptyset_{33} - 2\emptyset_{43} ,$$

$$\dot{\emptyset}_{54} = C_{21}\emptyset_{14} + C_{22}\emptyset_{24} + C_{23}\emptyset_{34} - 2\emptyset_{44} ,$$

$$\dot{\emptyset}_{55} = C_{21}\emptyset_{15} + C_{22}\emptyset_{25} + C_{23}\emptyset_{35} - 2\emptyset_{45} ,$$

$$\dot{\emptyset}_{56} = C_{21}\emptyset_{16} + C_{22}\emptyset_{26} + C_{23}\emptyset_{36} - 2\emptyset_{46} ,$$

$$\dot{\emptyset}_{61} = C_{31}\emptyset_{11} + C_{32}\emptyset_{21} + C_{33}\emptyset_{31} ,$$

$$\dot{\emptyset}_{62} = C_{31}\emptyset_{12} + C_{32}\emptyset_{22} + C_{33}\emptyset_{32} ,$$

$$\dot{\emptyset}_{63} = C_{31}\emptyset_{13} + C_{32}\emptyset_{23} + C_{33}\emptyset_{33} ,$$

$$\dot{\emptyset}_{64} = C_{31}\emptyset_{14} + C_{32}\emptyset_{24} + C_{33}\emptyset_{34} ,$$

$$\dot{\emptyset}_{65} = C_{31}\emptyset_{15} + C_{32}\emptyset_{25} + C_{33}\emptyset_{35} ,$$

$$\dot{\emptyset}_{66} = C_{31}\emptyset_{16} + C_{32}\emptyset_{26} + C_{33}\emptyset_{36} .$$

Appendix B – State Transition Matrix in ERTBP

The state transition matrix is a 6 X 6 matrix denoted by Φ and its variation is given by $\dot{\Phi} = A\Phi$ where

$$A = \begin{bmatrix} 0 & 0 & 0 & 1 & 0 & 0 \\ 0 & 0 & 0 & 0 & 1 & 0 \\ 0 & 0 & 0 & 0 & 0 & 1 \\ C_{11} & C_{12} & C_{13} & 0 & 2 & 0 \\ C_{21} & C_{22} & C_{23} & -2 & 0 & 0 \\ C_{31} & C_{32} & C_{33} & 0 & 0 & 0 \end{bmatrix}$$

$$C_{11} = \frac{\partial \ddot{x}}{\partial x} = \frac{1}{1 + e \cos(\nu)} \left[1 + \frac{3(1 - \mu)(x + \mu)^2}{r_1^5} - \frac{1 - \mu}{r_1^3} + \frac{3\mu(x - 1 + \mu)^2}{r_2^5} - \frac{\mu}{r_2^3} \right]$$

$$C_{22} = \frac{\partial \ddot{y}}{\partial y} = \frac{1}{1 + e \cos(\nu)} \left[1 + \frac{3y^2(1 - \mu)}{r_1^5} - \frac{1 - \mu}{r_1^3} + \frac{3\mu y^2}{r_2^5} - \frac{\mu}{r_2^3} \right]$$

$$C_{33} = \frac{\partial \ddot{z}}{\partial z} = \frac{1}{1 + e \cos(\nu)} \left[\frac{3z^2(1 - \mu)}{r_1^5} - \frac{1 - \mu}{r_1^3} + \frac{3\mu z^2}{r_2^5} - \frac{\mu}{r_2^3} - e \cos(\nu) \right]$$

$$C_{12} = \frac{\partial \ddot{x}}{\partial y} = 3y(1 - \mu) \frac{(x + \mu)}{r_1^5} + 3\mu y \frac{(x - (1 - \mu))}{r_2^5} = C_{21} = \frac{\partial \ddot{y}}{\partial x}$$

$$C_{13} = \frac{\partial \ddot{x}}{\partial z} = 3z(1 - \mu) \frac{(x + \mu)}{r_1^5} + 3\mu z \frac{(x - (1 - \mu))}{r_2^5} = C_{31} = \frac{\partial \ddot{z}}{\partial x}$$

$$C_{23} = \frac{\partial \ddot{y}}{\partial z} = 3z(1 - \mu) \frac{y}{r_1^5} + 3\mu z \frac{y}{r_2^5} = C_{32} = \frac{\partial \ddot{z}}{\partial y}$$

$$\dot{\Phi}_{11} = \Phi_{41} ; \dot{\Phi}_{12} = \Phi_{42} ; \dot{\Phi}_{13} = \Phi_{43} ; \dot{\Phi}_{14} = \Phi_{44} ; \dot{\Phi}_{15} = \Phi_{45} ; \dot{\Phi}_{16} = \Phi_{46}$$

$$\dot{\Phi}_{21} = \Phi_{51} ; \dot{\Phi}_{22} = \Phi_{52} ; \dot{\Phi}_{23} = \Phi_{53} ; \dot{\Phi}_{24} = \Phi_{54} ; \dot{\Phi}_{25} = \Phi_{55} ; \dot{\Phi}_{26} = \Phi_{56}$$

$$\dot{\Phi}_{31} = \Phi_{61} ; \dot{\Phi}_{32} = \Phi_{62} ; \dot{\Phi}_{33} = \Phi_{63} ; \dot{\Phi}_{34} = \Phi_{64} ; \dot{\Phi}_{35} = \Phi_{65} ; \dot{\Phi}_{36} = \Phi_{66}$$

$$\dot{\Phi}_{41} = C_{11}\Phi_{11} + C_{12}\Phi_{21} + C_{13}\Phi_{31} + 2\Phi_{51} ,$$

$$\dot{\Phi}_{42} = C_{11}\Phi_{12} + C_{12}\Phi_{22} + C_{13}\Phi_{32} + 2\Phi_{52} ,$$

$$\dot{\emptyset}_{43} = C_{11}\emptyset_{13} + C_{12}\emptyset_{23} + C_{13}\emptyset_{33} + 2\emptyset_{53} ,$$

$$\dot{\emptyset}_{44} = C_{11}\emptyset_{14} + C_{12}\emptyset_{24} + C_{13}\emptyset_{34} + 2\emptyset_{54} ,$$

$$\dot{\emptyset}_{45} = C_{11}\emptyset_{15} + C_{12}\emptyset_{25} + C_{13}\emptyset_{35} + 2\emptyset_{55} ,$$

$$\dot{\emptyset}_{46} = C_{11}\emptyset_{16} + C_{12}\emptyset_{26} + C_{13}\emptyset_{36} + 2\emptyset_{56} ,$$

$$\dot{\emptyset}_{51} = C_{21}\emptyset_{11} + C_{22}\emptyset_{21} + C_{23}\emptyset_{31} - 2\emptyset_{41} ,$$

$$\dot{\emptyset}_{52} = C_{21}\emptyset_{12} + C_{22}\emptyset_{22} + C_{23}\emptyset_{32} - 2\emptyset_{42} ,$$

$$\dot{\emptyset}_{53} = C_{21}\emptyset_{13} + C_{22}\emptyset_{23} + C_{23}\emptyset_{33} - 2\emptyset_{43} ,$$

$$\dot{\emptyset}_{54} = C_{21}\emptyset_{14} + C_{22}\emptyset_{24} + C_{23}\emptyset_{34} - 2\emptyset_{44} ,$$

$$\dot{\emptyset}_{55} = C_{21}\emptyset_{15} + C_{22}\emptyset_{25} + C_{23}\emptyset_{35} - 2\emptyset_{45} ,$$

$$\dot{\emptyset}_{56} = C_{21}\emptyset_{16} + C_{22}\emptyset_{26} + C_{23}\emptyset_{36} - 2\emptyset_{46} ,$$

$$\dot{\emptyset}_{61} = C_{31}\emptyset_{11} + C_{32}\emptyset_{21} + C_{33}\emptyset_{31} ,$$

$$\dot{\emptyset}_{62} = C_{31}\emptyset_{12} + C_{32}\emptyset_{22} + C_{33}\emptyset_{32} ,$$

$$\dot{\emptyset}_{63} = C_{31}\emptyset_{13} + C_{32}\emptyset_{23} + C_{33}\emptyset_{33} ,$$

$$\dot{\emptyset}_{64} = C_{31}\emptyset_{14} + C_{32}\emptyset_{24} + C_{33}\emptyset_{34} ,$$

$$\dot{\emptyset}_{65} = C_{31}\emptyset_{15} + C_{32}\emptyset_{25} + C_{33}\emptyset_{35} ,$$

$$\dot{\emptyset}_{66} = C_{31}\emptyset_{16} + C_{32}\emptyset_{26} + C_{33}\emptyset_{36} .$$

Bibliography

1. Moulton, F. R. (1914). An introduction to celestial mechanics. *The MacMillan company*, New York 1914, Second edition, pp. 319 -320.
2. Moulton, F. R., Buchanan, D., Buck, T., Griffin, F. L., Longley, W. R., MacMillan, W. D. (1920). Periodic orbits. *Carnegie Institution of Washington*, 1920.
3. Barrow-Green, J. E. (1993). Poincaré and the Three Body Problem. *Open University (United Kingdom)*.
4. Hill, G. W. (1878). Researches in the lunar theory. *American Journal of Mathematics*, 1(1), 5-26.
5. Broucke, R. (1969). Stability of periodic orbits in the elliptic, restricted three-body problem. *AIAA Journal*, 7, 1003–1009. <https://doi.org/10.2514/3.5267>
6. Szebehely, V. (1967). *Theory of Orbits: The Restricted Problem of Three Bodies*. Academic Press, New York.
7. Farquhar, R. W. (1967). Lunar communications with Libration-point satellites. *Journal of Spacecraft and Rockets*, 4(10), 1383-1384.
8. Farquhar, R. W., and Kamel, A. A. (1973). Quasi-periodic orbits about the translunar libration point. *Celestial Mechanics*, 7(4), 458-473.
9. Richardson, D. L., and Cary, N. D. (1975). A uniformly valid solution for motion about the interior libration point of the perturbed elliptic-restricted problem. In the *AIAA Conference on the Exploration of the Outer Planets*.
10. Richardson, D. L. (1980). Analytic construction of periodic orbits about the collinear points. *Celestial Mechanics*, 22(3), 241-253.
11. Richardson, D. L. (1980). Halo orbit formulation for the ISEE-3 mission. *Journal of Guidance and Control*, 3(6), 543-548.
12. Connor Howell, K. (1984). Three-dimensional, periodic halo orbits. *Celestial Mechanics*, 32(1), 53-71.
13. Howell, K. C., and Pernicka, H. J. (1987). Numerical determination of Lissajous trajectories in the restricted three-body problem. *Celestial Mechanics*, 41, 107–124. <https://doi.org/10.1007/BF01238756>.

14. Paffenroth, R., Doedel, E., Dichmann (2001). Continuation of periodic orbits around Lagrange points and AUTO 2000. *AAS Paper 01–303*. In: Proceedings of *AAS/AIAA Astrodynamics Specialist Conference*, Quebec City.
15. Pernicka, H. J. (1990). The numerical determination of nominal libration point trajectories and development of a station-keeping strategy. Ph. D. Thesis, *Purdue University*.
16. Dunham, D. W., Jen, S. J., Roberts, C. E., Seacord, A. W., Sharer, P. J., Folta, D. C., and Muhonen, D. P. (1992). Transfer trajectory design for the SOHO libration-point mission. In *Washington, DC International Astronautical Federation Congress*.
17. Sarris, E. (1989). Families of symmetric-periodic orbits in the elliptic three-dimensional restricted three-body problem. *Astrophysics and Space Science*, 162, 107–122. <https://doi.org/10.1007/BF00653348>.
18. Gordon, S. C. (1991). Representing the Nominal Path for an Interior Libration Point Orbit in the Sun-Earth Moon Elliptic Restricted Three-Body Problem. *Air Force Academy Colorado Springs CO*.
19. Farquhar, R. W. (1991). Halo-orbit and lunar-swingby missions of the 1990's. *Acta Astronautica*, 24, 227-234.
20. Cielaszyk, D., and Wie, B. (1994). Halo orbit determination and control for the elliptic restricted three-body system. In *Astrodynamics Conference* (p. 3729).
21. Cielaszyk, D., and Wie, B. (1996). New approach to halo orbit determination and control. *Journal of Guidance, Control, and Dynamics*, 19(2), 266-273.
22. Dunham, D. W., and Farquhar, R. W. (2003). Libration point missions, 1978–2002. In *Libration Point Orbits and Applications* (pp. 45-73).
23. Lo, M. W. (1997). Halo Orbit Generation Using the Center Manifold, Proceedings of the *AAS/AIAA Space Flight Mechanics Meeting*, Huntsville, AL, USA
24. Barden, B. T., and Howell, K. C. (1998). Fundamental motions near collinear libration points and their transitions. *The Journal of the Astronautical Sciences*, 46, 361-378.
25. Jorba, A., and Masdemont, J. (1997). Dynamics in the center manifold of the collinear points of the restricted three body problem. *Physica D: Nonlinear Phenomena*, 132(1-2), 189-213.
26. Gómez, G., Masdemont, J., and Simó, C. (1998). Quasihalo orbits associated with libration points. *The Journal of the Astronautical Sciences*, 46, 135-176.
27. J.L. Bell, M.W. Lo, and R.S. Wilson. (1999). Genesis Trajectory Design. In *AAS/AIAA Astrodynamics Specialist Conference*, Girdwood, AK. AAS 99-398.
28. Koon, W. S., Lo, M. W., Marsden, J. E., and Ross, S. D. (1999). The Genesis trajectory and heteroclinic connections. In the *AAS/AIAA Astrodynamics Specialist Conference* (pp. 99-451).

29. Koon, W.S., Lo, M.W., Marsden, J.E., Ross, S.D. (2000). Shoot the Moon. In: *AAS/AIAA Astrodynamics Specialist Conference*, Paper AAS 00–166.
30. M.W. Lo, S.D. Ross. (2001). The Lunar L₁ Gateway: Portal to the Stars and Beyond, in: *AIAA Space 2001 Conference*, Albuquerque, New Mexico.
31. Koon, W. S., Lo, M. W., Marsden, J. E., and Ross, S. D. (2000). Dynamical systems, the three-body problem and space mission design. In *Equadiff 99: (In 2 Volumes)* (pp. 1167-1181).
32. Gómez, G. (2001). Dynamics and mission design near libration points: fundamentals-the case of collinear libration points (Vol. 1). World Scientific.
33. Gomez, G., Jorba, A., Masdemont, J. J., and Simo, C. (2001). Dynamics and Mission Design Near Libration Points, Vol IV: Advanced Methods for Triangular Points (Vol. 5). World Scientific.
34. Gerard, G. (2001). Dynamics and Mission Design Near Libration Points: Advanced methods for collinear points. Vol. III (Vol. 4). World Scientific.
35. Canalias, E., Gomez, G., Marcote, M., and Masdemont, J. J. (2004). Assessment of mission design including utilization of libration points and weak stability boundaries. *ESA Advanced Concept Team*.
36. Canalias, E., and Masdemont, J. J. (2006). Homoclinic and heteroclinic transfer trajectories between planar Lyapunov orbits in the sun-earth and earth-moon systems. *Discrete and Continuous Dynamical Systems*, 14(2), 261.
37. Howell, K. C. (2001). Families of orbits in the vicinity of the collinear libration points. *The Journal of the Astronautical Sciences*, 49, 107-125.
38. Folta, D., and Beckman, M. (2003). Libration orbit mission design: applications of numerical and dynamical methods. In *Libration Point Orbits and Applications* (pp. 85-113).
39. McCaine, G. (2004). Halo orbit design and optimization. M. S. Thesis, *Naval Postgraduate School*, Monterey CA.
40. Farquhar, R. W., Dunham, D. W., Guo, Y., and McAdams, J. V. (2004). Utilization of libration points for human exploration in the Sun–Earth–Moon system and beyond. *Acta Astronautica*, 55(3-9), 687-700.
41. Rausch, R. R. (2005). Earth to halo orbit transfer trajectories. Master of Science Thesis, *Purdue University*, Indiana.
42. Kolemen, E., Kaskin, N. J., and Gurfil, P. (2007). Quasi-Periodic Orbits of the Restricted Three-Body Problem Made Easy. In *AIP Conference Proceedings* (Vol. 886, No. 1, pp. 68-77). *American Institute of Physics*.

43. Mondelo, J. M., Barrabés, E., Gómez, G., and Ollé, M. (2007). Numerical parametrizations of Libration Point trajectories and their invariant manifolds. *Advances in the Astronautical Sciences*, 129, 1153-1168.
44. Campagnola, S., Lo, M., Newton, P. (2008). Subregions of motion and elliptic halo orbits in the elliptic restricted three-body problem. *Advances in Astronautical Sciences*, 130 part 2, 1541–1555.
45. Olikara, Z. P., and Howell, K. C. (2010). Computation of quasi-periodic invariant tori in the restricted three-body problem. Paper No. AAS, 1-15.
46. Olikara, Z. P. (2010). Computation of quasi-periodic tori in the circular restricted three-body problem (Doctoral dissertation, *Purdue University*).
47. Alessi, E. M. (2010). The role and usage of libration point orbits in the earth-moon system. *Universitat de Barcelona*.
48. Alessi, E. M., Gómez, G., and Masdemont, J. J. (2012). A methodology for the computation of constrained orbits and its application to the design of Solar System trajectories. *The Journal of the Astronautical Sciences*, 59, 477-501.
49. Zhang, H., Li, Y., and Zhang, K. (2011). A novel method of periodic orbit computation in circular restricted three-body problem. *Science China Technological Sciences*, 54, 2197-2203.
50. Mahajan, B., and Pernicka, H. (2012). Halo orbits near small bodies in the elliptic restricted problem. In the *AIAA/AAS Astrodynamics Specialist Conference* (p. 4876).
51. Folta, D. C., Bosanac, N., Guzzetti, D., and Howell, K. C. (2015). An Earth–Moon system trajectory design reference catalog. *Acta Astronautica*, 110, 341-353.
52. Peng, H., and Xu, S. (2014). Numerical stability study of multi-circle elliptic halo orbit in the elliptic restricted three-body problem. In *Proceedings 24th International Symposium on Space Flight Dynamics—24th ISSFD*. Luarel, United States (pp. 1-20).
53. Peng, H., Bai, X., and Xu, S. (2017). Continuation of periodic orbits in the Sun-Mercury elliptic restricted three-body problem. *Communications in Nonlinear Science and Numerical Simulation*, 47, 1-15.
54. Bosanac, N., Webster, C. M., Howell, K. C., and Folta, D. C. (2017). Trajectory design and station-keeping analysis for the wide field infrared survey telescope mission. In the *AAS/AIAA Astrodynamics Specialist Conference*.
55. Nath, P., Ramanan, R. V. (2016). Precise halo orbit design and optimal transfer to halo orbits from earth using differential evolution. *Advances in Space Research*, 57, 202–217.

56. Srivastava, V. K., Kumar, J., Mishra, P., and Kushvah, B. S. (2018). Halo orbit of regularized circular restricted three-body problem with radiation pressure and oblateness. *Journal of Astrophysics and Astronomy*, 39, 1-14.
57. Abouelmagd, E. I., Pal, A. K., and Guirao, J. L. G. (2021). Analysis of nominal halo orbits in the Sun–Earth system. *Archive of Applied Mechanics*, 91(12), 4751-4763.
58. Baresi, N., Olikara, Z. P., and Scheeres, D. J. (2018). Fully numerical methods for continuing families of quasi-periodic invariant tori in astrodynamics. *The Journal of the Astronautical Sciences*, 65, 157-182.
59. Ferrari, F., Lavagna, M. (2018). Periodic motion around Libration points in the Elliptic Restricted Three-Body Problem. *Nonlinear Dynamics*, 93(2), 453–462.
60. Antoniadou, K. I., and Libert, A. S. (2018). Origin and continuation of 3/2, 5/2, 3/1, 4/1 and 5/1 resonant periodic orbits in the circular and elliptic restricted three-body problem. *Celestial Mechanics and Dynamical Astronomy*, 130, 1-30.
61. Wu, T., Pan, X., Xu, M., Qu, Q., Xia, Q., Liu, S. (2019). Parallely generating halo orbit and its transfer trajectory in the full ephemeris model. *Astrophysics and Space Science*, 364(1), 1-15.
62. Lujan, D., and Scheeres, D. J. (2022). Earth–Moon L 2 Quasi-Halo Orbit Family: Characteristics and Manifold Applications. *Journal of Guidance, Control, and Dynamics*, 45(11), 2029-2045.
63. Paez, R. I., and Guzzo, M. (2022). On the analytical construction of halo orbits and halo tubes in the elliptic restricted three-body problem. *arXiv preprint arXiv:2203.16315*.
64. D'Amario, L. A., and Edelbaum, T. N. (1974). Minimum impulse three-body trajectories. *AIAA Journal*, 12(4), 455-462.
65. L. A. Amario. Minimum Impulse Three-Body Trajectories. *Ph.D. Dissertation, Department of Aeronautics and Astronautics, Massachusetts Institute of Technology, Cambridge, Massachusetts, July 1973*.
66. Farquhar, R. W., Muhonen, D., and Richardson, D. (1977). Mission design for a halo orbiter of the Earth. In the *Astrodynamics Conference* (p. 810).
67. Farquhar, R. W., Muhonen, D. P., Newman, C. R., and Heuberger, H. S. (1980). Trajectories and orbital maneuvers for the first libration-point satellite. *Journal of Guidance and Control*, 3(6), 549-554.
68. Rodriguez-Canabal, J., Hechler, M. (1989). Orbital aspects of the SOHO mission design, AAS 89–171. In: *Orbital Mechanics and Mission Design, Advances in the Astronautical Sciences*, vol. 69, San Diego, pp. 347–357.

69. Hiday, L., "Optimal Transfers Between Libration-Point Orbits in the Elliptic Restricted Three-Body Problem," Ph.D. Dissertation, *School of Aeronautics and Astronautics, Purdue Univ.*, West Lafayette, IN, 1992.
70. Gómez, G., Jorba, À., Masdemont, J., and Simó, C. (1991). Moon's Influence on the Transfer from the Earth to a Halo Orbit Around L_1 . *Predictability, Stability, and Chaos in N-Body Dynamical Systems*, 283-290.
71. Gómez, G., Jorba, A., Masdemont, J., and Simó, C. (1993). Study of the transfer from the Earth to a halo orbit around the equilibrium point L_1 . *Celestial Mechanics and Dynamical Astronomy*, 56, 541-562.
72. Howell, K. C., Mains, D. L., and Barden, B. T. (1994). Transfer trajectories from Earth parking orbits to Sun-Earth halo orbits. *Spaceflight mechanics 1994*, 399-422.
73. Howell, K. C., Barden, B. T., and Lo, M. W. (1997). Application of dynamical systems theory to trajectory design for a libration point mission. *The Journal of the Astronautical Sciences*, 45, 161-178.
74. Wilson, R. S., "Trajectory Design in the Sun-Earth-Moon Four Body Problem," Ph.D. Dissertation, *School of Aeronautics and Astronautics, Purdue University*, West Lafayette, IN, 1998.
75. Wilson, R. S., and Howell, K. C. (1998). Trajectory Design in the Sun-Earth-Moon System Using Lunar Gravity Assists. *Journal of Spacecraft and Rockets*, Vol. 35, No. 2, pp. 191–198.
76. Folta, D., Cooley, S., Howell, K., and Bauer, F. H. (2001). Trajectory design strategies for the NGST L_2 libration point mission (No. AAS-01-206).
77. Mains, D. L. (1993). Transfer trajectories from Earth parking orbits to L_1 halo orbits. *Master's Thesis, Department of Aeronautics and Astronautics, Purdue University*, Purdue, USA.
78. Barden, B. T. (1994). Using stable manifolds to generate transfers in the circular restricted problem of three bodies. *Master degree thesis*. West Lafayette: School of Aeronautics and Astronautics, Purdue University.
79. Howell, K. C., Mains, D. L., and Barden, B. T. (1994). Transfer trajectories from Earth parking orbits to Sun-Earth halo orbits. *Spaceflight mechanics 1994*, 399-422.
80. Sharer, P.; Harrington, T. (1996). Trajectory Optimization for the ACE Halo Orbit Mission. In *Proceedings of the AIAA/AAS Astrodynamics Specialist Conference*, San Diego, CA, USA. AIAA paper 96-3601-CP.
81. Anderson, J. Earth-to-Lissajous Transfers and Recovery Trajectories Using an Ephemeris Model, *M.S. Thesis, School of Aeronautics and Astronautics, Purdue University*, 2001

82. Howell, K. C., Guzman, J. J., and Anderson, J. P. (2001). Trajectory arcs with lunar encounters for transfers to small amplitude Lissajous orbits. In *Proceedings of the 11 th Annual AAS/AIAA Space Flight Mechanics Meeting*, Santa Barbara, CA, Feb. 11-15, 2001, (Vol. 2, pp. 1481-1502).
83. Farquhar, R. W. (2001). The flight of ISEE-3/ICE: origins, mission history, and a legacy. *The Journal of the astronautical sciences*, 49, 23-73.
84. Corrêa, A. A., Prado, A. F. B. A., Stuchi, T. J., and Beaugé, C. (2007). Comparison of transfer orbits in the restricted three and four-body problems. *Nonlinear dynamics and systems theory*, 7(3), 267-277.
85. Rosales, J. J., Jorba, À., and Jorba-Cuscó, M. (2021). Transfers from the Earth to L 2 Halo orbits in the Earth–Moon bicircular problem. *Celestial Mechanics and Dynamical Astronomy*, 133(11-12), 55.
86. Hou, X. Y., Tang, J. S., and Liu, L. (2007). Transfer to the collinear libration point L_3 in the Sun–Earth Moon system. In *Proceedings of the 20th International Symposium on Space Flight Dynamics*. Nasa Technical Report 20080012700
87. D. P. Gordon, “Transfers to Earth–Moon L_2 Halo Orbits Using Lunar Proximity and Invariant Manifolds,” *M.S. Thesis, School of Aeronautics and Astronautics, Purdue University*, August 2008.
88. Parker, J. S., Born, G. H. (2008). Direct Lunar halo orbit transfers. *Journal of the Astronautical Sciences*, 56(4), 441–476.
89. Masdemont Soler, J., Gómez Muntané, G., and Alessi, E. M. (2009). Transfer orbits in the Earth–Moon system and refinement to JPL ephemerides. In the *21st International Symposium on Space Flight Dynamics*.
90. Alessi, Elisa Maria., Gerard, Gómez., Josep J, Masdemont. (2010). Two-maneuvers transfers between LEOs and Lissajous orbits in the Earth–Moon system. *Advances in Space Research*. 45(10), 1276-1291.
91. Li, M., and Zheng, J. (2010). Indirect transfer to the Earth–Moon L_1 libration point. *Celestial mechanics and dynamical astronomy*, 108, 203-213. DOI 10.1007/s10569-010-9301-7
92. Mingtao, L., and Jianhua, Z. (2010). Impulsive lunar halo transfers using the stable manifolds and lunar flybys. *Acta Astronautica*, 66(9-10), 1481-1492.
93. Folta, D. C., Pavlak, T. A., Haapala, A. F., and Howell, K. C. (2013). Preliminary design considerations for access and operations in Earth–Moon L_1/L_2 orbits. In *AAS/AIAA Spaceflight Mechanics Meeting* (No. GSFC-500-13-D-0037).

94. Renk, F., Hechler, M., and Messerschmid, E. (2010). Exploration missions in the Sun–Earth–Moon system: A detailed view on selected transfer problems. *Acta Astronautica*, 67(1-2), 82-96.
95. Zanzottera, A., Mingotti, G., Castelli, R., and Dellnitz, M. (2012). Intersecting invariant manifolds in spatial restricted three-body problems: design and optimization of Earth-to-halo transfers in the Sun–Earth–Moon scenario. *Communications in Nonlinear Science and Numerical Simulation*, 17(2), 832-843.
96. Davis, K., Born, G., and Butcher, E. (2013). Transfers to Earth–Moon L_3 halo orbits. *Acta Astronautica*, 88, 116-128.
97. Kokou, P., Le Bihan, B., Receveur, J. B., and Lizy-Destrez, S. (2014). Computing an optimized trajectory between Earth and an EM L_2 halo orbit. In *AIAA Guidance, Navigation, and Control Conference* (p. 0450).
98. Zeng, H., Zhang, J., Qi, R., and Li, M. (2017). Study of time-free transfers into libration point orbits with multiple constraints. *Journal of Guidance, Control, and Dynamics*, 40(11), 2752-2770.
99. Conte, D., He, G., Spencer, D. B., and Melton, R. G. (2018). Trajectory Design for LEO to Lunar Halo Orbits Using Manifold Theory and Fireworks Optimization. *Advances in the Astronautical Sciences*, 167, 1335-1353.
100. He, G., Conte, D., Melton, R. G., and Spencer, D. B. (2020). Fireworks Algorithm Applied to Trajectory Design for Earth to Lunar Halo Orbits. *Journal of Spacecraft and Rockets*, 57(2), 235-246.
101. Mezentsev, G., and Aksenov, S. (2021). Computer simulation of single burn transfers between low-Earth and halo orbits in the Sun-Earth system. In *Journal of Physics: Conference Series* (Vol. 1740, No. 1, p. 012018). IOP Publishing.
102. Ren, J., Wang, Y., Li, M., and Zheng, J. (2022). A trajectory design and optimization framework for transfers from the Earth to the Earth-Moon triangular L_4 point. *Advances in Space Research*, 69(2), 1012-1026.
103. Campagnola, S., and Lo, M. (2007). BepiColombo gravitational capture and the elliptic restricted three-body problem. In *PAMM: Proceedings in Applied Mathematics and Mechanics* (Vol. 7, No. 1, pp. 1030905-1030906). Berlin: WILEY-VCH Verlag.
104. Storn, R., Price, K. (1997). Differential evolution—A simple and efficient heuristic for global optimization over continuous spaces. *Journal of global optimization*, 11(4), 341–359.
105. Price, K. V, Storn, R.M., Lampinen, J.A. (2005). *Differential evolution: a practical approach to global optimization, Natural computing series*. Springer, Berlin.

106. Peng, H., Xu, S. (2015). Transfer to a multi-revolution elliptic halo orbit in Earth–Moon Elliptic Restricted Three-Body Problem using stable manifold. *Advances in Space Research*. 55(4), 1015–1027. <https://doi.org/10.1016/J.ASR.2014.11.013>
107. Peng, H., Xu, S. (2015). Low-energy transfers to a Lunar multi-revolution elliptic halo orbit. *Astrophysics and Space Science*. 357(1), 1–15.
108. Shirobokov, M., Trofimov, S., & Ovchinnikov, M. (2017). Survey of station-keeping techniques for libration point orbits. *Journal of Guidance, Control, and Dynamics*, 40(5), 1085-1105.
109. NASA. (2016). General Mission Analysis Tool (GMAT) v.R2016a (No. GSC-17177-1). Retrieved from <https://software.nasa.gov/software/GSC-17177-1>
110. Miguel Hermanns. (2002). Parallel Programming in Fortran 95 using OpenMP. https://www.openmp.org/wp-content/uploads/F95_OpenMPv1_v2.pdf